Copy No. 165

RM No. L6H28c





NACA

# RESEARCH MEMORANDUM

## INVESTIGATION OF DIVE BRAKES AND A DIVE-RECOVERY FLAP ON A HIGH-ASPECT-RATIO WING IN THE LANGLEY 8-FOOT HIGH-SPEED TUNNEL

By

Axel T. Mattson

Langley Memorial Aeronautical Laboratory
Langley Field, Va.



NATIONAL ADVISORY COMMITTEE
FOR AERONAUTICS

NATIONAL ADVISORY COMMITTEE FOR AERONAUTICS

RESEARCH MEMORANDUM

# INVESTIGATION OF DIVE BRAKES AND A DIVE-RECOVERY FLAP ON A HIGH-ASPECT-RATIO WING IN THE LANGLEY 8-FOOT HIGH-SPEED TUNNEL

By Axel T. Mattson

## SUMMARY

The results of tests made to determine the aerodynamic characteristics of a solid brake, a slotted brake, and a dive-recovery flap mounted on a high-aspect-ratio wing at high Mach numbers are presented. The data were obtained in the Langley 8-foot high-speed tunnel for corrected Mach numbers up to 0.940. The results have been analyzed with regard to the suitability of dive-control devices for a proposed high-speed airplane in limiting the airplane terminal Mach number by the use of dive brakes and in achieving favorable dive-recovery characteristics by the use of a dive-recovery flap. The analysis of the results indicated that the slotted brake would limit the proposed airplane terminal Mach number to values below 0.880 for altitudes up to 35,000 feet and a wing loading of 80 pounds per square foot and the dive-recovery flap would produce trim changes required for controlled pull-outs at 25,000 feet for a Mach number range from 0.800 to 0.900. Basic changes in spanwise loading are presented to aid in the evaluation of the wing strength requirements.

## INTRODUCTION

The investigation presented was undertaken because of the adverse compressibility phenomena that affect the longitudinal stability and control of high-speed airplanes and because of the vital need for safety in dives at high Mach numbers. The investigation was conducted in the Langley 8-foot high-speed tunnel in order to obtain data for use in evaluating the aerodynamic characteristics of dive-control devices at high Mach numbers. The aerodynamic characteristics of a low-drag wing equipped with a

solid brake, a slotted brake, and a dive-recovery flap for application as dive-control devices are presented. The dive brakes were investigated primarily to determine their application as speed-limiting devices at high Mach numbers. Some evaluation of their flight characteristics was also made. The dive-recovery flap was investigated to determine its effectiveness in producing a controlled pull-out from a high-speed dive.

The high-speed aerodynamic characteristics, which include the lift, span loading, pitching moment, drag, and wake widths for the high-aspect-ratio wing have been analyzed and are presented in reference 1. The data presented herein include the same aerodynamic characteristics as affected by a solid brake, a slotted brake, and a dive-recovery flap. Also included in the present investigation are increments in average downwash resulting from the addition of a dive-recovery flap. Data for Mach numbers up to 0.940 are presented.

## SYMBOLS AND COEFFICIENTS

$a$ speed of sound in undisturbed stream, feet per second

$b$ span of model, feet (3.15)

$c$ section chord of model, feet

$c'$ mean aerodynamic chord (0.37 ft)

$M$ Mach number in undisturbed stream $(V/a)$

$p_o$ static pressure in undisturbed stream, pounds per square foot

$p$ local static pressure at a point on airfoil section, pounds per square foot

$P$ pressure coefficient $\left(\frac{p - p_o}{q}\right)$

$q$ undisturbed-stream dynamic pressure, pounds per square foot $\left(\frac{1}{2}\rho V^2\right)$

$S$ area of complete model, square feet (1.10)

$V$ velocity in undisturbed stream, feet per second

$x$ distance along chord from leading edge of section, feet

$y$ distance along semispan from wing center line, feet

$\alpha$ angle of attack, degrees

$\rho$ mass density in undisturbed stream, slugs per cubic foot

$M_T$ estimated terminal Mach number

$R$ Reynolds number

$\Delta\varepsilon$ increment in downwash angle, degrees

$i_t$ angle of incidence of stabilizer, degrees

$\Delta H$ loss of total pressure between free stream and station in wake

$W/S$ airplane wing loading, pounds per square foot

Subscripts:

cr critical

L lower surface of airfoil section

U upper surface of airfoil section

The coefficients are defined as follows:

$c_n$ section normal-force coefficient

$$c_n = \frac{1}{c}\int_0^c \left(P_L - P_U\right)dx$$

$c_m$ section pitching-moment coefficient about 25-percent-chord station

$$c_m = \frac{1}{c^2}\int_0^c (P_U - P_L)\left(x - \frac{c}{4}\right)dx$$

$C_N$ wing normal-force coefficient

$$C_N = \frac{2}{S}\int_0^{b/2} cc_n dy$$

$C_{m_{c/4}}$ wing pitching-moment coefficient about 25-percent-chord station

$$C_{m_{c/4}} = \frac{2}{Sc'}\int_0^{b/2} c^2 c_m dy$$

$C_{D_o}$ wing profile-drag coefficient

$c_n c\frac{b}{S}$ section loading

## APPARATUS AND METHODS

The Langley 8-foot high-speed tunnel, in which the tests were conducted, is of the single-return, closed-throat type. The Mach number at the throat is continuously controllable. The air-stream turbulence in the tunnel is small but slightly higher than in free air. A complete description of the basic model and tunnel setup is given in reference 1 with the corrections for model constriction, wake constriction, lift-vortex interference, and model inaccuracies. All the data presented are for corrected Mach numbers unless otherwise specified.

The high-aspect-ratio wing used in this investigation is the same wing used in the tests of reference 1 with dive-control devices added. The wing has an NACA 65-210 section, an aspect ratio of 9.0, a taper ratio of 2.5:1.0, no sweepback, twist, or dihedral (reference 1). The effective span of the model is 37.8 inches, the root chord is 6 inches, and the tip chord is 2.4 inches. The model wing included 20 static-pressure orifices placed

at each of eight stations along the span. The spanwise locations of the stations in percent of the semispan are 11, 20, 30, 43, 56, 64, 80, and 95. The four inboard stations were placed on the left half of the wing and the four outboard stations were placed on the right half of the wing. The wing and the locations of the orifices are shown in figure 1.

In the investigation two types of dive brake having the same over-all dimensions and the same location were mounted on the model wing. (See fig. 2.) The solid brake consisted of a solid plate having a span approximately 20 percent of the wing semispan and a height the same as the wing thickness (10 percent of the local wing chord). The face of the slotted brake includes three banks of four slots inclined 10° to the air stream. Each slot was approximately 25 percent of the brake span and 10 percent of the brake height. (See fig. 3.)

The dive brakes were located on both the upper and lower surface of the model wing at 50 percent of the wing chord. The dive brakes were located spanwise, symmetrical about the wing center line; the center of the upper-surface brake was located at approximately 20 percent of the wing semispan; and the center of the lower-surface brake was located at approximately 12 percent of the wing semispan. (See fig. 4.) The unsymmetrical spanwise location of the brakes was used because of a possible installation in which the brakes could be applied by rotating in a plane normal to the chord line about a common support. The inboard location was necessary to insure adequate model strength.

The dive-recovery flap was located on the lower surface of the model wing. (See fig. 5.) The model flap was of the wedge type with a chord 10 percent of the local wing chord and a span 20 percent of the wing semispan. (See fig. 6.) The leading edge of the flap was located at 30 percent of the wing chord and the center of the flap was approximately 20 percent of the wing semispan from the model center line. The flap was deflected 30° with reference to the wing chord line. Pressure orifices were installed on the dive-recovery flap at corresponding wing stations A, B, and C. (See fig. 6.)

No force measurements were made during the tests. All the lift and moment data were obtained from

integrations of the pressure-distribution measurements. The pressures at the 164 orifices were recorded simultaneously by photographing a multiple tube manometer. The pressure-distribution measurements were made for a corrected Mach number range from 0.400 to 0.940. The tunnel choked at an uncorrected Mach number of 0.945.

The brake configurations were tested at angles of attack of 0°, 2°, 4°, 7°, and 10° for Mach numbers of 0.400 and 0.600 and at angles of attack of 0°, 2° and 4° for the complete Mach number range. The dive-recovery flaps were tested at angles of attack of -2°, 0°, 2°, 4°, and 7° for the complete Mach number range.

The wake-survey drag measurements were made independently of the pressure measurements. These measurements were made for uncorrected Mach numbers of 0.400, 0.600, 0.725, 0.760, 0.800, 0.850, and 0.880. As pointed out in reference 1, the tunnel choked with the wake-survey rake-support strut installed when the uncorrected Mach number in the region of the model was 0.880. A calibration of the tunnel with the wake-survey strut in place indicated that the results are essentially unaffected by choking effects up to the choking Mach number of the wake-survey strut. (See reference 1.) Wake-survey measurements were made at six spanwise stations 1.4 root chords behind the 25-percent-chord line of the wing. These stations were 11, 20, 26.5, 30.2, 33.3, and 42.9 percent of the wing semispan from the model-support plate. Wake-survey measurements for outboard stations of 60, 80, 95, and 102 percent semispan were obtained from the data of reference 1. These measurements were made for the complete Mach number and angle-of-attack ranges. In order to obtain wake-width measurements at a typical tail location, wake surveys were made at a station 2.82 root chords behind the 25-percent-chord line of the wing, 5 inches from the support plate or 26.4 percent wing semispan.

Downwash measurements were made at a station 2.87 root chords behind the 25-percent-chord line of the wing for the wing with dive-recovery flap and wing alone and 26.4 percent of the wing semispan from the support plate. The measurements were made by a small calibrated yaw head. The yaw-head measurements were made at a point located 70 percent of the chord above the center line of the tunnel. The measurements were made for a Mach number range from 0.400 to 0.880 at angles of attack of 0°, 2°, 4°, and 7°.

The variation of model Reynolds number in the Langley 8-foot high-speed tunnel, based on the mean aerodynamic chord of the model wing (0.37 ft), as a function of test Mach number is presented in figure 7. The variation of level-flight airplane lift coefficient with Mach number for wing loadings of 60 and 80 pounds per square foot are presented in figure 8.

In order to aid in locating the various figures in this report, a figure index has been prepared giving the figure number, title, Mach number range, and angle-of-attack range. (See table I.)

## RESULTS

### Pressure Distribution and Span Loadings

Basic pressure distributions.- The basic chordwise pressure distributions for the solid brake, slotted brake, and dive-recovery flap for spanwise stations of 11, 20, 30, and 43 percent semispan for Mach numbers of approximately 0.600, 0.800, and 0.930 and angles of attack of 0°, 4°, and 10° are presented in figures 9 to 20. These data illustrate the section chordwise loadings that occur with the application of the dive-control devices and the appearance of compressibility effects. The chordwise pressure-distribution measurements for all spanwise stations have been integrated to determine the corresponding section normal-force and moment coefficients. The spanwise variations in section loading are presented in figures 21 to 23. When compared with the results of reference 1 figures 21 to 23 illustrate the changes in aerodynamic forces along the span of the model caused by the application of the dive-control devices for variations in angle of attack and Mach number.

Normal force and pitching moments.- The spanwise variations in normal-force and pitching-moment coefficients were integrated along the wing semispan for each angle of attack and test Mach number to obtain total wing normal-force coefficients and total pitching-moment coefficients. The total wing pitching-moment coefficients are based on the mean aerodynamic chord of the wing (0.37 ft) and were calculated about a point located at 25 percent of the chord. These normal-force and pitching-moment coefficients are presented for the solid brake, slotted brake,

and dive-recovery flap at each angle of attack plotted against Mach number in figures 24, 25, and 26, respectively. The results for the model wing alone are presented in reference 1.

The effects of the solid brake, slotted brake, and dive-recovery flap on the static longitudinal stability characteristics of the wing are shown in figure 27. The variation of $dC_n/d\alpha$ and $dC_m/d\alpha$ with Mach number for an airplane level-flight wing loading of 60 pounds per square foot for the wing alone and for the wing with solid brake, slotted brake, and dive-recovery flap are presented in figures 28 and 29. In order to illustrate further the effects of the dive-control devices on the aerodynamic characteristics of the wing, the increments in normal-force and moment coefficients due to the solid brake, slotted brake, and dive-recovery flap are presented against Mach number in figures 30 to 32.

## Drag

Section wake surveys at five spanwise stations have been reduced to total profile-drag coefficients by use of expressions including the effects of compressibility similar to those presented in reference 1. These results are presented for each dive-control configuration in figures 33 to 35 for constant angles of attack through a range of Mach number from 0.400 to 0.865. The wake-survey measurements taken at stations 11.0 and 20.2 percent of the wing semispan - that is, directly behind the brakes - are subject to errors introduced by difficulty in obtaining measurements of the extreme total-pressure losses in the wake. The errors are believed to be a small part of the total drag and become unimportant when the total drag is used to estimate the terminal Mach number. The data and calculations presented are believed to be closely representative of the drag increases that can be expected.

From the drag results obtained an estimated variation of airplane drag coefficient with Mach number for the solid and slotted brakes at wing loadings of 60 and 80 pounds per square foot are presented in figures 36 and 37. In these figures the variation of wing drag coefficient for 0° angle of attack obtained from results presented in reference 1 are presented as a check on the variation of estimated airplane drag coefficient with

Mach number obtained from reference 2. The generalized drag curve obtained from unpublished data was extrapolated up to a Mach number of 1.0 and the extrapolations are used only to illustrate the high terminal Mach numbers to be expected for this airplane with a wing loading of 60 and 80 pounds per square foot. The increments obtained for the solid and slotted brakes were added to the estimated airplane variation. From these data, the terminal Mach number estimated for the complete airplane with and without the solid and slotted brakes are presented in figures 38 and 39 for wing loadings of 60 and 80 pounds per square foot for altitudes up to 35,000 feet.

## Wake Profiles

Vertical variations in total-pressure loss in the wake $\Delta H/q$ were measured at a station representing a typical horizontal-tail location and are presented for the wing with the dive-control devices for various angles of attack and Mach numbers in figures 40 to 42. This survey station is 2.82 root chords behind the 25-percent-chord line and 5 inches from the support plate (26.4-percent wing semispan), which represents a possible tail location. All the wake dimensions are given in terms of the wing root chord. These results show the wake width in the region of the tail and the wake spread with increase in Mach number.

## Downwash and Estimated Stability

Changes in downwash for model configurations with and without the dive-recovery flap were measured in a region representing a typical horizontal-tail location. These changes in downwash angles are representative of changes in tail loads resulting from the action of the dive-recovery flap. The variation in increments in downwash with Mach number for constant angles of attack are presented in figure 43.

An estimated qualitative comparison of elevator-fixed static longitudinal stability characteristics estimated for a proposed high-speed airplane with dive-recovery flaps is presented in figure 44.

## DISCUSSION

### Dive-Brake Characteristics

The primary purpose of a dive brake is to limit the terminal Mach number of a high-speed airplane without creating a serious stability problem, trim change, and flight hazard such as buffeting excited by low-frequency wake fluctuations. The slotted brake was designed primarily to decrease, with a minimum loss in braking effectiveness, some of the serious effects usually associated with a solid brake such as lift loss, moment changes, and buffeting tendencies.

Drag.- A large increase in wing profile drag resulted from the application of the dive-control brakes. The results presented illustrate the drag coefficients that can be obtained when air brakes are introduced in flow fields induced by the wing and corresponding wing-interference drag. (See figs. 33 and 34.) The drag variation with Mach number for both the solid and slotted brakes indicated rapid increases up to the highest test Mach number. The profile-drag coefficient for the slotted brake at a Mach number of 0.4 and an angle of attack of 0° is approximately 30 percent lower than the corresponding value obtained for the solid brake. The profile-drag coefficient for the slotted brake, however, increases more rapidly with Mach number so that for a Mach number of 0.85 the slotted brake presents a reduction in profile-drag coefficient of approximately 8 percent lower than that of the total solid-brake drag. This greater rate in drag increase with Mach number can be accounted for by a choking condition for the slotted brake; that is, a constant mass flow through the brake slots, which with increasing Mach number will effectively cause the slotted brake to approach the characteristics of the solid brake. The variation of drag for the wing with dive brakes with angle of attack indicates a decrease in profile-drag coefficient with increase in angle of attack. This variation is expected since at 0° angle of attack the brakes are normal to the free-stream air-flow direction, whereas with increases in wing angle of attack corresponding changes in brake angles occur. This change in brake angle may be visualized as a decrease in effective brake frontal area with increasing angles of attack.

Estimated terminal Mach number.- The effectiveness of the solid and slotted dive brakes in limiting the terminal Mach number of a high-speed airplane for wing loadings of 60 and 80 pounds per square foot has been estimated by use of a generalized drag curve from reference 2 and the drag results presented herein. (See figs. 36 to 39.) The estimated terminal Mach number for the airplane with a wing loading of 60 pounds per square foot at 25,000 feet altitude is approximately 0.950. With the application of the slotted brake the estimated terminal Mach number for these same conditions is 0.695 and with the application of the solid brake, 0.675. At 35,000 feet, the slotted brake will limit the estimated terminal Mach number to 0.805 and the solid brake will limit the estimated terminal Mach number to approximately 0.795. For a wing loading of 80 pounds per square foot and 35,000 feet altitude, which represents the most severe condition considered, the slotted brake will limit the estimated terminal Mach number to 0.880 and the solid brake will limit the estimated terminal Mach number to 0.870.

Wake profiles.- The wake widths for the dive brakes at a station approximating the probable tail location for various angles of attack and Mach numbers are presented in figures 40 and 41. The solid brake produces a broad erratic wake that slightly increases in width with Mach number. The width of the wake ranges from approximately 70 percent of the wing root chord below the wing chord line to approximately 70 percent above the wing chord line for 0° angle of attack. At an angle of attack of 4° and a Mach number of 0.883, the wake boundary for the solid brake has increased to 1 wing chord above the wing chord line. The slotted brake provides a decrease in wake widths of approximately 20 percent compared with the solid brake. The wake boundaries for the slotted brake do not seem to be as erratic as those indicated for the solid brake, especially for the lower-surface brake, which suggests a possible reduction in magnitude of the wake vorticity. At an angle of attack of 4° and a Mach number of 0.884, the wake boundary for the wing with the slotted brake is approximately 80 percent of the wing chord above the wing chord line as compared with 1 chord length for the solid brake. The wake of the brakes if located in front of the horizontal tail will envelop the tail for a recommended tail location of 70 percent above the wing chord (references 1 and 3).

Normal force and pitching moments.- The variation of normal-force and pitching-moment coefficients with Mach number for the solid and slotted brakes are presented in figures 24 and 25, respectively. The variation of normal-force coefficient with Mach number for the solid brake below the force break for angles of attack of 0° and 2° is small; however, a more rapid increase is indicated for the larger angles of attack. At the higher Mach numbers, that is from 0.800 to 0.900, there is a decrease in normal-force coefficient and, consequently, an increase in angle for zero lift. For the slotted brake the variation of normal-force coefficient with Mach number indicates a premature break in the normal-force-coefficient variation occurring at a Mach number of approximately 0.600 for angles of attack of 0° and 2°. (See fig. 25.) This premature force break is not considered serious and examination of the spanwise section loadings indicates shifts that at the higher Mach numbers move inboard toward the brake. (See fig. 22.) At the higher Mach numbers, this shift in span loading increases the section loading at a station approximately 50 percent of the wing semispan. It may be reasoned that, for a Mach number range from 0.600 to 0.760, a choking condition is occurring for the flow through the slotted brake, which demands a readjustment of the flow over the wing. Beyond a Mach number of approximately 0.800, the usual decrease in normal-force coefficient occurs; however, the force break is not so severe as that encountered for the wing alone in reference 1. (See figs. 24 and 25.) The data also indicate an increase in normal force beyond a Mach number of 0.900 for angles of attack of 0° and 2°. The variation of pitching-moment coefficients about the wing 25-percent chord with Mach number for both the solid and slotted brakes indicates no unusual characteristics and both types of brake seemed to improve the wing-alone variations.

In order to evaluate more completely the effects of the dive brakes with regard to changes in wing characteristics, the variation of increments in normal force and pitching moments produced by the dive brakes with Mach number is considered. These data are presented in figures 30 and 31. The results indicate a loss in normal-force coefficient for both the solid and slotted brakes; however, a greater loss is indicated for the solid brake.

Both the solid and slotted brake produce positive increments in wing pitching-moment coefficients. The

slotted brake, however, produces a slightly greater increment than the solid brake.

Stability.- The static longitudinal stability characteristics for the wing with dive brakes compared with those for the wing alone are presented in figure 27. In general, the wing alone (reference 1) tends to become more stable with increases in Mach number. For example, at a Mach number of 0.400 for a normal-force-coefficient range from 0.1 to 0.4 the wing alone is neutrally stable, becoming slightly unstable at the larger normal-force coefficients. As the Mach number is increased, the wing alone becomes increasingly stable with large increases in stability occurring at a Mach number of 0.900. The application of the solid and slotted brakes increases to a small degree the stability of the wing except at high Mach numbers. The wing stability variations for both the solid and slotted brakes are displaced to a desirable positive or pull-out pitching-moment coefficient range, which may be indicative of a positive trim change.

Application to complete airplane.- The wing static longitudinal stability characteristics as defined by normal-force and moment coefficients for the slotted brake seem to be, in general, satisfactory with regard to application at high Mach numbers, and the effectiveness of the slotted brake in limiting the airplane terminal Mach number compares favorably with that of the solid brake.

It should be noted here that the inboard location of the dive brakes investigated was determined by model strength. Unpublished downwash measurement and fluctuations made behind the brakes at a tail location recommended in references 1 and 3 (70 percent above the wing chord line) indicated erratic flow produced by the dive brakes. Wake envelopment of the horizontal tail in the recommended location would be encountered. (See section entitled "Wake profile".) These results indicate the undesirability of a brake location in front of the horizontal tail. An outboard location of the dive brakes is recommended. It is believed that an outboard location of the dive brakes would insure proper functioning of the horizontal tail and increase the trim lift coefficient for the airplane but an investigation of a specific airplane configuration will be necessary to determine these effects.

## Dive-Recovery-Flap Characteristics

Normal force and pitching moments.- The variation of normal-force coefficient for the dive-recovery flap with Mach number indicates a rapid increase in normal-force coefficient up to a Mach number of 0.800 for 0° angle of attack. The normal-force coefficients decreased rapidly with further increases in Mach number. The pitching-moment coefficient for constant angles of attack have small or nearly constant variations for a Mach number range from 0.400 to approximately 0.650. From a Mach number of 0.650 to 0.850 an increase in positive or pull-out moment is indicated; however, at Mach numbers from 0.800 to 0.925 a slight decrease occurs. At the highest Mach number the pitching moments for all angles of attack assume a positive moment coefficient. (See fig. 26.)

Increments in normal-force and moment coefficients.- The dive-recovery flap, the fundamental purposes of which are to increase wing lift and to produce favorable pull-out moment changes at high Mach numbers, indicates an increase in normal-force and positive moment coefficient through most of the test Mach number range for angles of attack of 0°, 2°, and 4°. For angles of attack of 0°, 2°, and 4°, the normal-force coefficient increment for the dive-recovery flap increases rapidly with Mach number. For an angle of attack of 0° at a Mach number of 0.900 the increment in normal-force coefficient produced by the dive-recovery flap is approximately 0.3. For the highest test angle of attack - that is, 7° - a loss in normal-force coefficient occurs for all Mach numbers. (See fig. 32.)

The basic chordwise pressure distributions and section loadings illustrate the variations discussed. (See figs. 17 to 20 and 23.) In general, the dive-recovery flap with its forward-chord location (30 percent of wing chord) increases the local pressures over the forward part of the lower surface of the airfoil with separated flow developed behind the flap and a corresponding decrease in pressures over the upper surface of the airfoil. At low Mach numbers this chordwise pressure distribution does not represent an increase in over-all lift mainly because of the separated region induced behind the flap, which tends to nullify the increased lift experienced over the forward part of the airfoil. The small increment in normal force that occurs for a Mach number of 0.400 can be seen in figure 32.

With increases in Mach number, corresponding increases in local velocities distribute the chordwise pressures so that rapid increases in lift occur over the forward part of the airfoil with the effect of the separated flow behind the flap tending to remain the same. At a Mach number of approximately 0.929, however, the rearward shift in upper-surface pressures seems to nullify some of the important increase in lift produced by the dive-recovery flap; a loss in flap effectiveness above a Mach number of 0.900 is thus indicated. (See figs. 17 and 20.) The changes in wing moment produced by the dive-recovery flap is apparent from these corresponding changes in chordwise loading. The increased loading for the forward part of the airfoil, which increases with increase in Mach number until the rearward shift in upper-surface loading occurs, will increase the pull-out moment for most conventional airplane center-of-gravity locations. The effects of the dive-recovery flaps on the variation in spanwise section loadings have been compared with the wing alone for angles of attack of 0° and 4°. (See fig. 23.) For a Mach number of 0.400 and an angle of attack of 4° the dive-recovery flap decreases the section loading; however, a slight increase in section loading occurs outboard of the flap. With increase in Mach number the dive-recovery flap for constant angle of attack up to approximately 4° produces increases in section loading over most of the span.

Stability.- The wing with the dive-recovery flap for a Mach number range up to 0.850 follows closely the wing-alone static longitudinal stability variation, the curve being displaced to a positive moment direction. (See fig. 27.) For Mach numbers of 0.900 and 0.925, however, the wing and dive-recovery flap become slightly unstable with some decrease in the positive moment. At the higher normal-force coefficients and Mach numbers, a large increase in stability occurs. The effects of the stability changes for the dive-recovery flap will be discussed further by use of downwash measurements and unpublished tail characteristics to estimate over-all airplane static longitudinal stability characteristics at high Mach numbers.

Downwash.- The dive-recovery flap produces slight decrease in downwash, from a Mach number of 0.400 to approximately 0.750. At a Mach number of 0.800 to a Mach number of 0.890 for angles of attack of 0°, 2°, and 4° a rapid increase in downwash occurs. (See fig. 43.) For

0° angle of attack at a Mach number of 0.800 the downwash increment produced is essentially 0°; however, at a Mach number of 0.890 the downwash increment has increased to approximately 4°. The large increase in downwash due to the dive-recovery flap will produce a large pull-out moment for this range of Mach number. At an angle of attack of 7° the dive-recovery flap does not contribute to an increased downwash but shows a decrease in downwash of approximately 1° at a Mach number of 0.850. (See fig. 43.) These downwash measurements were made at a station corresponding to 25.8 percent of the semispan. Examination of spanwise variation in section normal force for the dive-recovery flap compared with the wing alone (fig. 23) shows that the variation in section loading at the 25.8-percent station with Mach number agrees qualitatively with the measured increment in downwash.

Application to complete airplane.- The general aerodynamic merits of the dive-recovery flap with regard to wing alone have been discussed; however, further analysis is needed to evaluate more completely the effectiveness of the dive-recovery flap in producing desirable airplane pull-out characteristics. By use of the wing results of reference 1, downwash measurements, unpublished tail characteristics, and the results presented herein, the longitudinal stability and trim changes were calculated for the airplane with and without the dive-recovery flap for Mach numbers of 0.800, 0.825, 0.850, and 0.890. (See fig. 44.) These calculations are not considered quantitatively exact; however, they illustrate the over-all elevator-fixed static longitudinal stability characteristics and trim changes that may be encountered with the application of the dive-recovery flap. These calculations indicate that a rather large decrease in trim lift coefficient will occur for the airplane without the dive-recovery flap for a Mach number increase from 0.800 to 0.890. The application of the dive-recovery flap, however, produces an increase in trim with elevator fixed for a Mach number of 0.800 and a similar but slightly greater increase in trim lift coefficient for a Mach number of 0.890. These calculations represent a stick-fixed trim change that, for a wing loading of 60 pounds per square foot at 25,000 feet at Mach numbers of 0.800 and 0.890, will correspond to approximately a 3.6g pull-out; however, at lower altitudes the normal acceleration will be somewhat greater. (See figs. 8 and 44.) From the results and calculations of the present paper the dive-recovery flap investigated may be concluded to

provide satisfactory pull-outs for an airplane configuration in the range of Mach number from 0.800 to 0.900.

Wake profiles.- The dive-recovery flap produces a wake approximately 1 chord in width displaced below the wing chord line. At a Mach number of 0.867 and an angle of attack of 4°, the flap upper-wake boundary is approximately 50 percent of the wing chord above the chord line; however, at this point a wake loss ($\Delta H/q$ of approx. 0.04) was measured that is believed to be introduced by an upper-surface shock disturbance. This disturbance is apparent for all angles of attack and, for an angle of attack of 4° at a Mach number of 0.887, extends to 140 percent of the wing chord above the wing chord. (See fig. 42.) The amplitude and fluctuations in the wake produced by this indicated shock disturbance should not be serious and is similar to that analyzed in reference 2, which may give an indication of the structural stiffness needed for the fuselage and tail design.

Drag.- The variation of drag coefficient with Mach number for the dive-recovery flap indicates a large increase in wing profile drag from a Mach number of 0.750 to the highest Mach number tested. At a Mach number of 0.850 for an angle of attack of 4°, the dive-recovery flap represents an increase of approximately 59 percent of the wing-alone drag. (See reference 1 and fig. 35.)

## CONCLUDING REMARKS

The present investigation of similar solid and slotted dive brakes mounted on a model of a high-aspect-ratio wing has shown that the slotted brakes are slightly less effective than the solid brakes in limiting the terminal Mach number of a proposed high-speed bomber. The slotted brake was estimated to limit an airplane terminal Mach number to values below 0.880 for altitudes up to 35,000 feet and wing loadings up to 80 pounds per square foot: The slotted brake decreased slightly the serious effects usually associated with a solid brake such as lift loss, wing moment changes, and wake fluctuations. It is recommended that the slotted brake be located outboard on the wing to prevent wake envelopment of the horizontal tail.

A dive-recovery flap of the same relative dimensions and location investigated herein installed on a high-speed airplane should produce trim changes required for pull-outs at 25,000 feet for a Mach number range from 0.300 to 0.900.

Langley Memorial Aeronautical Laboratory
National Advisory Committee for Aeronautics
Langley Field, Va.

## REFERENCES

1. Whitcomb, Richard T.: Investigation of the Characteristics of a High-Aspect-Ratio Wing in the Langley 8-Foot High-Speed Tunnel. NACA RM No. L6H28a, 1946.

2. Bielat, Ralph P.: A Simple Method for Estimating Terminal Velocity Including Effect of Compressibility on Drag. NACA ACR No. L5G31, 1945.

3. Ferri, Antonio: Preliminary Investigation of Downwash Fluctuations of a High-Aspect-Ratio Wing in Langley 8-Foot High-Speed Tunnel. NACA RM No. L6H28b, 1946.

TABLE I.- INDEX OF FIGURES

| Figure | Title | Range | |
|---|---|---|---|
| | | Mach number | Angle of attack (deg) |
| **Model details** | | | |
| 1 | Pressure-orifice locations on 65-210 wing | ---------- | ---------- |
| 2 | Solid and slotted dive brakes mounted on wing in Langley 8-foot high-speed tunnel | ---------- | ---------- |
| 3 | Slotted dive brakes | ---------- | ---------- |
| 4 | Solid and slotted dive brakes at 50-percent-chord location on 65-210 wing | ---------- | ---------- |
| 5 | Dive-recovery flap mounted on wing | ---------- | ---------- |
| 6 | Location of 30° dive-recovery flap at 30-percent-chord location on lower surface of 65-210 wing | ---------- | ---------- |
| **Reynolds number** | | | |
| 7 | Variation of test Reynolds number with Mach number | 0.400 to 0.875 | ---------- |
| **Level-flight lift** | | | |
| 8 | Variation of level-flight lift coefficient with Mach number | 0.400 to 0.900 | ---------- |

TABLE I.- INDEX OF FIGURES - Continued

| Figure | Title | Range | |
|---|---|---|---|
| | | Mach number | Angle of attack (deg) |
| Pressure distribution | | | |
| 9 | Pressure distribution at the 11-percent-semispan station for wing with solid brake | 0.600 to 0.925 | 0 to 10.0 |
| 10 | Pressure distribution at the 20-percent-semispan station for wing with solid brake | ↓ | ↓ |
| 11 | Pressure distribution at the 30-percent-semispan station for wing with solid brake | ↓ | ↓ |
| 12 | Pressure distribution at the 43-percent-semispan station for wing with solid brake | ↓ | ↓ |
| 13 | Pressure distribution at the 11-percent-semispan station for wing with slotted brake | ↓ | ↓ |
| 14 | Pressure distribution at the 20-percent-semispan station for wing with slotted brake | ↓ | ↓ |
| 15 | Pressure distribution at the 30-percent-semispan station for wing with slotted brake | ↓ | ↓ |

TABLE I.- INDEX OF FIGURES - Continued

| Figure | Title | Range | |
|---|---|---|---|
| | | Mach number | Angle of attack (deg) |
| Pressure distribution - Continued | | | |
| 16 | Pressure distribution at the 43-percent-semispan station for wing with slotted brake | 0.600 to 0.925 | 0 to 10.0 |
| 17 | Pressure distribution at the 11-percent-semispan station for wing with dive-recovery flap | | 0 to 4.0 |
| 18 | Pressure distribution at the 20-percent-semispan station for wing with dive-recovery flap | | |
| 19 | Pressure distribution at the 30-percent-semispan station for wing with dive-recovery flap | | |
| 20 | Pressure distribution at the 43-percent-semispan station for wing with dive-recovery flap | | |
| Spanwise section loading | | | |
| 21 | Spanwise variation in section loading for wing with solid brake | 0.400 to 0.940 | 0 to 10.0 |

TABLE I.- INDEX OF FIGURES - Continued

| Figure | Title | Range | |
|---|---|---|---|
| | | Mach number | Angle of attack (deg) |
| | Spanwise section loading - Continued | | |
| 22 | Spanwise variation in section loading for wing with slotted brake | 0.400 to 0.937 | 0 to 10.0 |
| 23 | Spanwise variation in section loading for wing with dive-recovery flap | 0.400 to 0.929 | -2.0 to 7.0 |
| | Normal force and pitching moments | | |
| 24 | Variation of normal-force and pitching-moment coefficients with Mach number for wing with solid brake | 0.400 to 0.925 | 0 to 10.0 |
| 25 | Variation of normal-force and pitching-moment coefficients with Mach number for wing with slotted brake | ↓ | ↓ |
| 26 | Variation of normal-force and pitching-moment coefficients with Mach number for wing with dive-recovery flap | ↓ | -2.0 to 7.0 |
| | Stability | | |
| 27 | Stability characteristics for various model configurations | 0.400 to 0.925 | -2.0 to 10.0 |

TABLE I.- INDEX OF FIGURES - Continued

| Figure | Title | Range | |
|---|---|---|---|
| | | Mach number | Angle of attack (deg) |
| | Normal-force and pitching-moment slopes | | |
| 28 | Slope of normal-force-coefficient curve for a loading of 60 pounds per square foot at an altitude of 35,000 feet | 0.400 to 0.925 | ---------- |
| 29 | Slope of pitching-moment-coefficient curve for a loading of 60 pounds per square foot at an altitude of 35,000 feet | ↓ | ---------- |
| | Normal-force and pitching-moment increments | | |
| 30 | Variation of incremental normal-force and pitching-moment coefficients with Mach number for solid brake | 0.400 to 0.925 | 0 to 10.0 |
| 31 | Variation of incremental normal-force and pitching-moment coefficients with Mach number for slotted brake | ↓ | ↓ |
| 32 | Variation of incremental normal-force and pitching-moment coefficients with Mach number for dive-recovery flap | ↓ | 0 to 7.0 |

TABLE I.- INDEX OF FIGURES - Continued

| Figure | Title | Range | |
|---|---|---|---|
| | | Mach number | Angle of attack (deg) |
| | **Profile drag** | | |
| 33 | Variation of profile-drag coefficient with Mach number for wing with solid brake | 0.400 to 0.865 | 0 to 10.0 |
| 34 | Variation of profile-drag coefficient with Mach number for wing with slotted brake | 0.400 to 0.860 | ↓ |
| 35 | Variation of profile-drag coefficient with Mach number for wing with dive-recovery flap | 0.400 to 0.850 | -2.0 to 4.0 |
| | **Terminal Mach number** | | |
| 36 | Estimated variation of airplane drag coefficient with Mach number for terminal Mach number prediction for airplane wing loading of 60 pounds per square foot at various altitudes | 0.400 to 0.900 | ---------- |
| 37 | Estimated variation of airplane drag coefficient with Mach number for terminal Mach number prediction for airplane wing loading of 80 pounds per square foot at various altitudes | ↓ | ---------- |

TABLE I.- INDEX OF FIGURES - Continued

| Figure | Title | Range | |
|---|---|---|---|
| | | Mach number | Angle of attack (deg) |
| | Terminal Mach number - Continued | | |
| 38 | Estimated variation of terminal Mach number with altitude for wing loading of 60 pounds per square foot | 0.400 to 0.900 | ---------- |
| 39 | Estimated variation of terminal Mach number with altitude for wing loading of 80 pounds per square foot | ↓ | ---------- |
| | Wake profiles | | |
| 40 | Wake profiles for several Mach numbers 2.82 root chords behind the 25-percent-chord line for wing with solid brake | 0.700 to 0.883 | 0 to 4.0 |
| 41 | Wake profiles for several Mach numbers 2.82 root chords behind the 25-percent-chord line for wing with slotted brake | 0.760 to 0.884 | ↓ |
| 42 | Wake profiles for several Mach numbers 2.82 root chords behind the 25-percent-chord line for wing with dive-recovery flap | 0.760 to 0.887 | ↓ |

TABLE I.- INDEX OF FIGURES - Concluded

| Figure | Title | Range | |
|---|---|---|---|
| | | Mach number | Angle of attack (deg) |
| | Downwash | | |
| 43 | Variation of change in downwash angle with Mach number for the dive-recovery flap measured 70 percent of chord above the center line | 0.400 to 0.900 | 0 to 7.0 |
| | Estimated comparative stability | | |
| 44 | Estimated comparison of elevator-fixed static longitudinal stability characteristics for complete airplane with dive-recovery flap | 0.8 to 0.89 | ---------- |

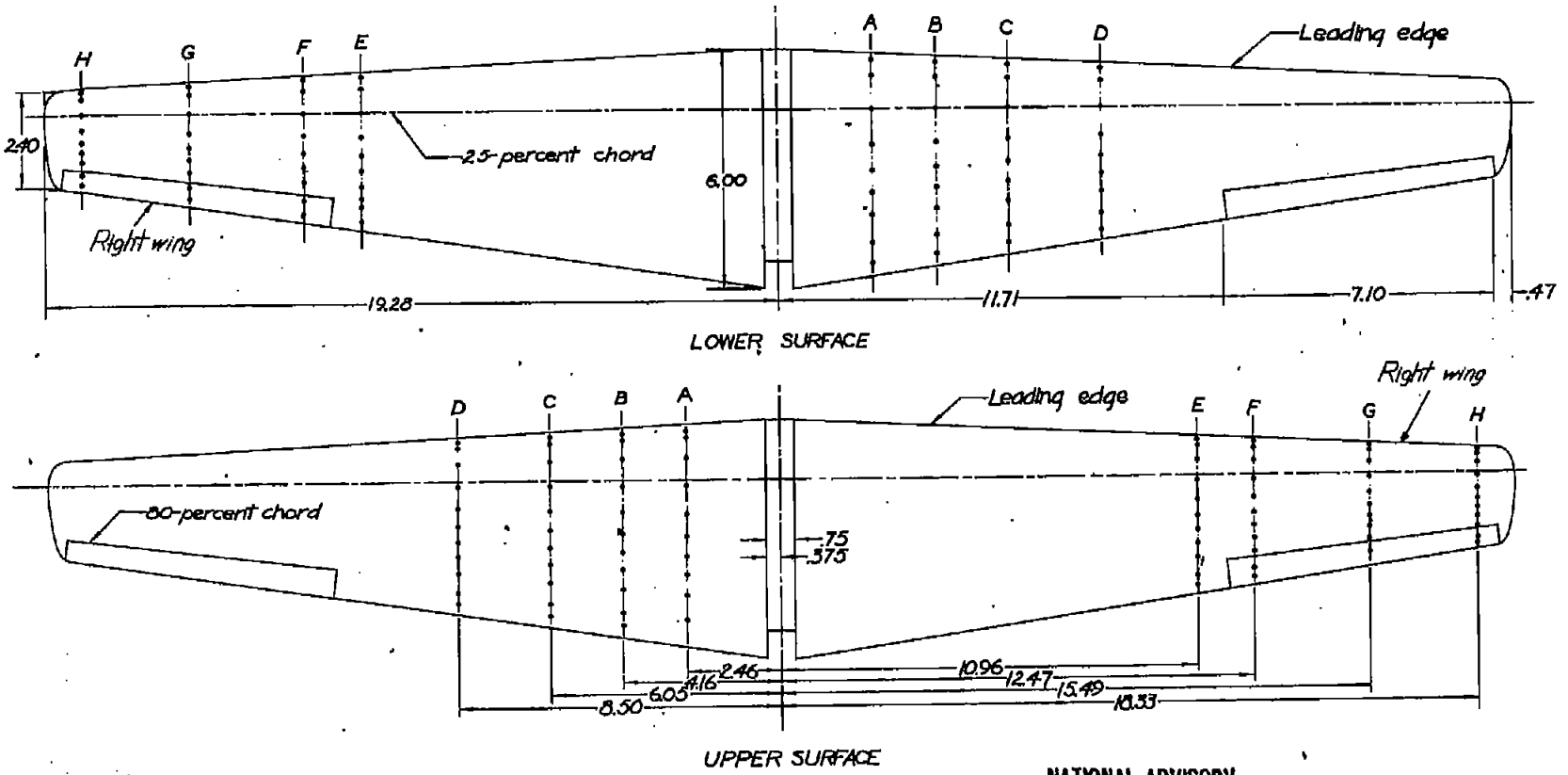


NATIONAL ADVISORY
COMMITTEE FOR AERONAUTICS



| Station | Station location, percent semispan | Orifice location, percent chord | | | | | | | | | | | | | | | | | | | | | | | |
|---|---|---|---|---|---|---|---|---|---|---|---|---|---|---|---|---|---|---|---|---|---|---|---|---|---|
| | | Upper surface | | | | | | | | | | | | | Lower surface | | | | | | | | | | |
| A | 11 | 2 | 6 | 15 | 27.5 | 40 | 50 | 59 | 62.5 | 72.5 | | 88 | | | 3 | 10 | 25 | 41 | 52.5 | 62.5 | 72.5 | | 85 | 94 |
| B | 20 | 2 | 6 | 15 | 27.5 | 40 | 50 | 59 | 62.5 | 72.5 | | 88 | 94 | | 3 | 10 | 25 | 41 | 52.5 | 62.5 | 72.5 | | 85 | 94 |
| C | 30 | 2 | 6 | 15 | 27.5 | 40 | 50 | 59 | 62.5 | 72.5 | | 88 | 94 | | 3 | 10 | 25 | 41 | 52.5 | 62.5 | 72.5 | | 85 | 94 |
| D | 43 | 2 | 6 | 15 | 27.5 | 40 | 50 | 59 | 62.5 | 72.5 | | 88 | 94 | | 3 | 10 | 25 | 41 | 52.5 | 62.5 | 72.5 | | 85 | 94 |
| E | 56 | | 6 | 15 | 27.5 | 40 | 50 | 59 | 62.5 | 72.5 | | 88 | 94 | | 3 | 10 | 25 | 41 | 52.5 | 62.5 | 72.5 | 80 | 85 | 94 |
| F | 64 | 2 | 6 | 15 | 27.5 | 40 | 50 | 59 | 62.5 | 72.5 | 80 | 88 | 94 | | 3 | 10 | 25 | 41 | 52.5 | 62.5 | 72.5 | 80 | 85 | 94 |
| G | 80 | 2 | 6 | 15 | 27.5 | 40 | 50 | 59 | 62.5 | 72.5 | 80 | 88 | | | 3 | 10 | 25 | 41 | 52.5 | 62.5 | 72.5 | 80 | 85 | 94 |
| H | 95 | 2 | 6 | 15 | 27.5 | 40 | 50 | 59 | 62.5 | 72.5 | 80 | 88 | 94 | | 3 | 10 | 25 | 41 | 52.5 | 62.5 | 72.5 | 80 | 85 | 94 |

Figure 1.— Pressure-orifice locations.

CONFIDENTIAL

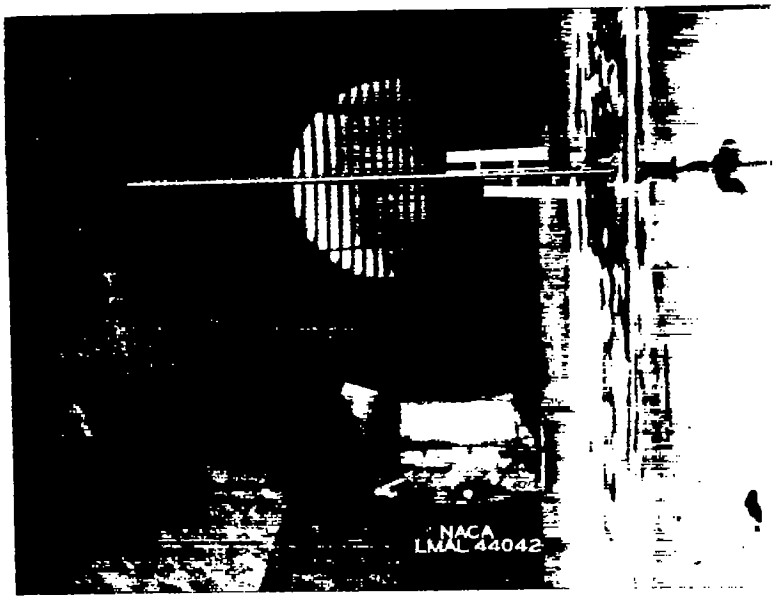


(a) Solid brake.

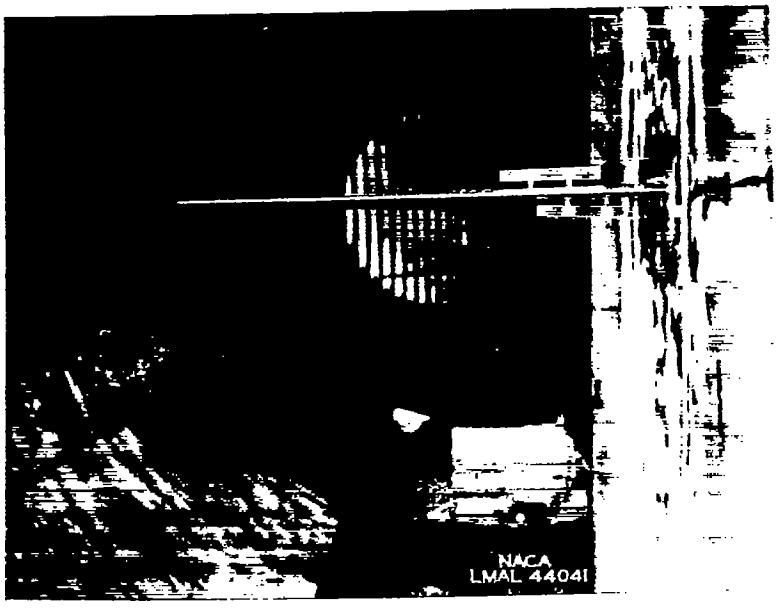


(b) Slotted brake.

Figure 2.- Solid and slotted dive brakes mounted on wing in Langley 8-foot high-speed tunnel.

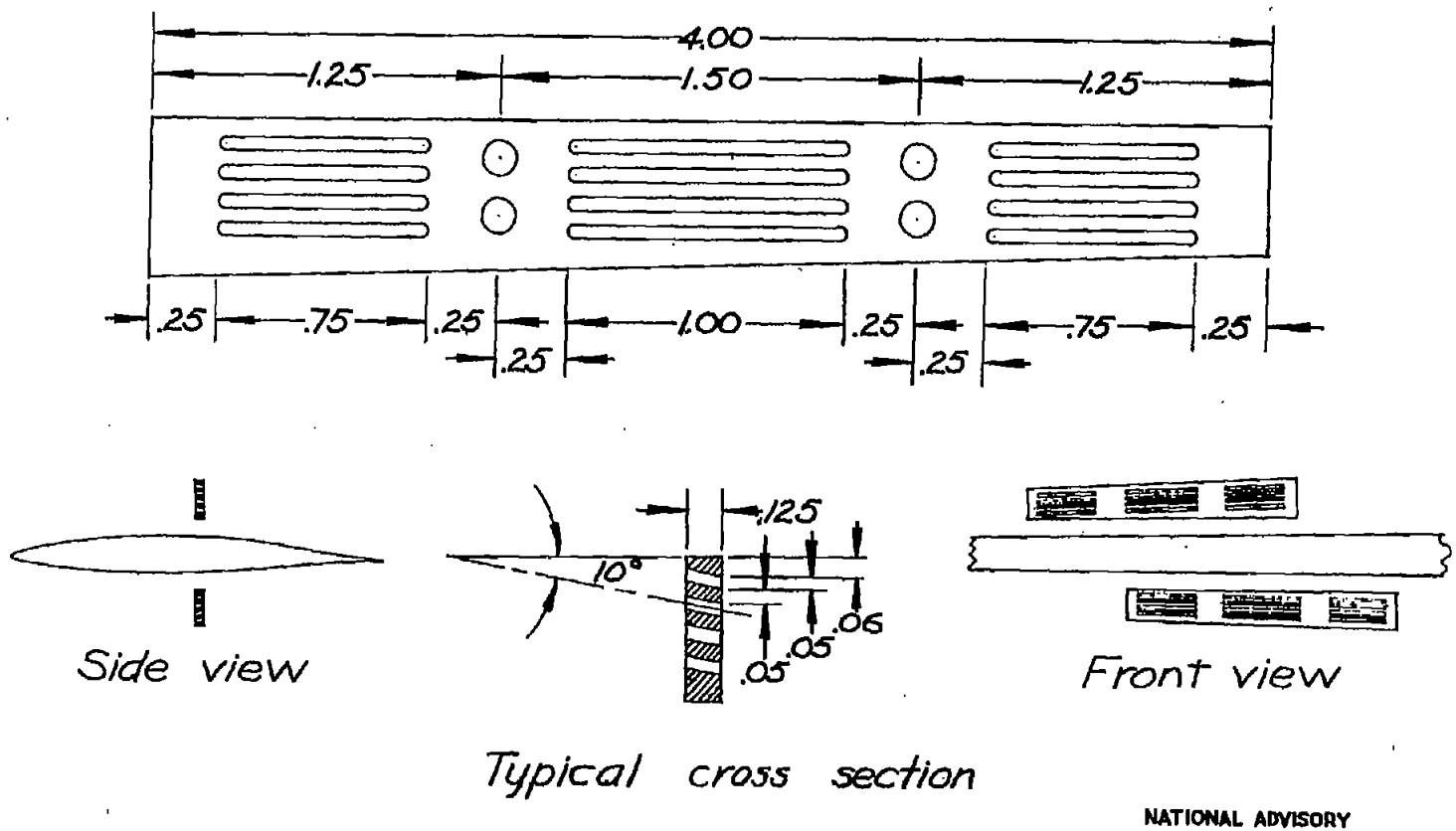


NATIONAL ADVISORY
COMMITTEE FOR AERONAUTICS

Figure 3.—Detail of slotted dive brake.

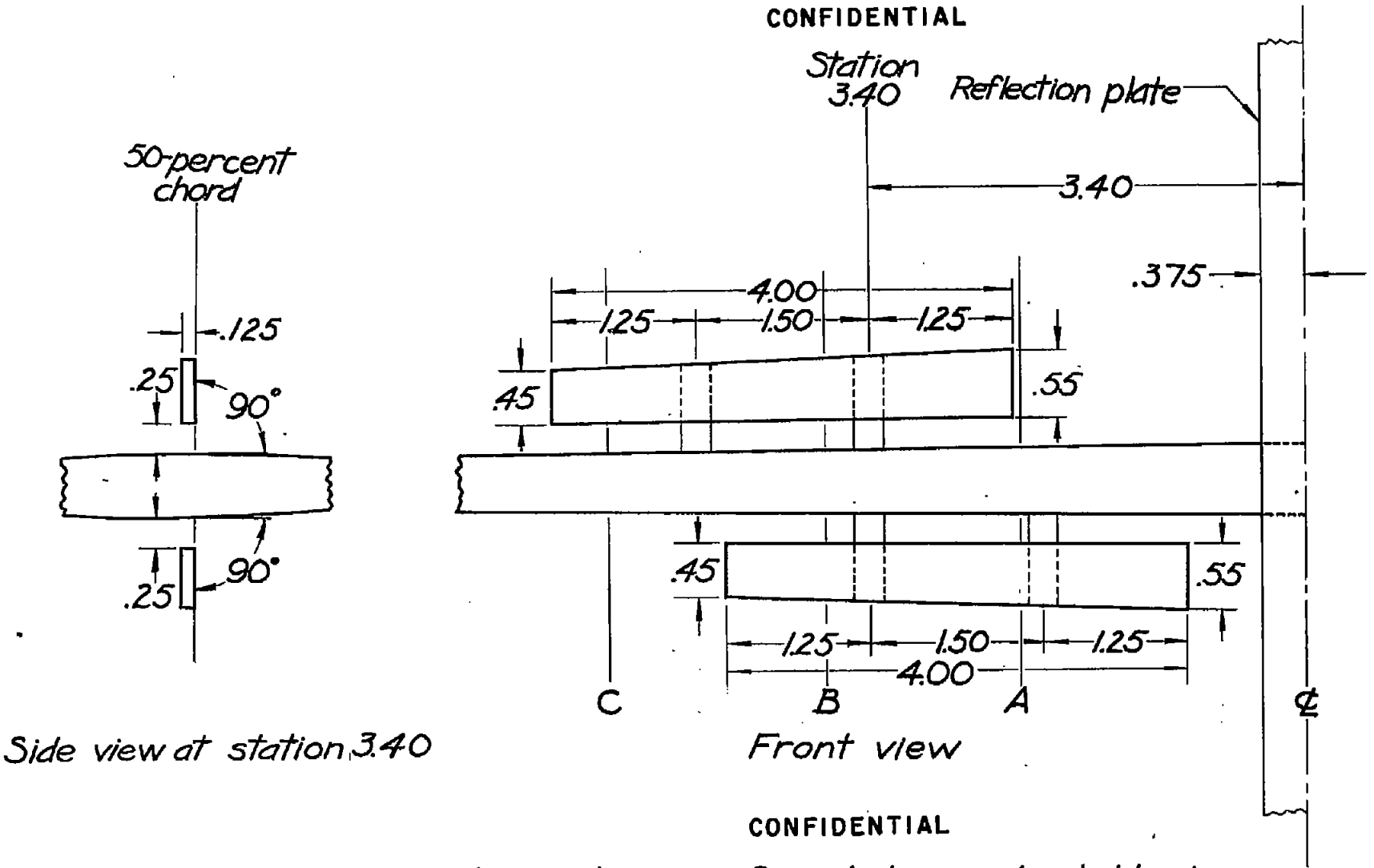




Figure 4.—Location of solid and slotted dive brakes on 65-210 wing. All dimensions are in inches.

NATIONAL ADVISORY COMMITTEE FOR AERONAUTICS

CONFIDENTIAL

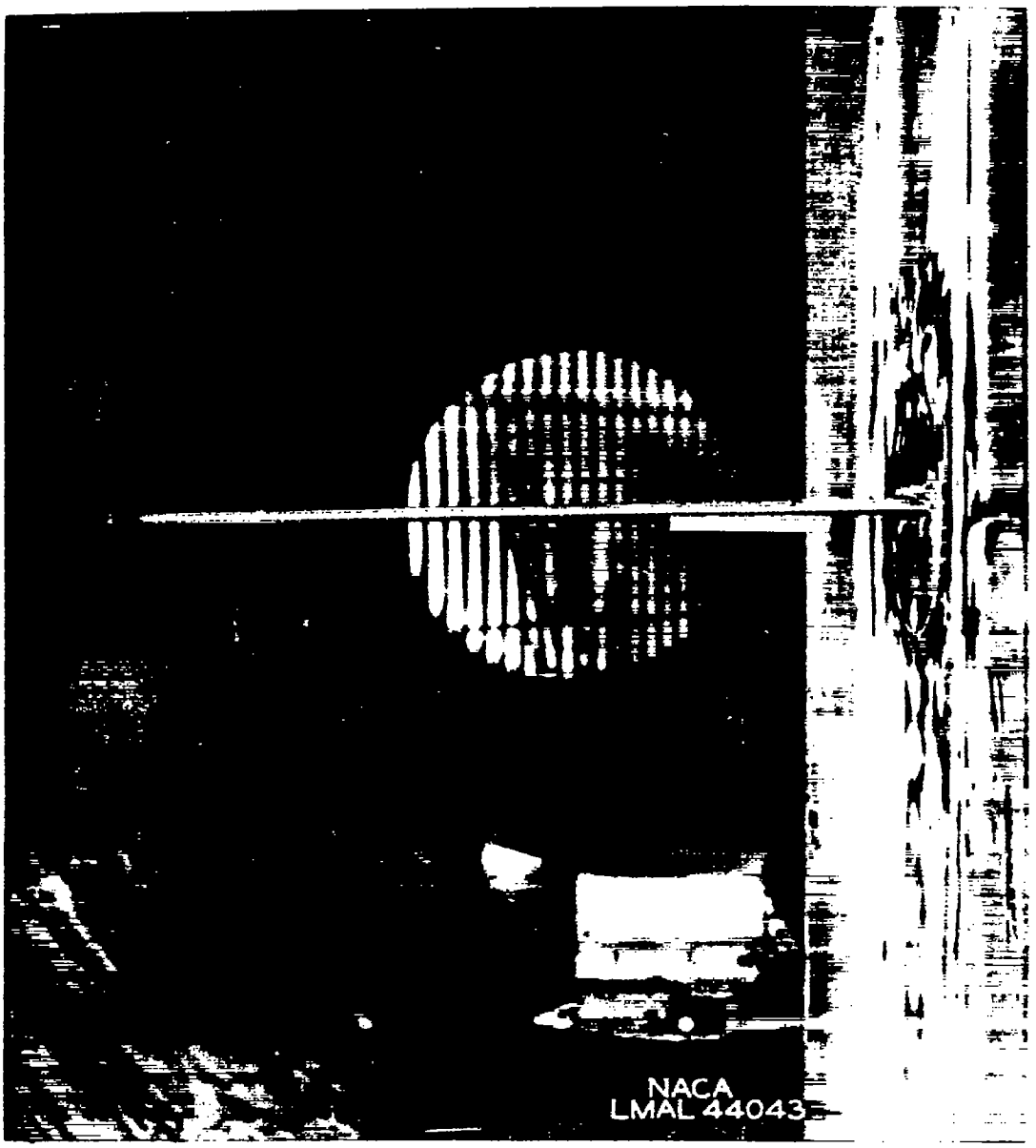


Figure 5.- Dive-recovery flap mounted on wing.

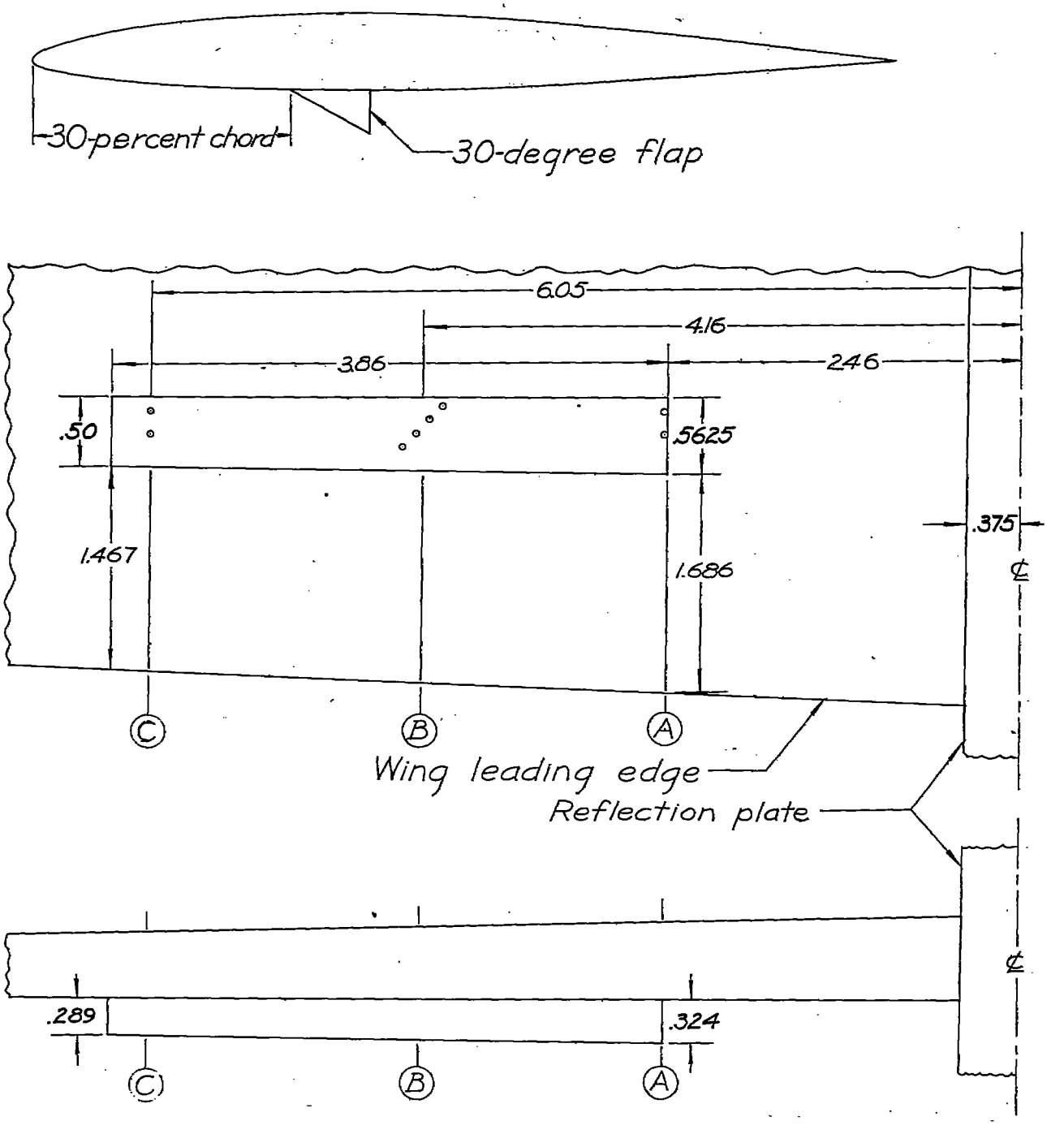


Figure 6.—Location of 30-degree dive-recovery flap on wing lower surface. All dimensions are in inches.

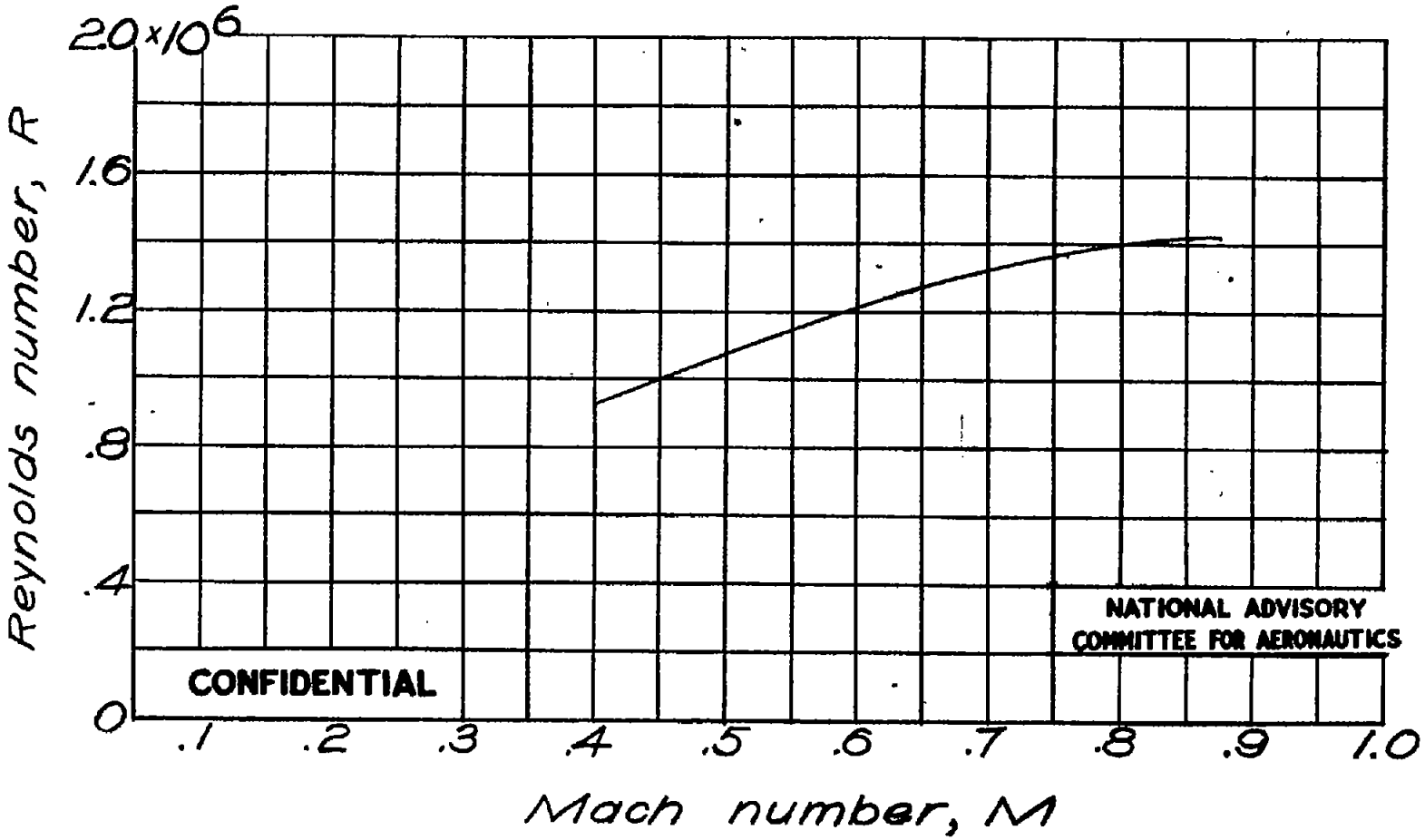


Figure 7.-Variation of test Reynolds number with Mach number.

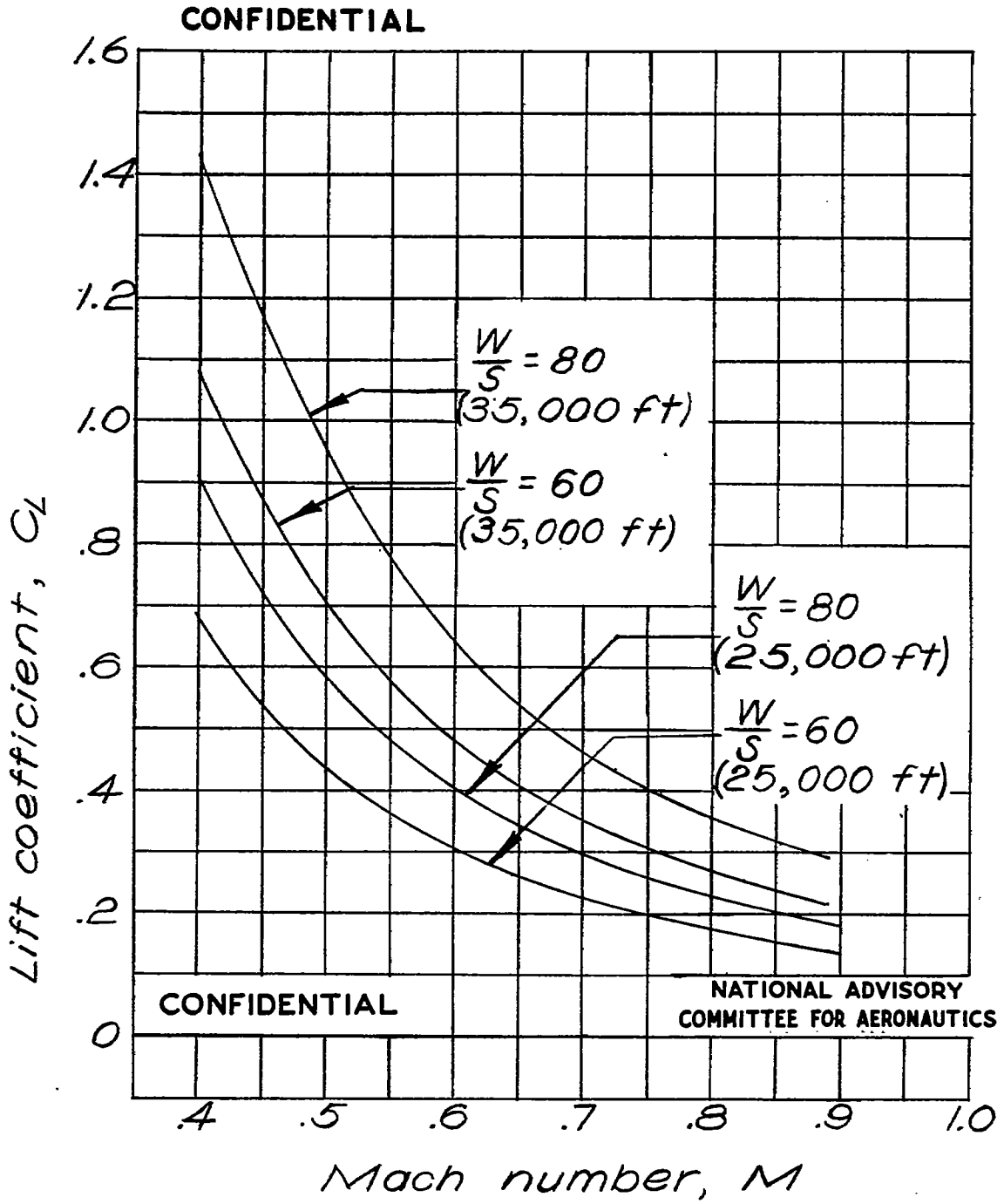


Figure 8.-Variation of level-flight lift coefficient with Mach number.

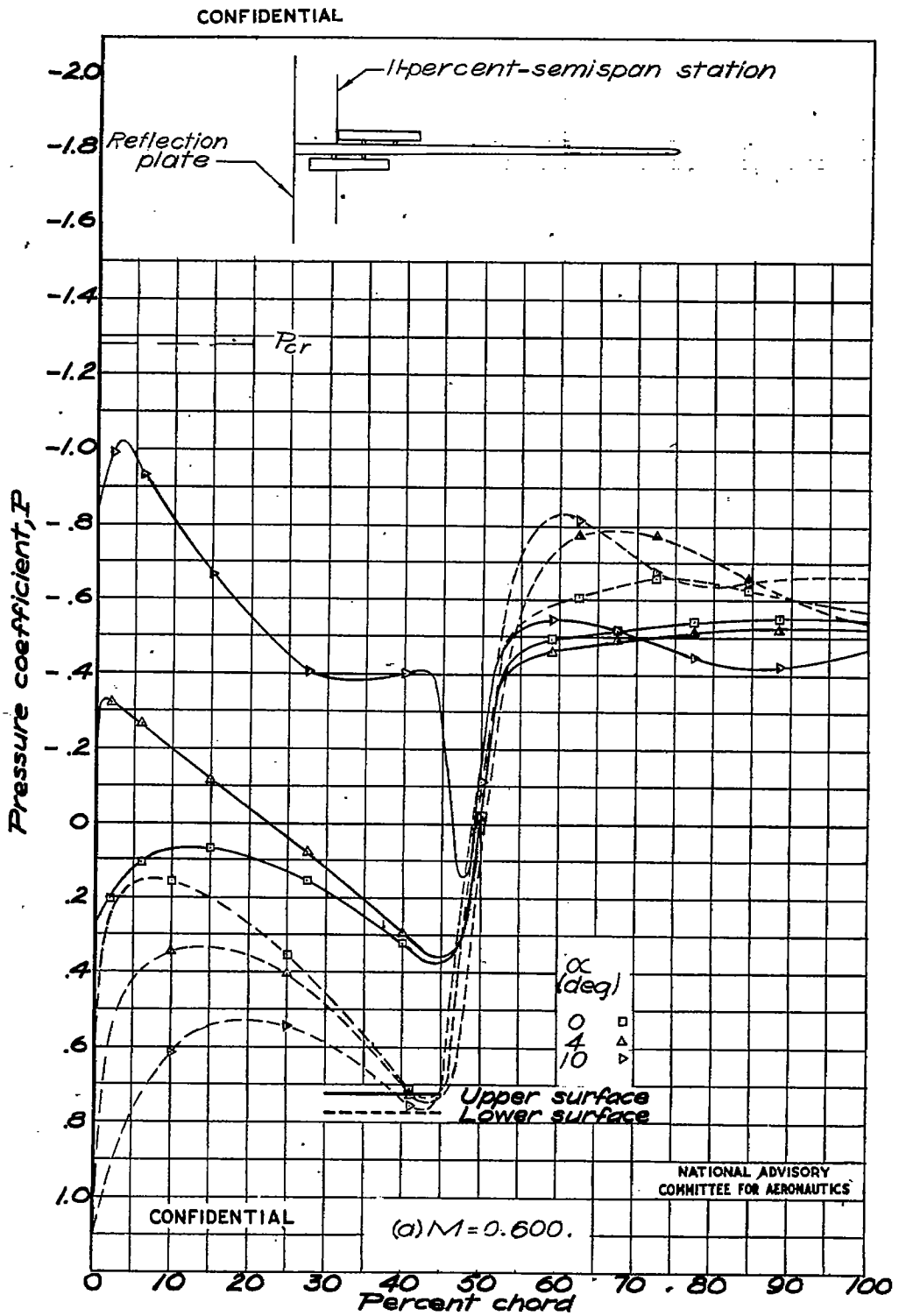


Figure 9.- Pressure distribution at the 11-percent-semispan station for wing with solid brake.

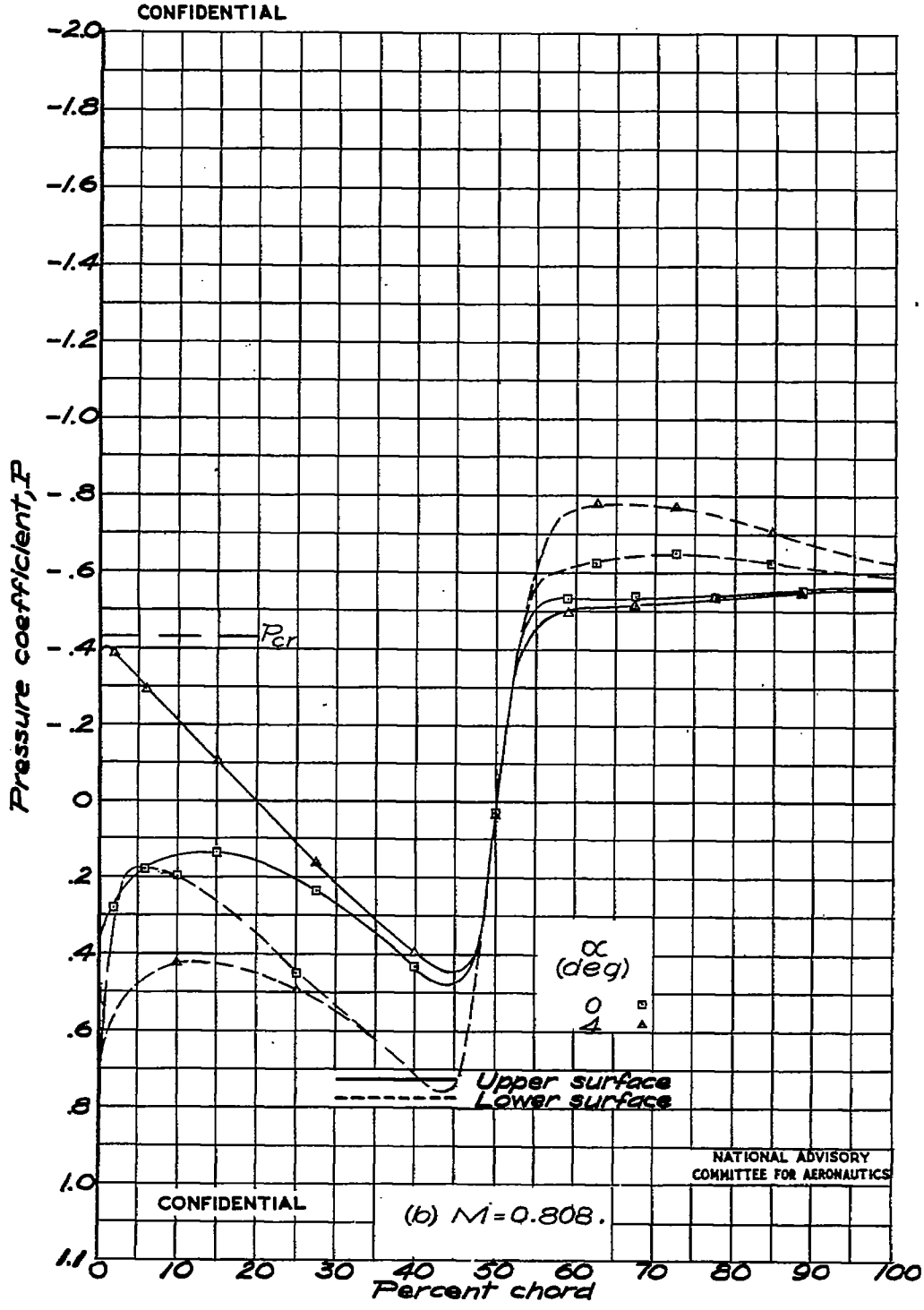


Figure 9.- Continued.

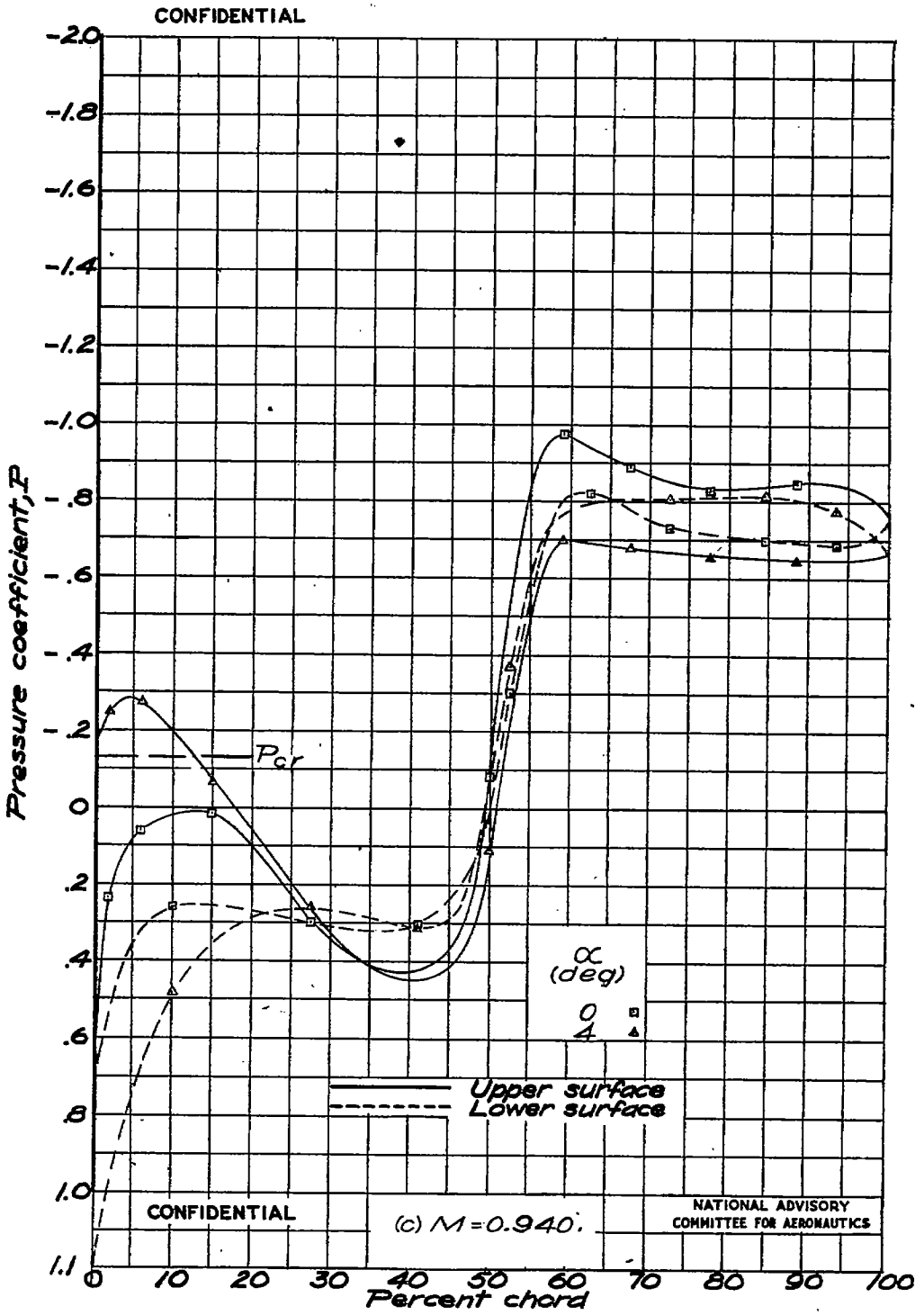


Figure 9.- Concluded.

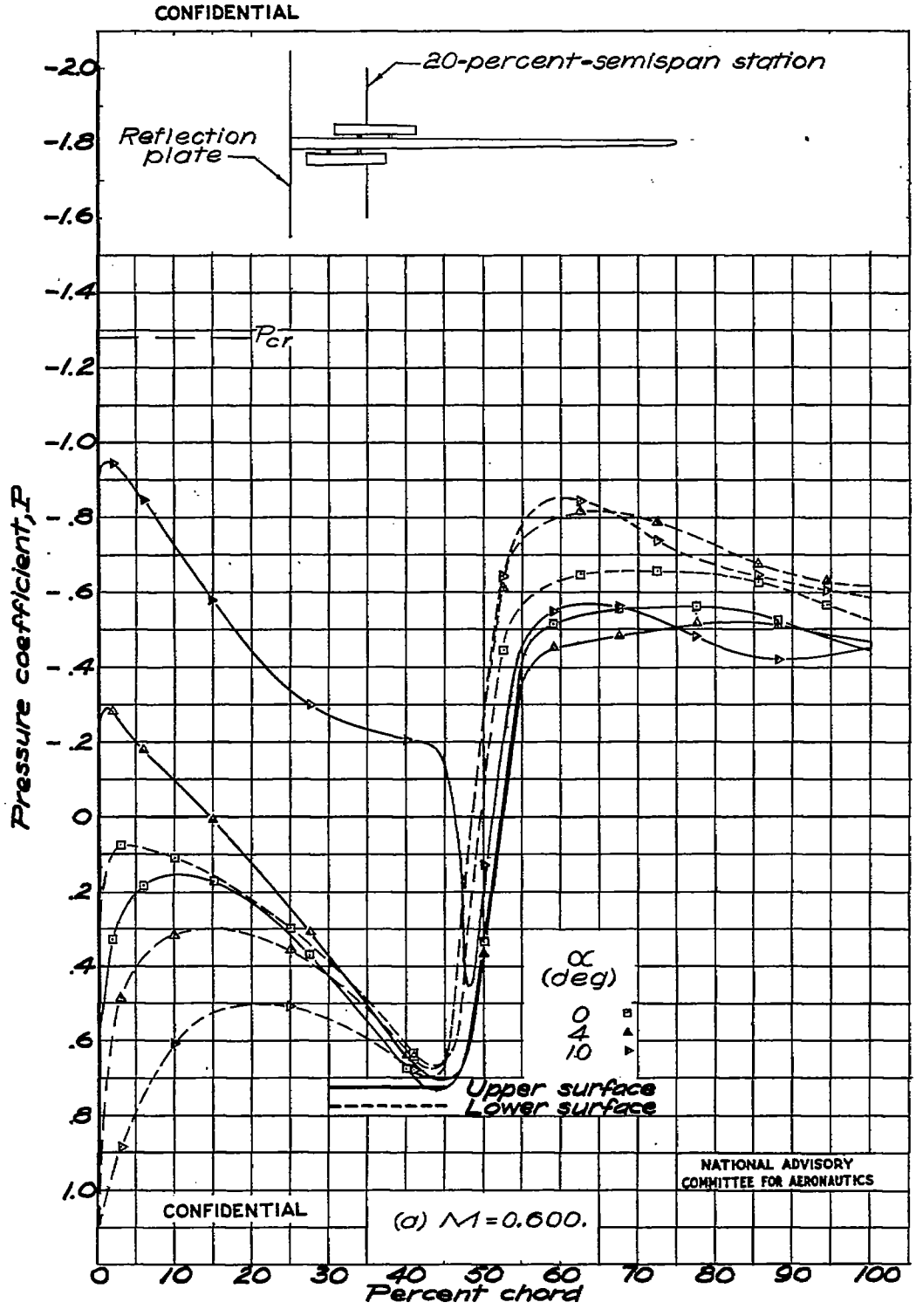


Figure 10.- Pressure distribution at the 20-percent-semispan station for wing with solid brake.

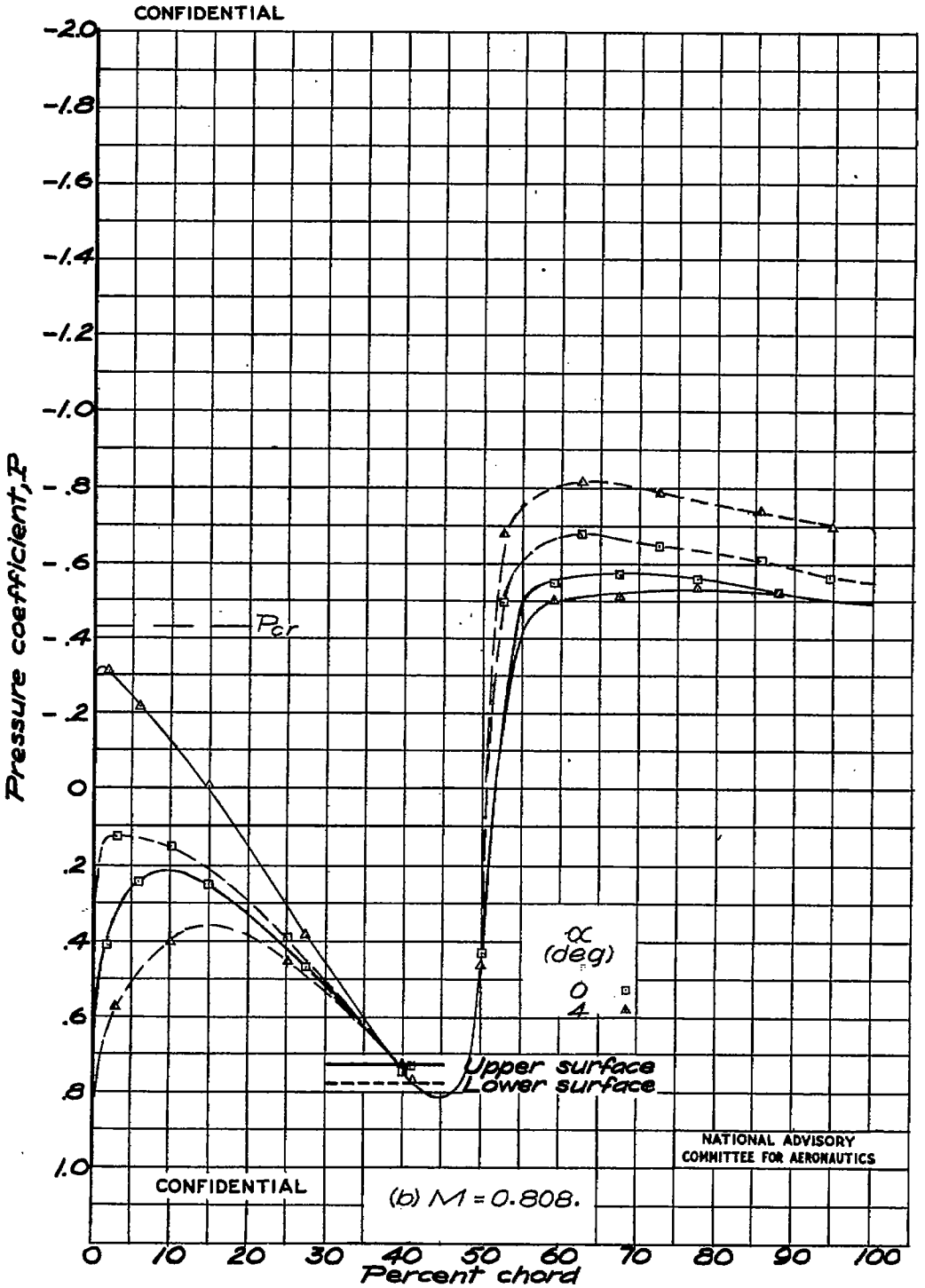


Figure 10.- Continued.

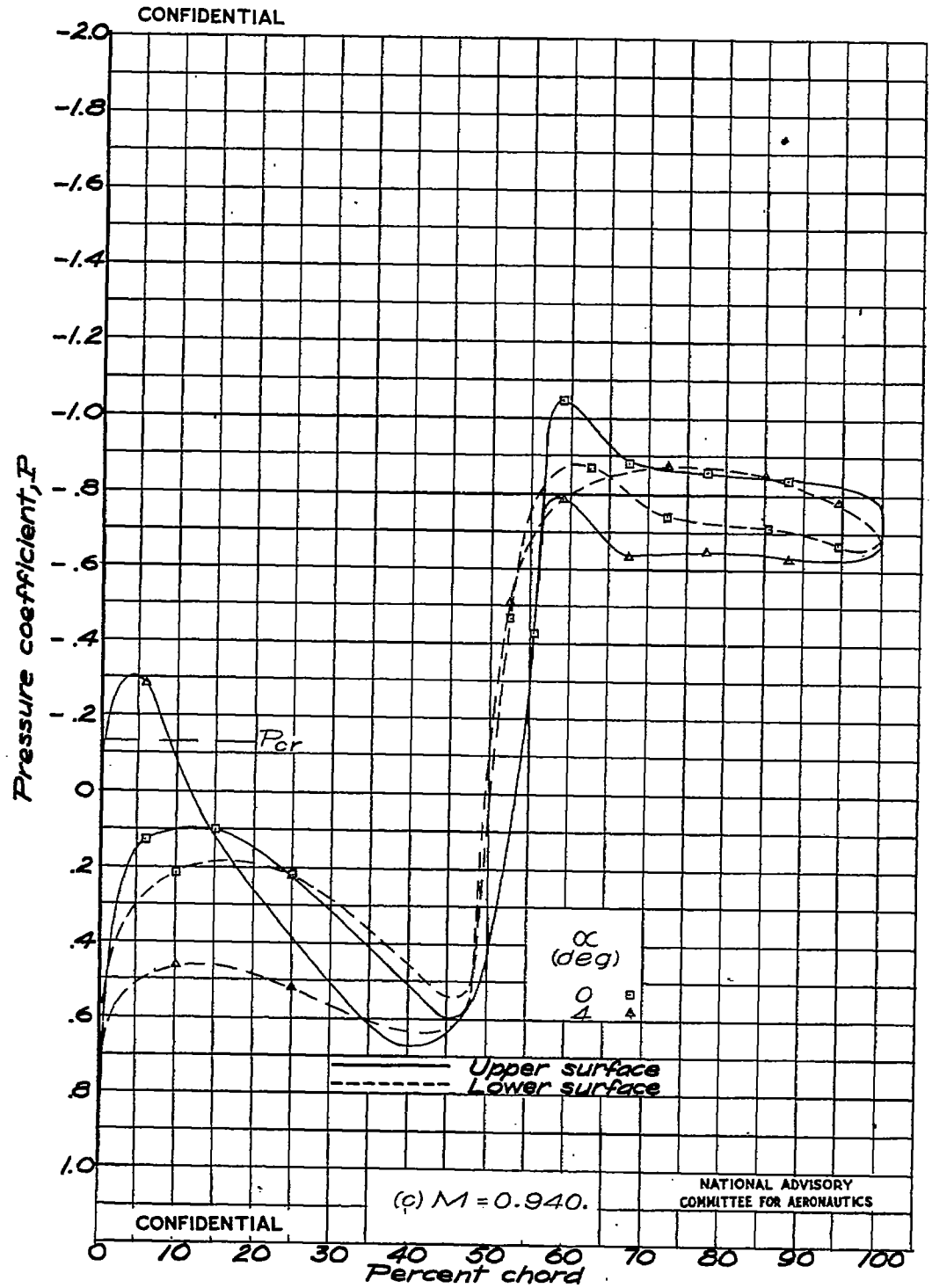


Figure 10.- Concluded.

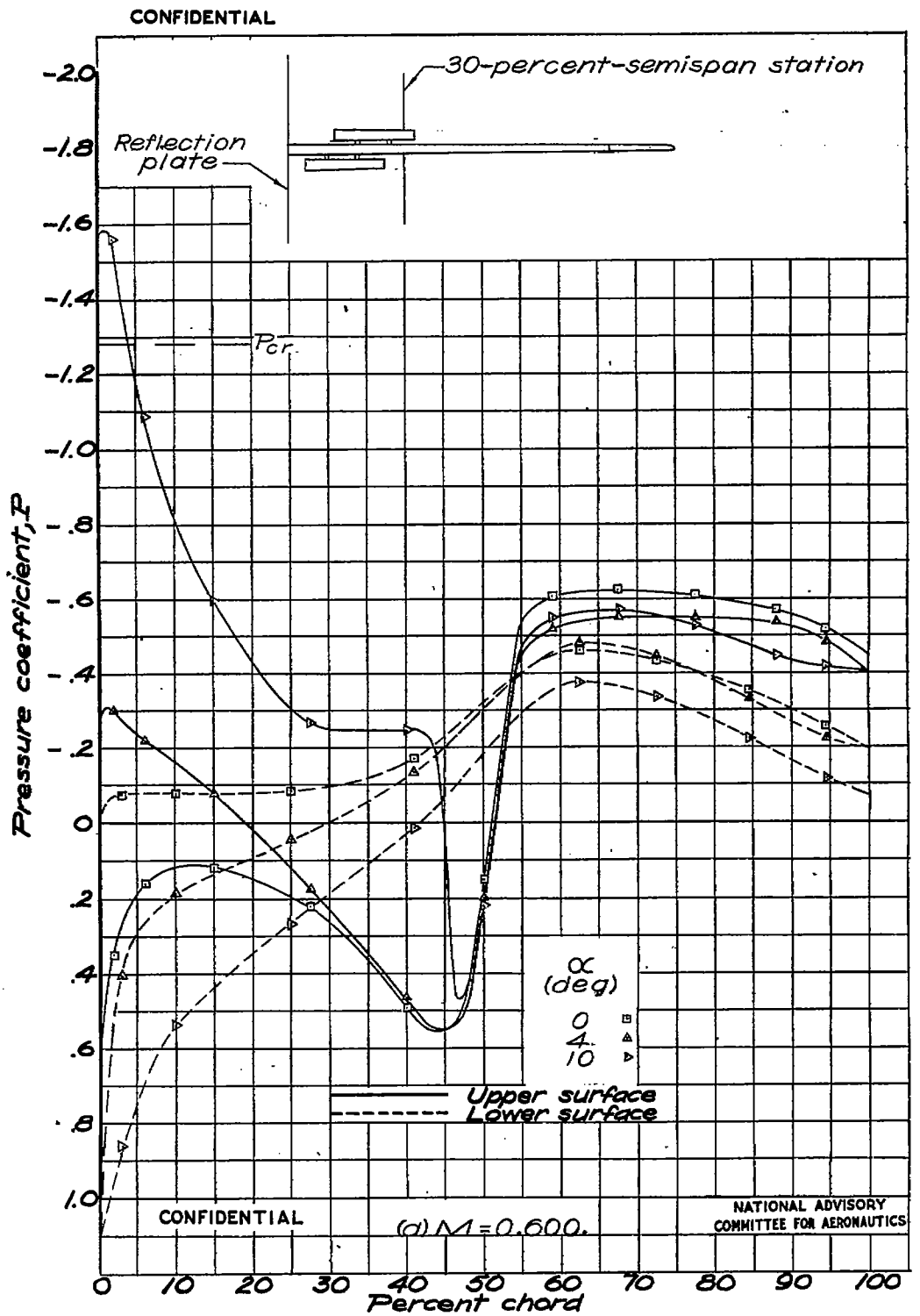


Figure 11 .- Pressure distribution at the 30-percent-semispan station for wing with solid brake.

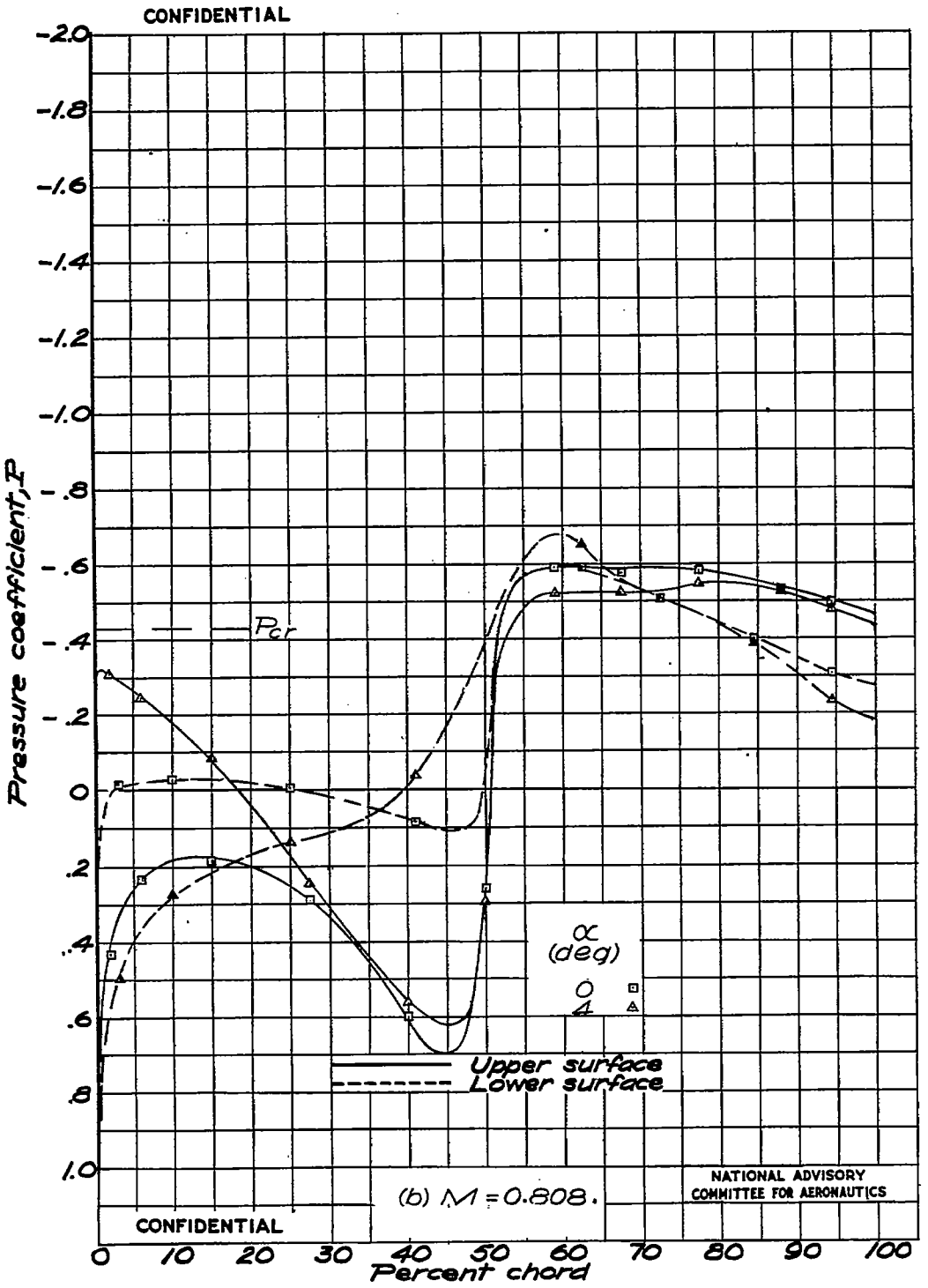


Figure 11.- Continued.

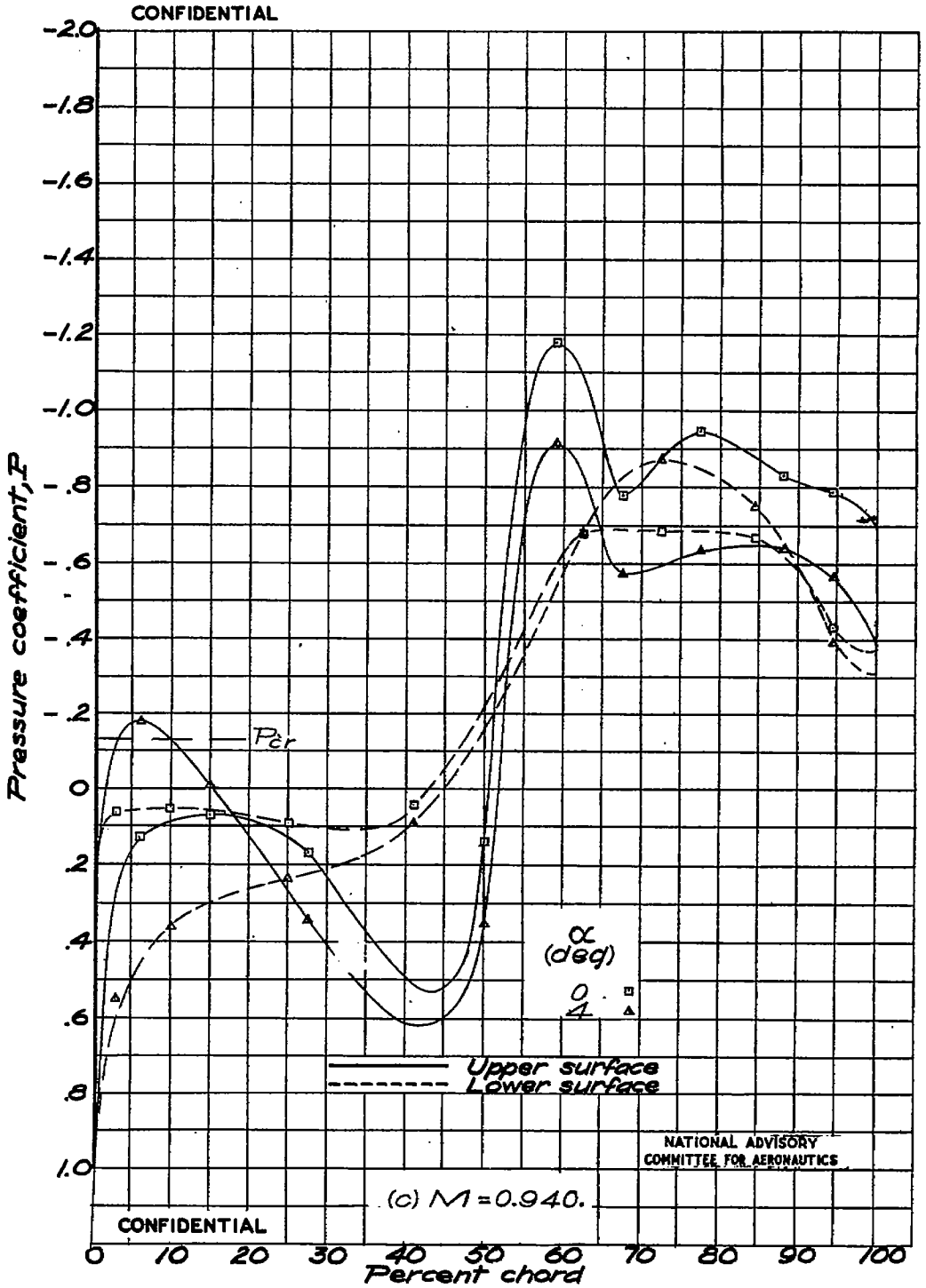


Figure 11.- Concluded.

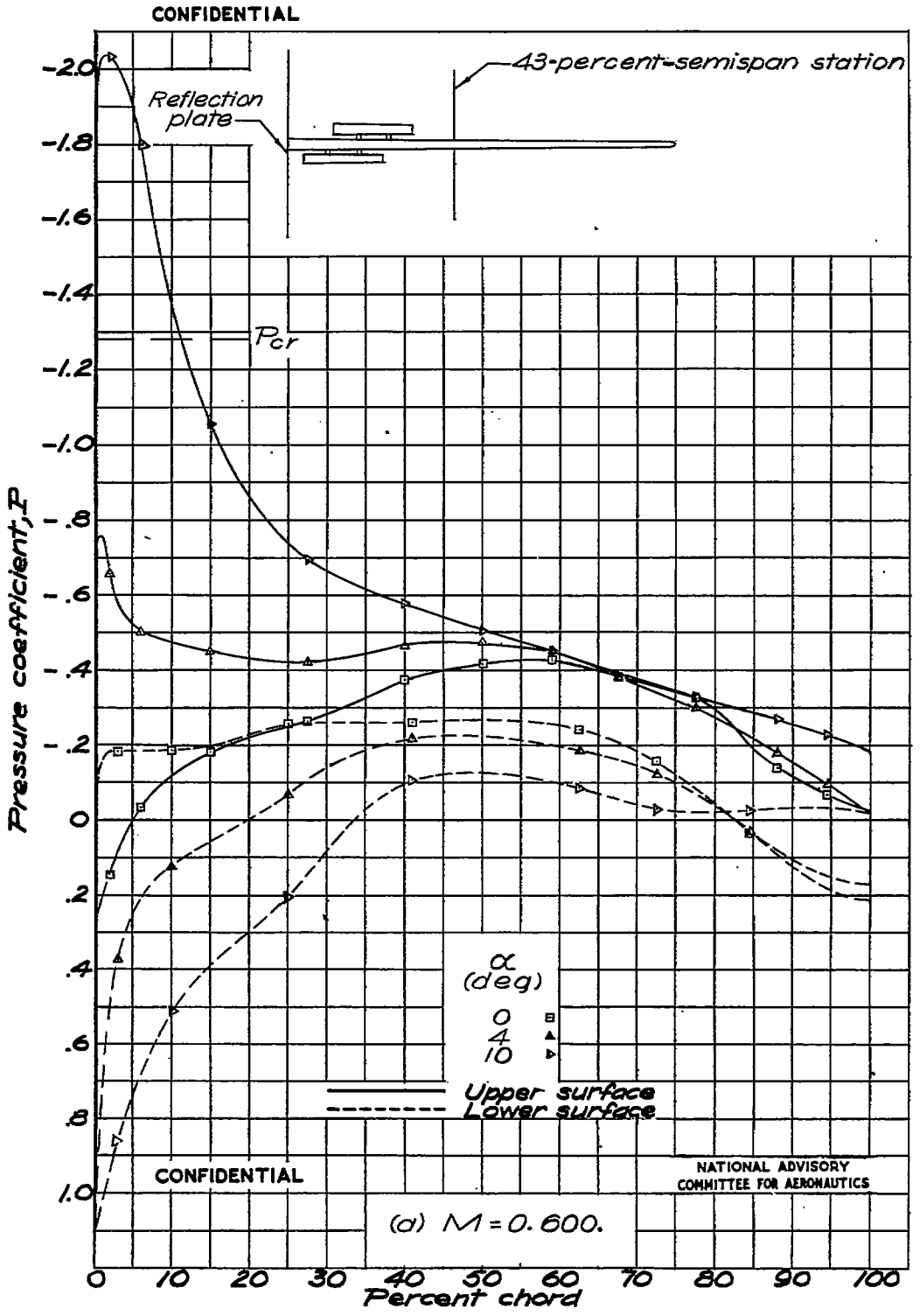


**Figure 12.**— Pressure distribution at the 43-percent-semispan station for wing with solid brake.

CONFIDENTIAL

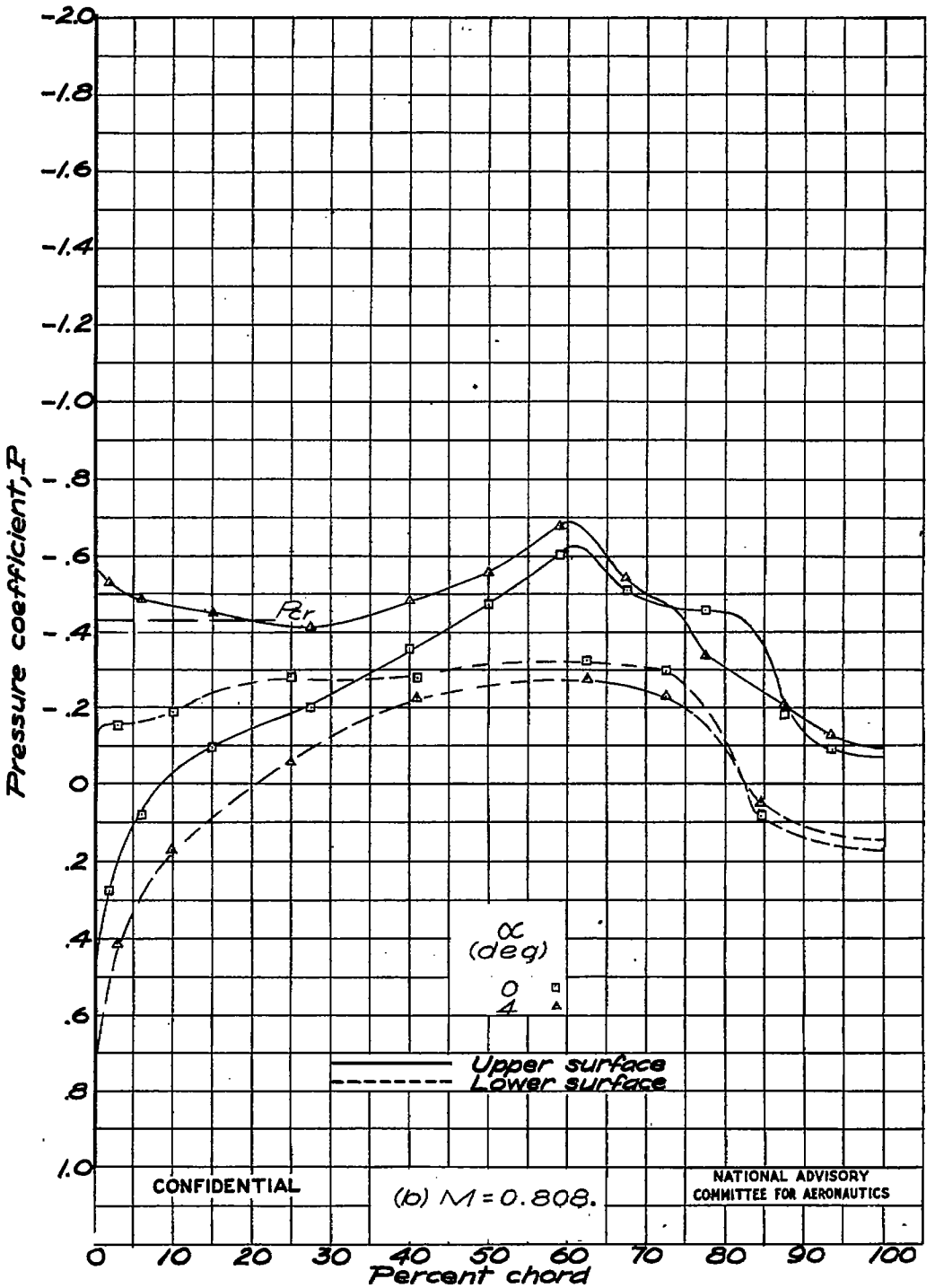


Figure 12.- Continued.

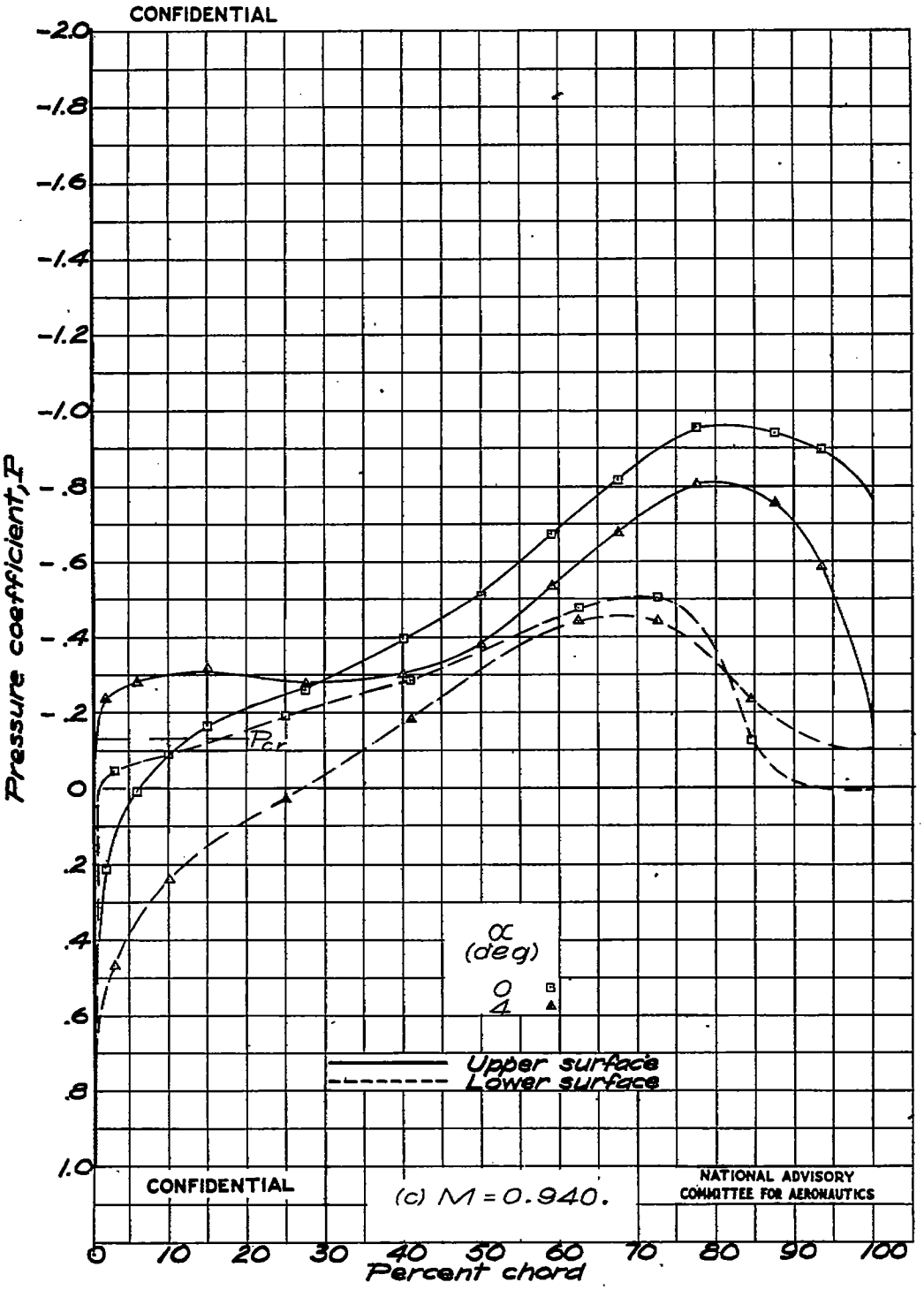


Figure 12.- Concluded.

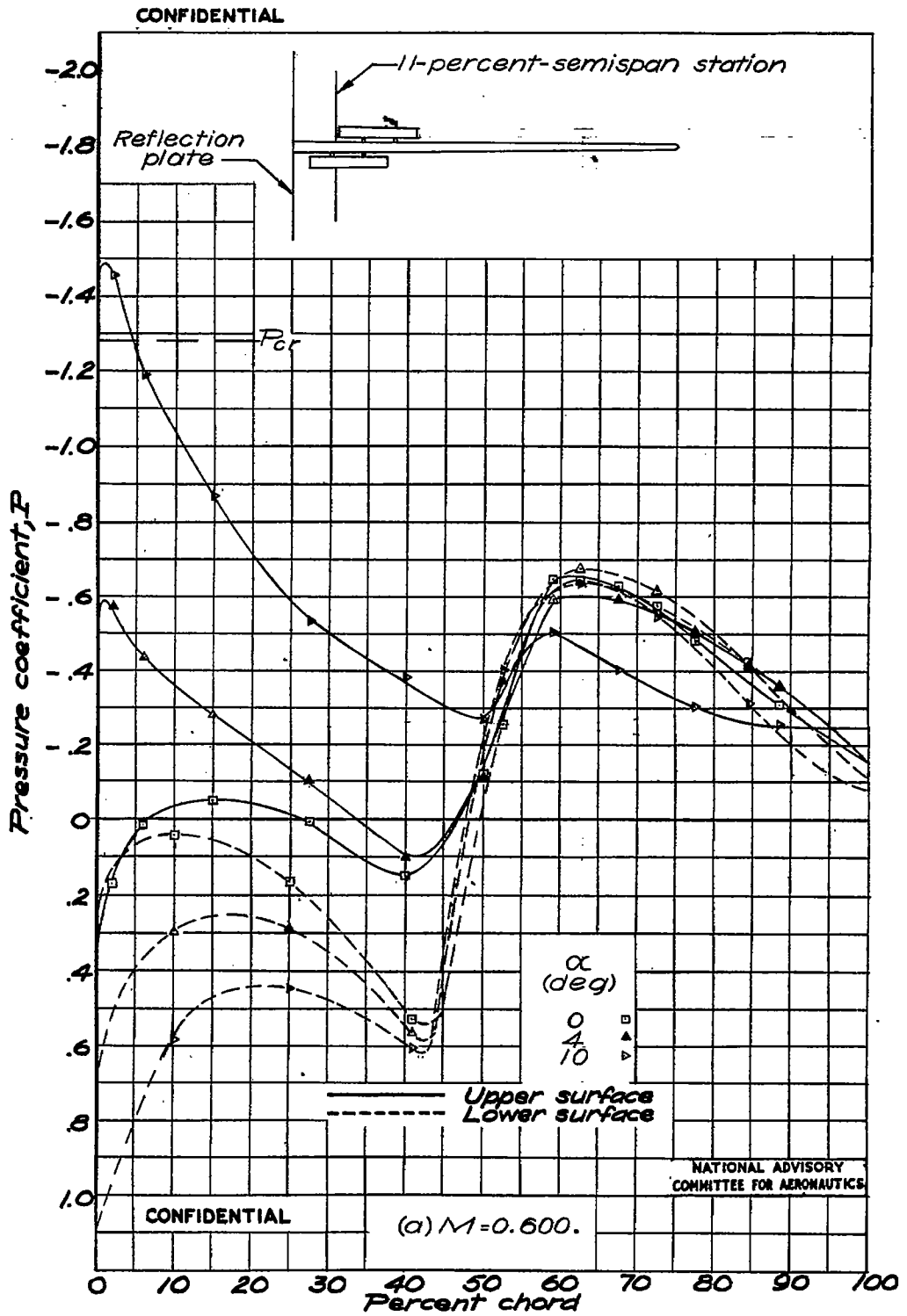


Figure 13.- Pressure distribution at the 11-percent-semispan station for wing with slotted brake.

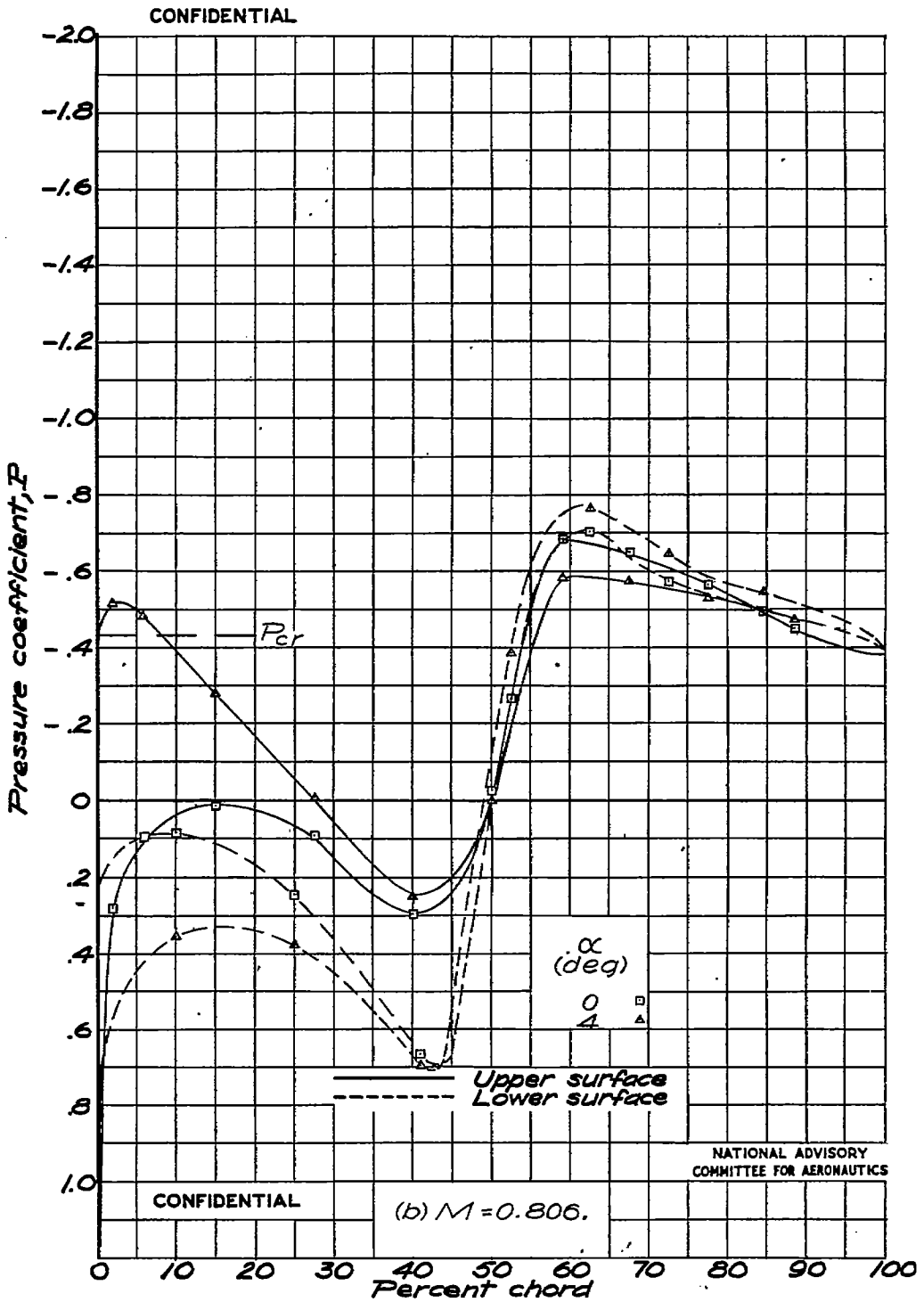


Figure 13.- Continued.

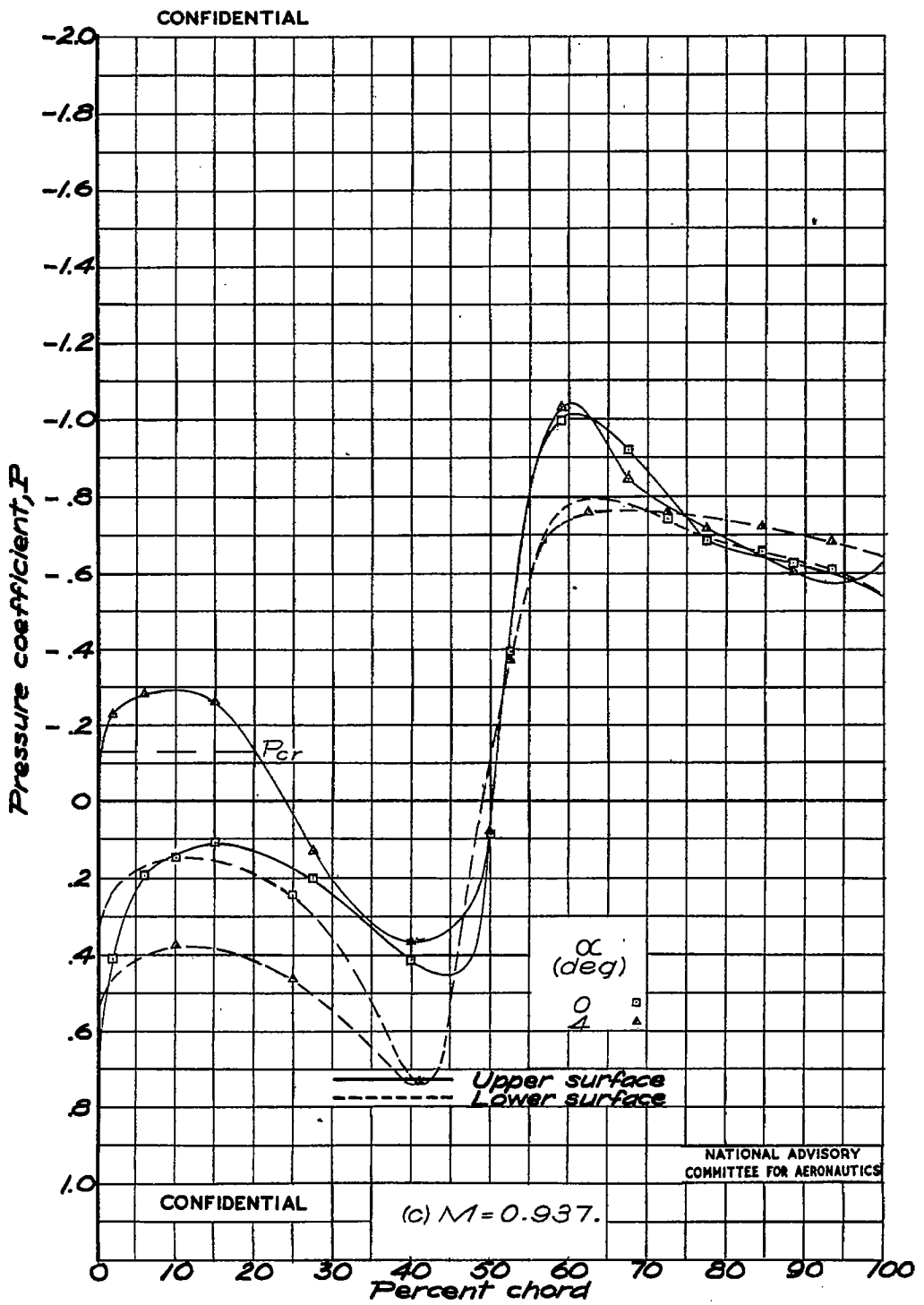


Figure 13.- Concluded.

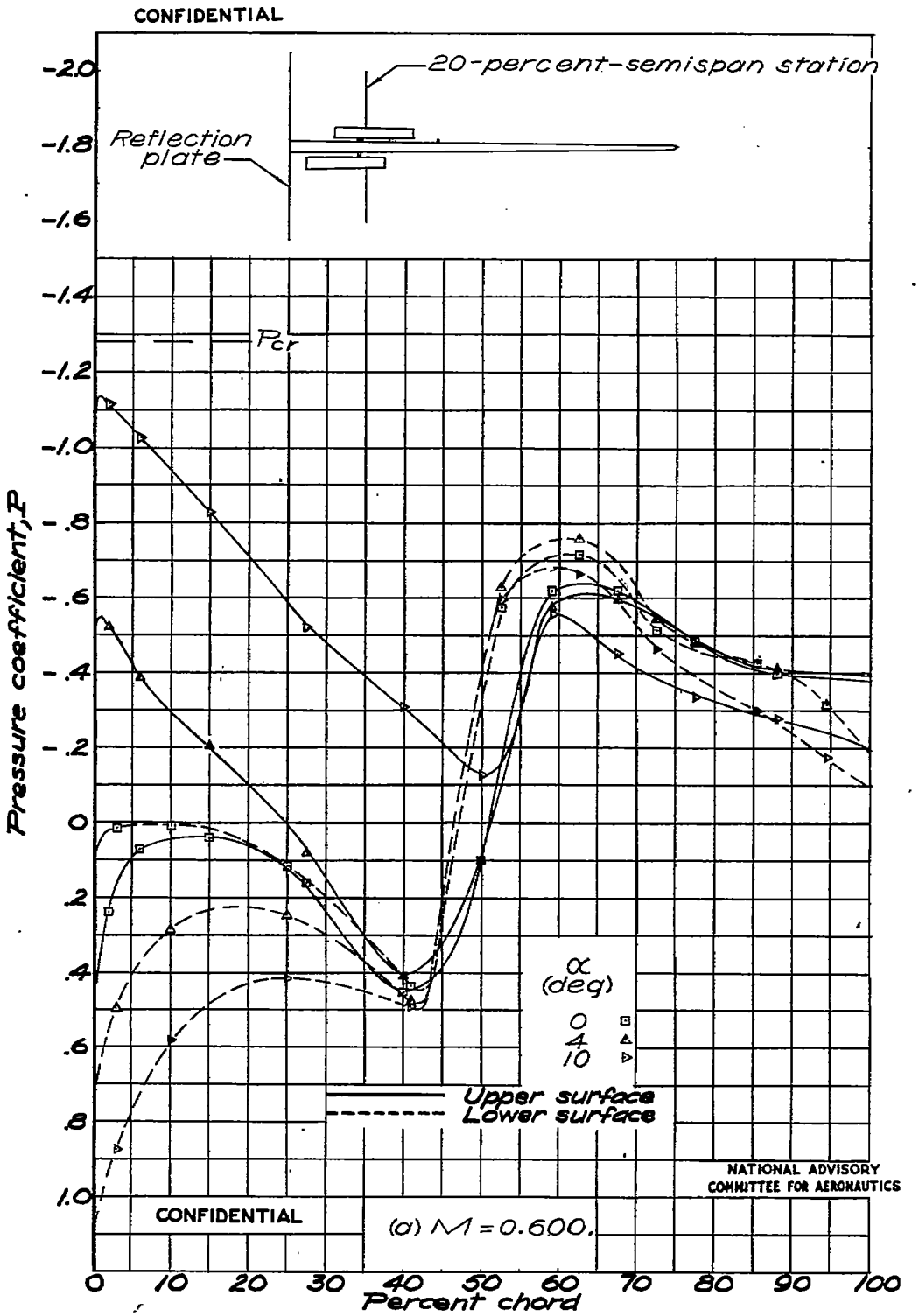


**Figure 14.-** Pressure distribution at the 20-percent-semispan station for wing with slotted brake.

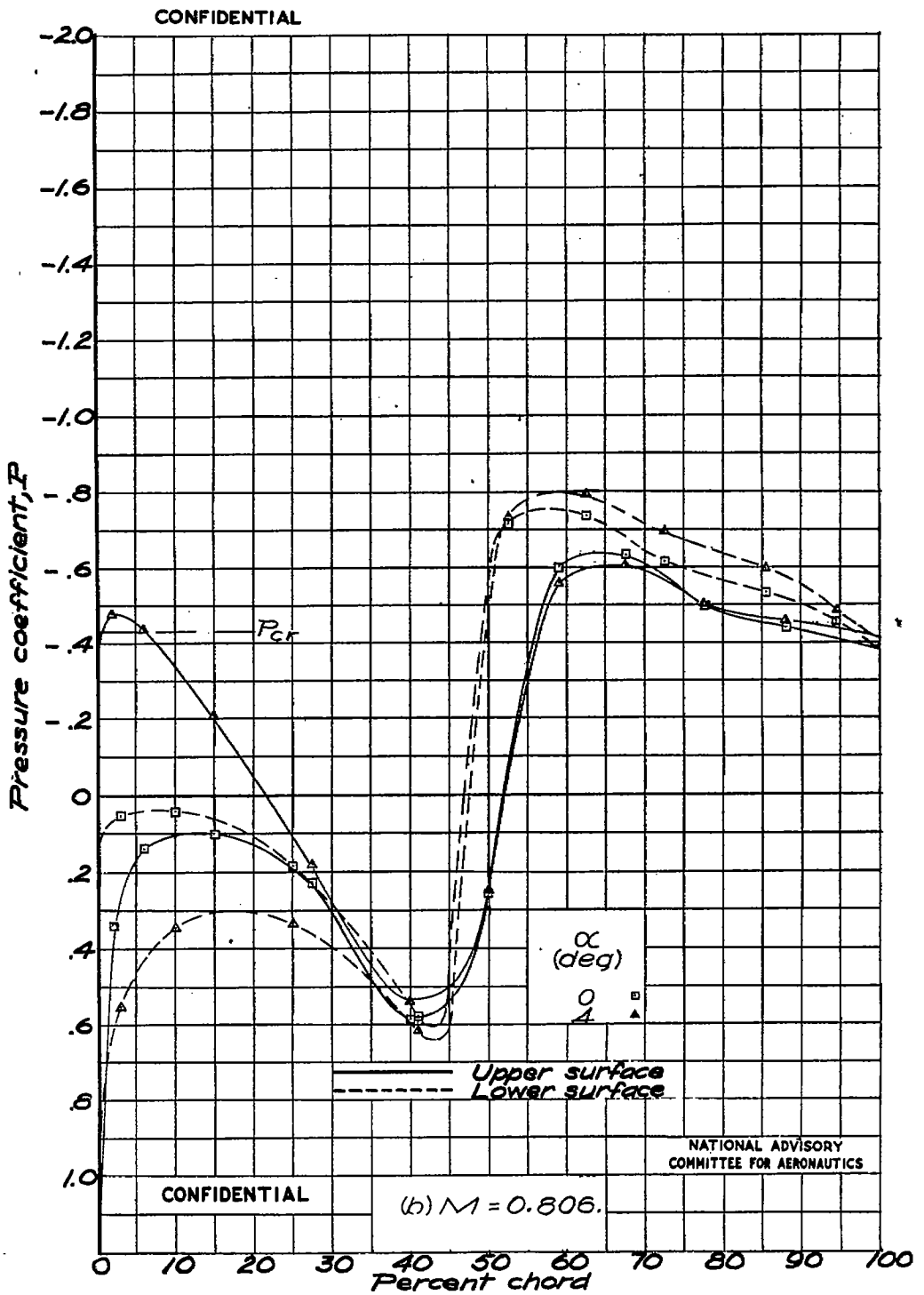


Figure 14.- Continued.

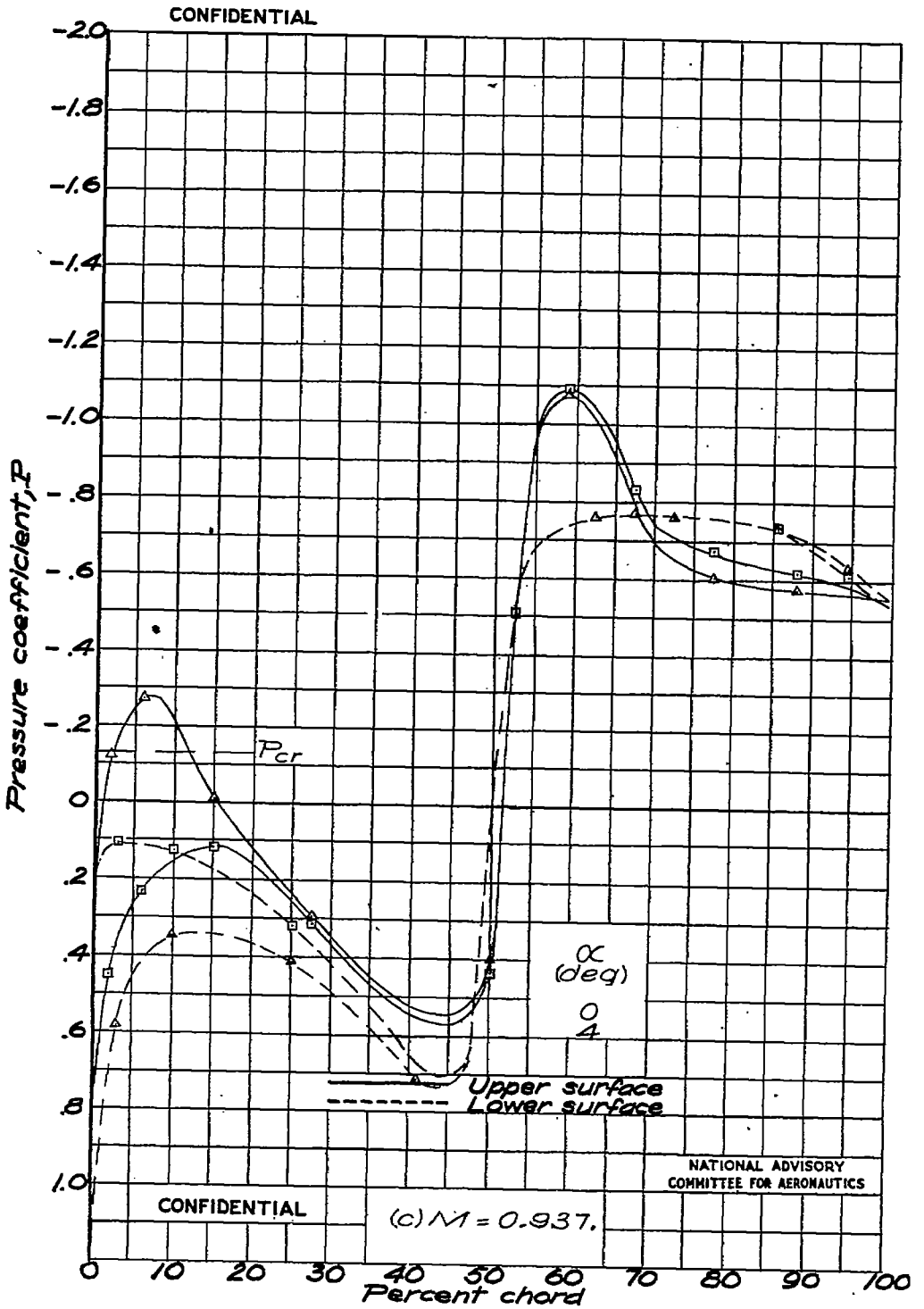


Figure 14.- Concluded.

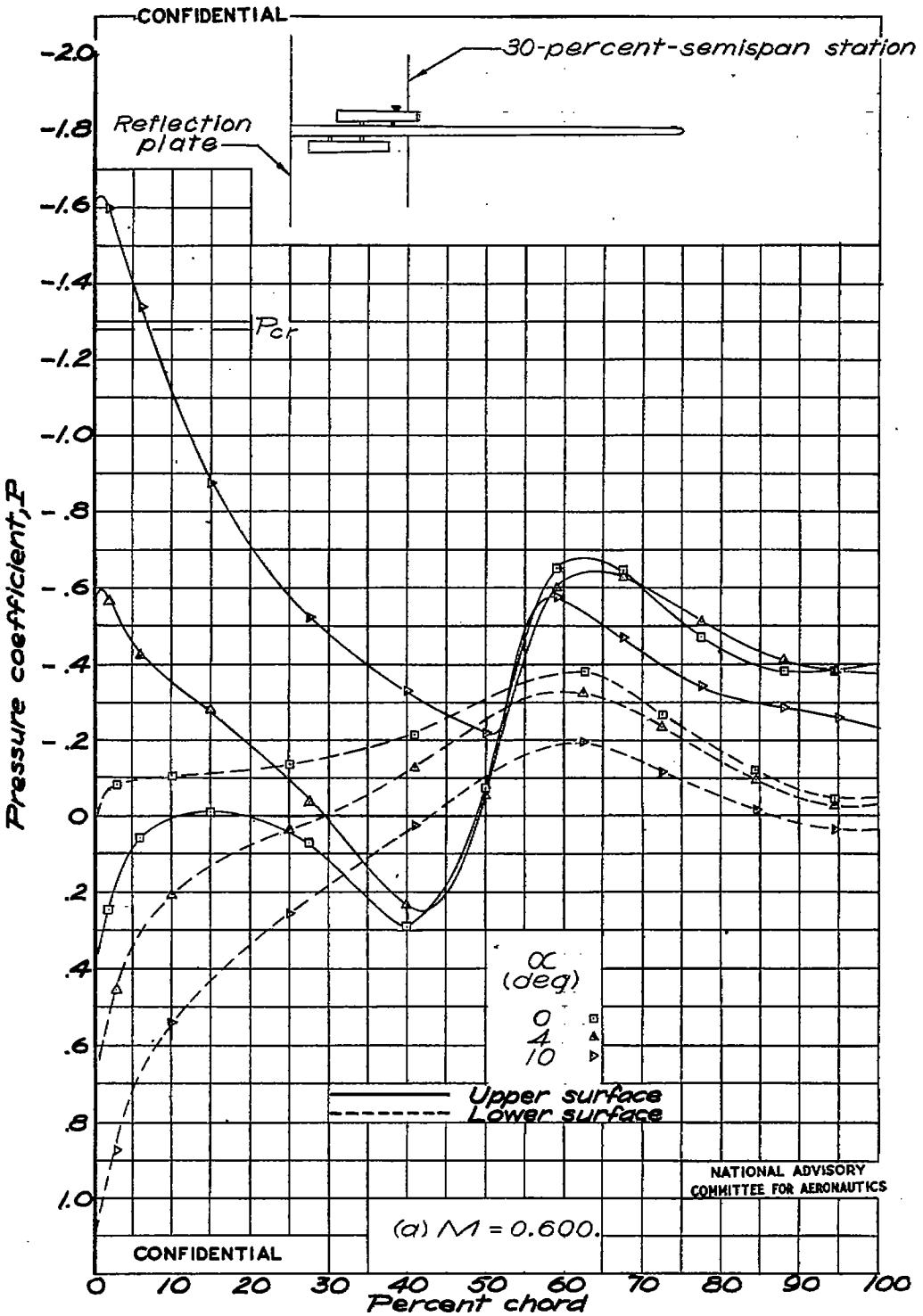


**Figure 15.**— Pressure distribution at the 30-percent-semispan station for wing with slotted brake.

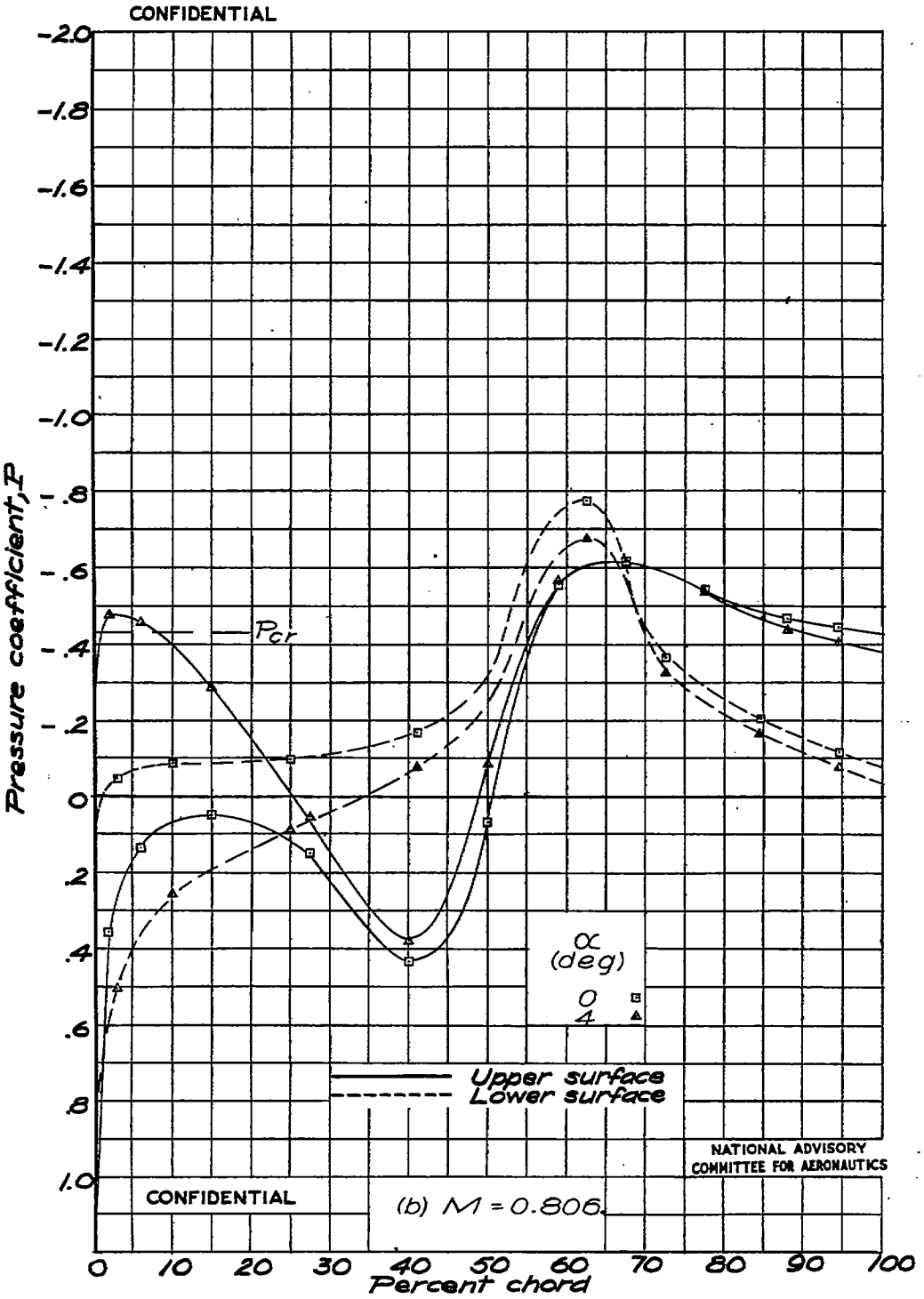


Figure 15.- Continued.

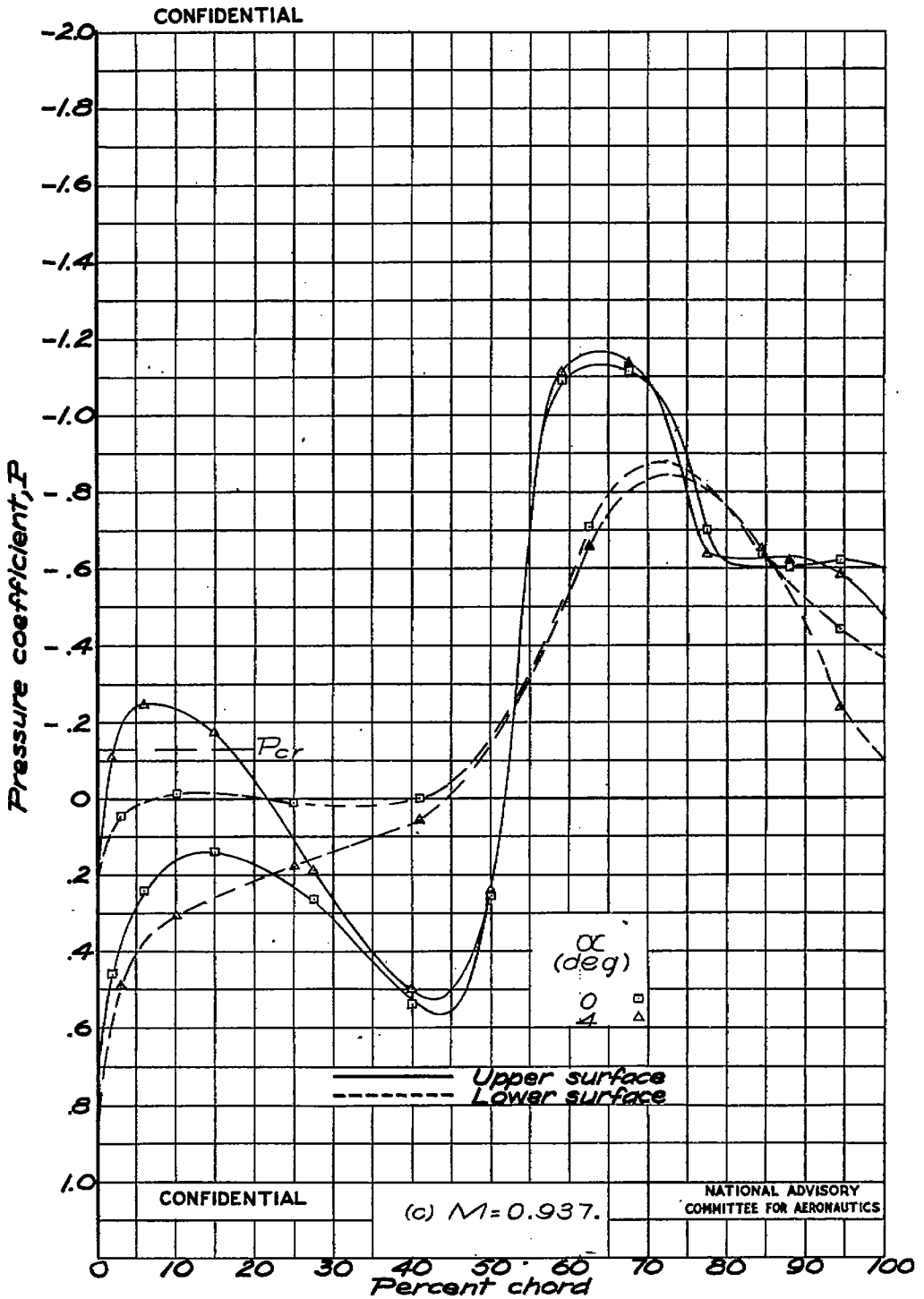


Figure 15.- Concluded.

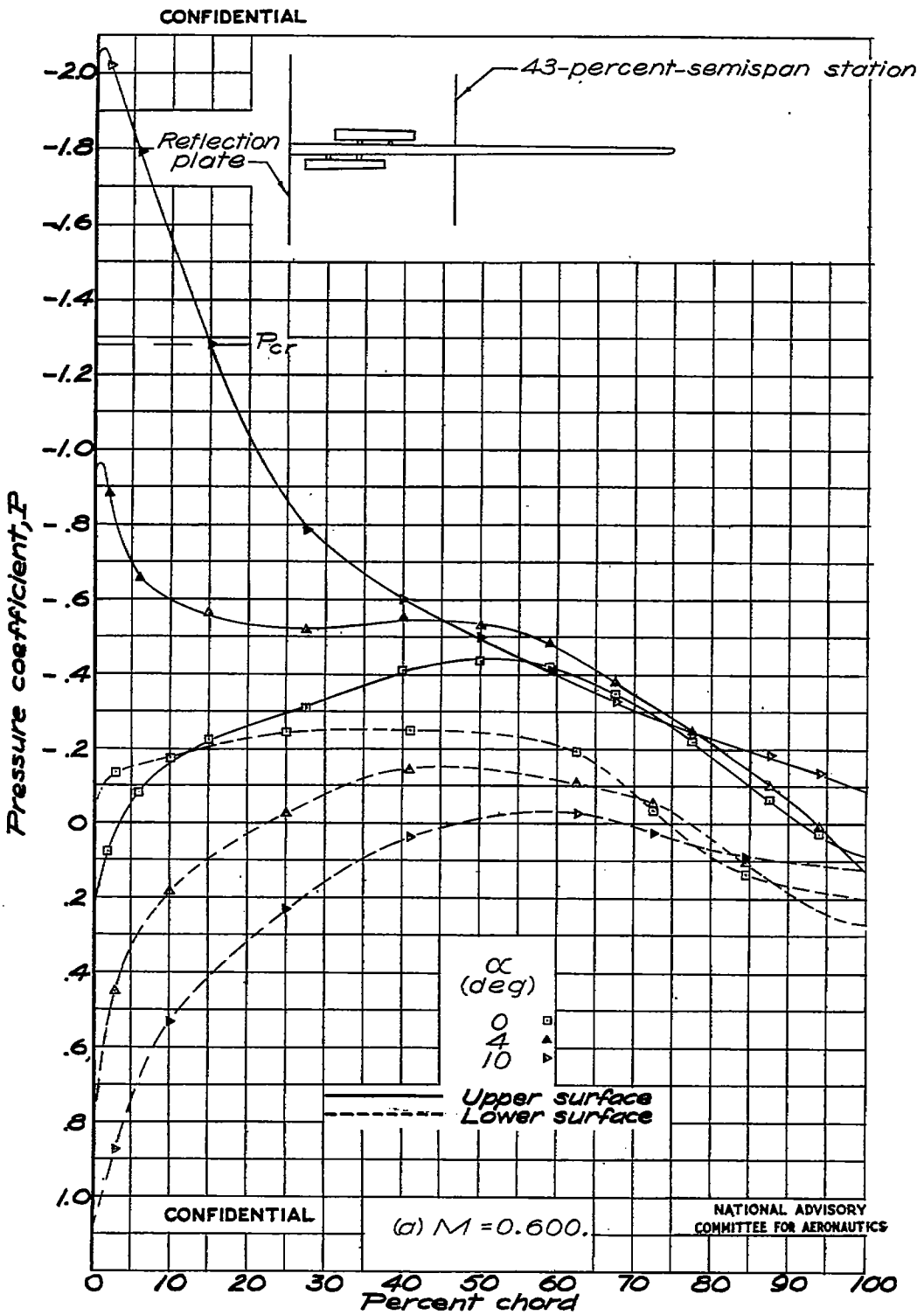


**Figure 16.** – Pressure distribution at the 43-percent-semispan station for wing with slotted brake.

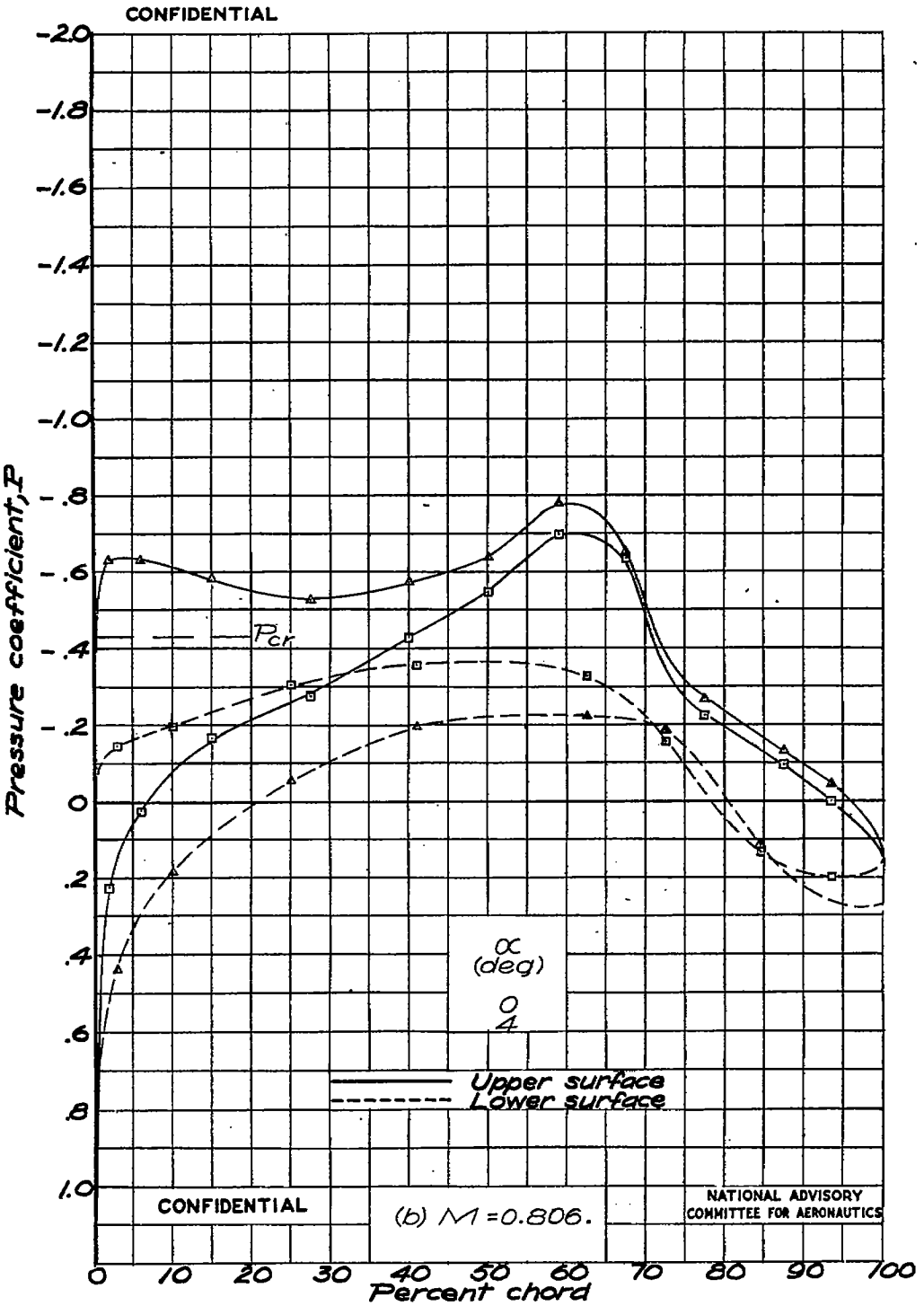


Figure 16.- Continued.

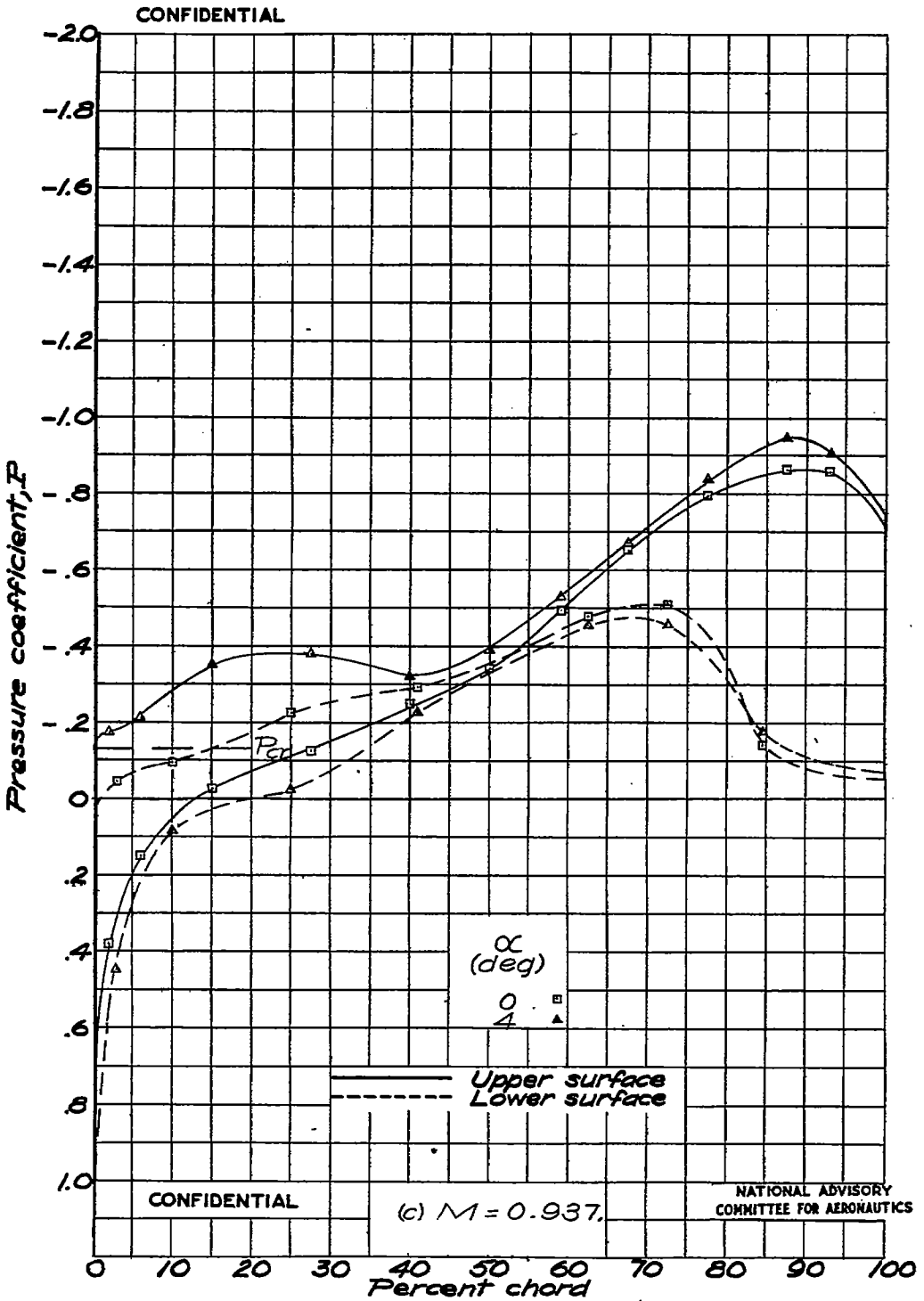


Figure 16.- Concluded.

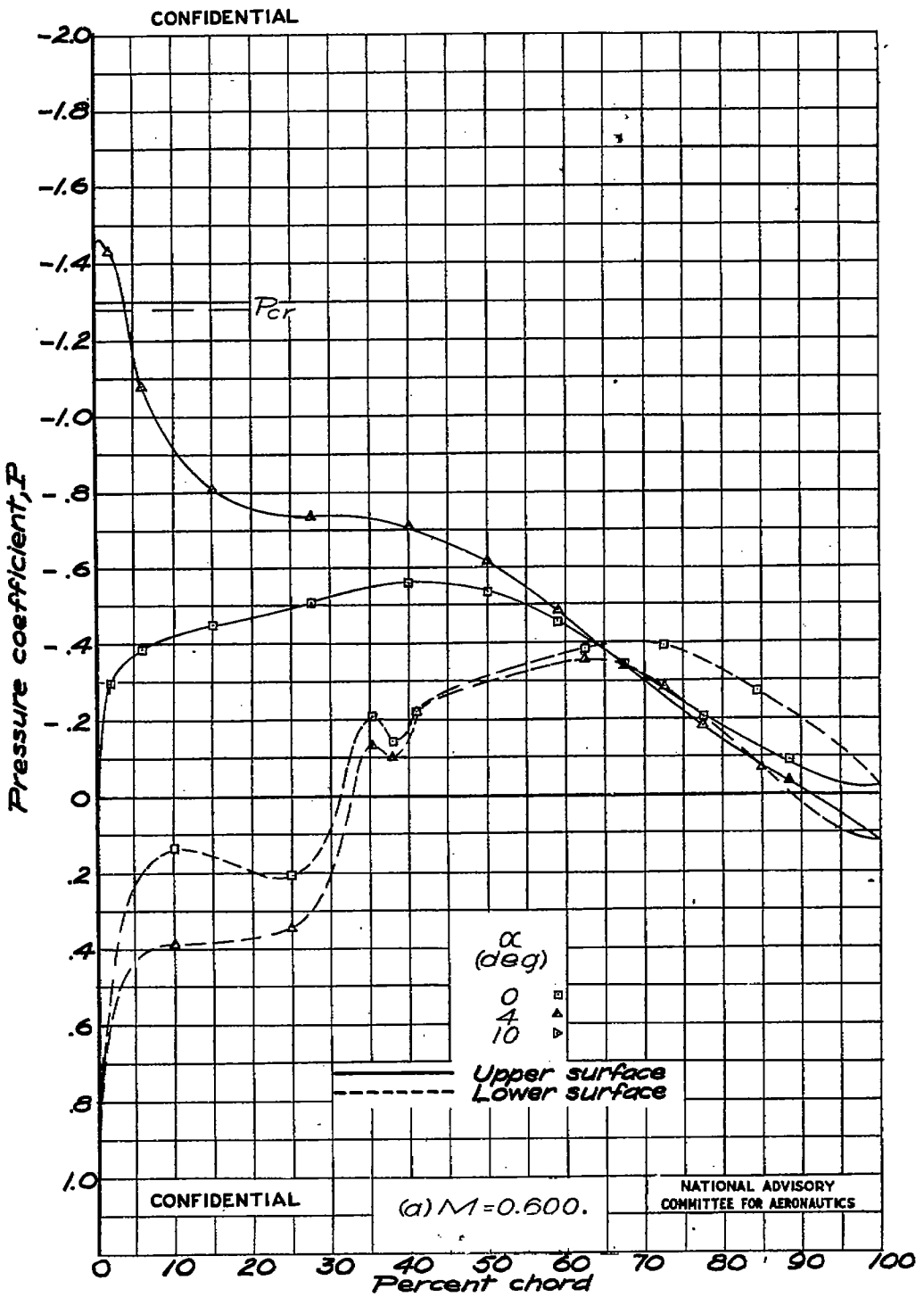


Figure 17.- Pressure distribution at the 11-percent-semispan station for wing with dive-recovery flap.

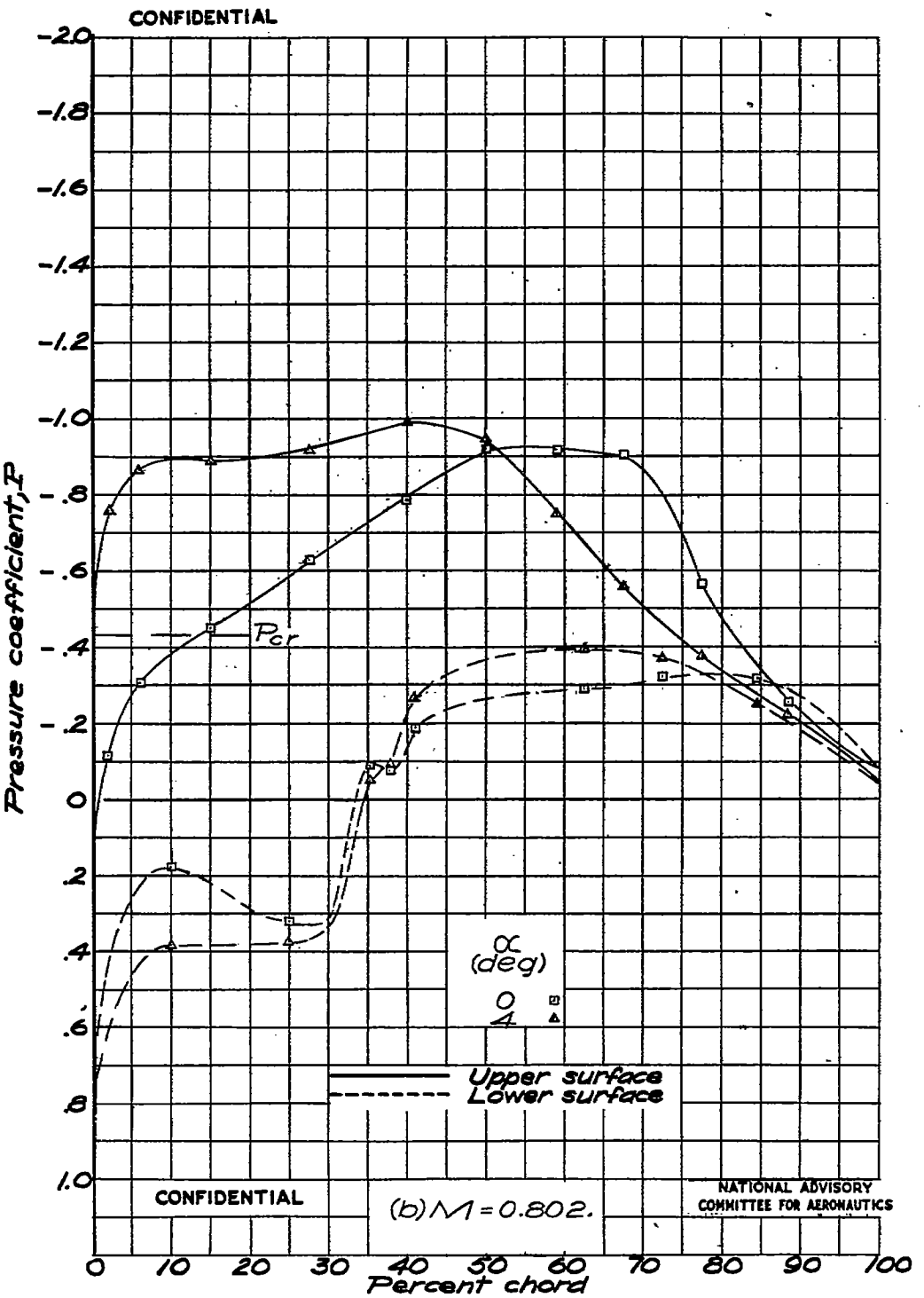


Figure 17.- Continued.

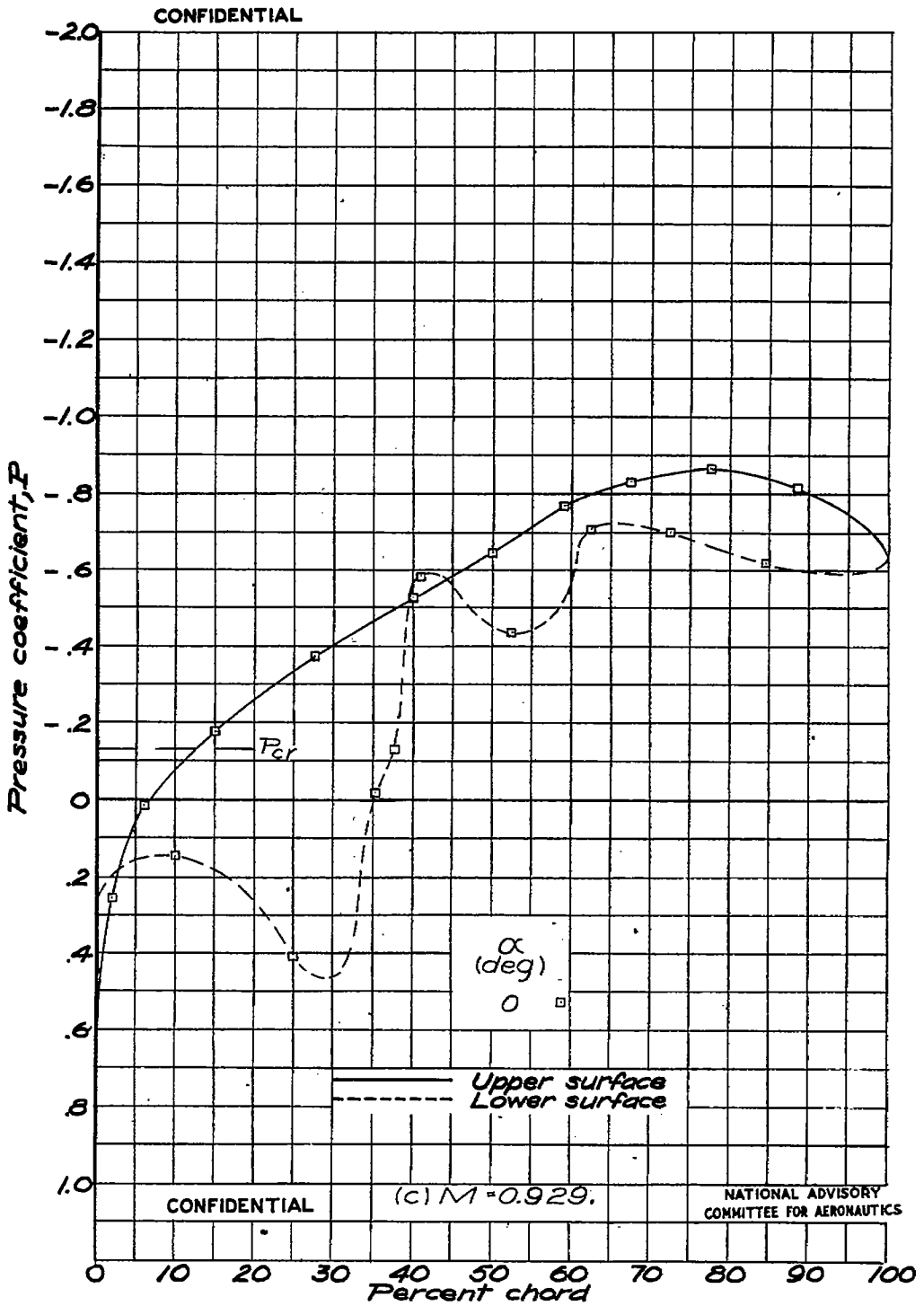


Figure 17.- Concluded.

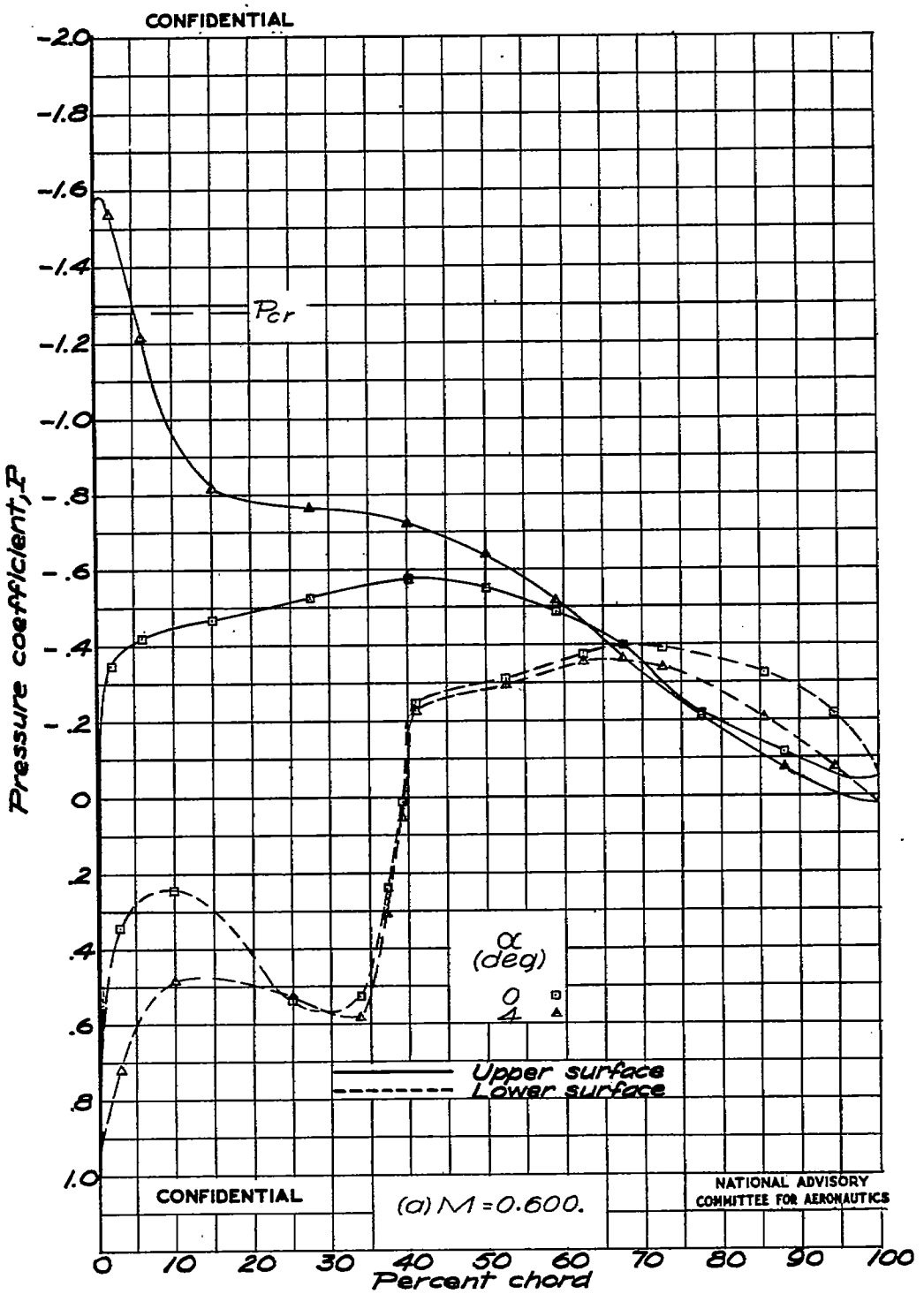


Figure 18.- Pressure distribution at the 20-percent-semispan station for wing with dive-recovery flap.

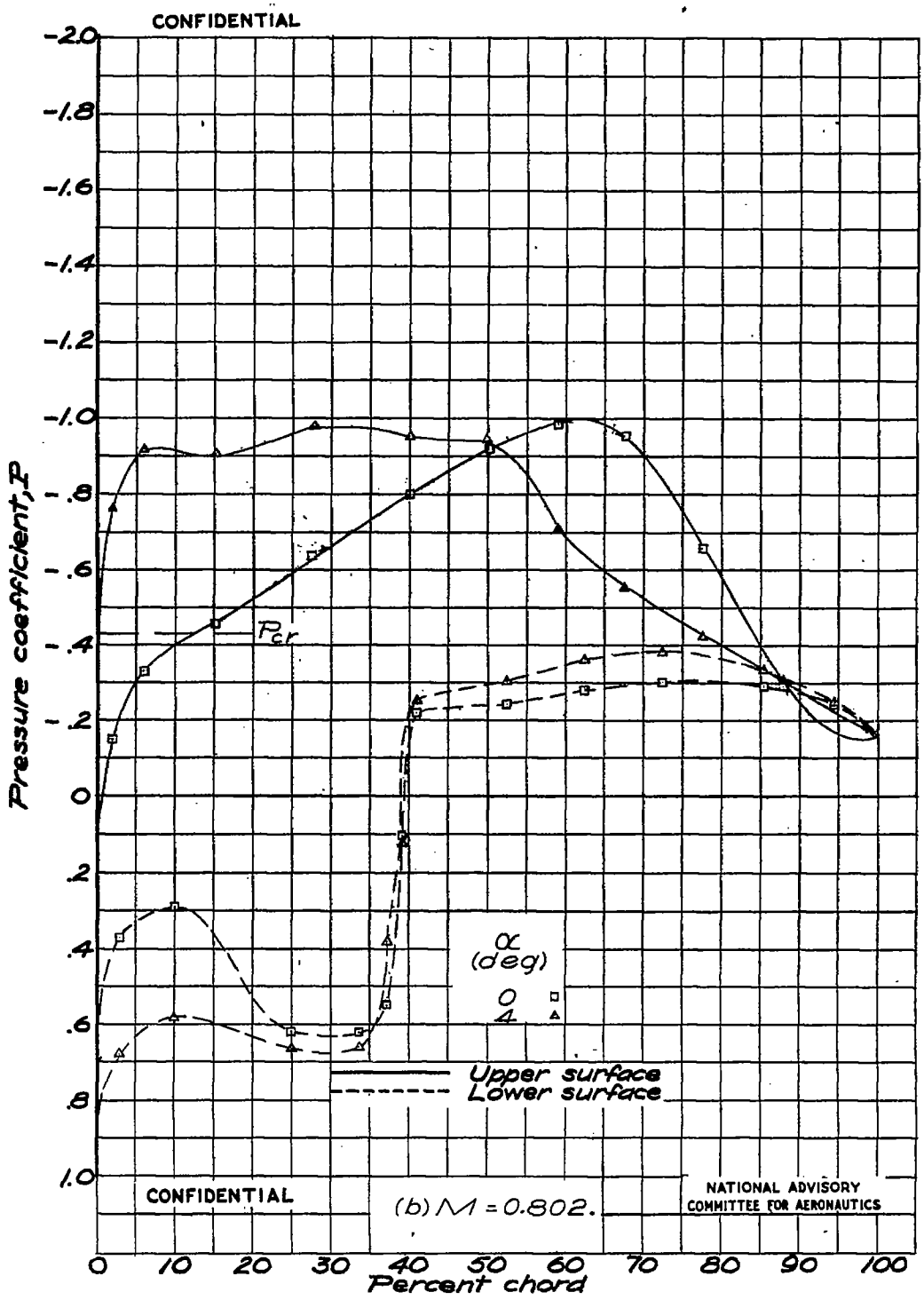


Figure 18.- Continued.

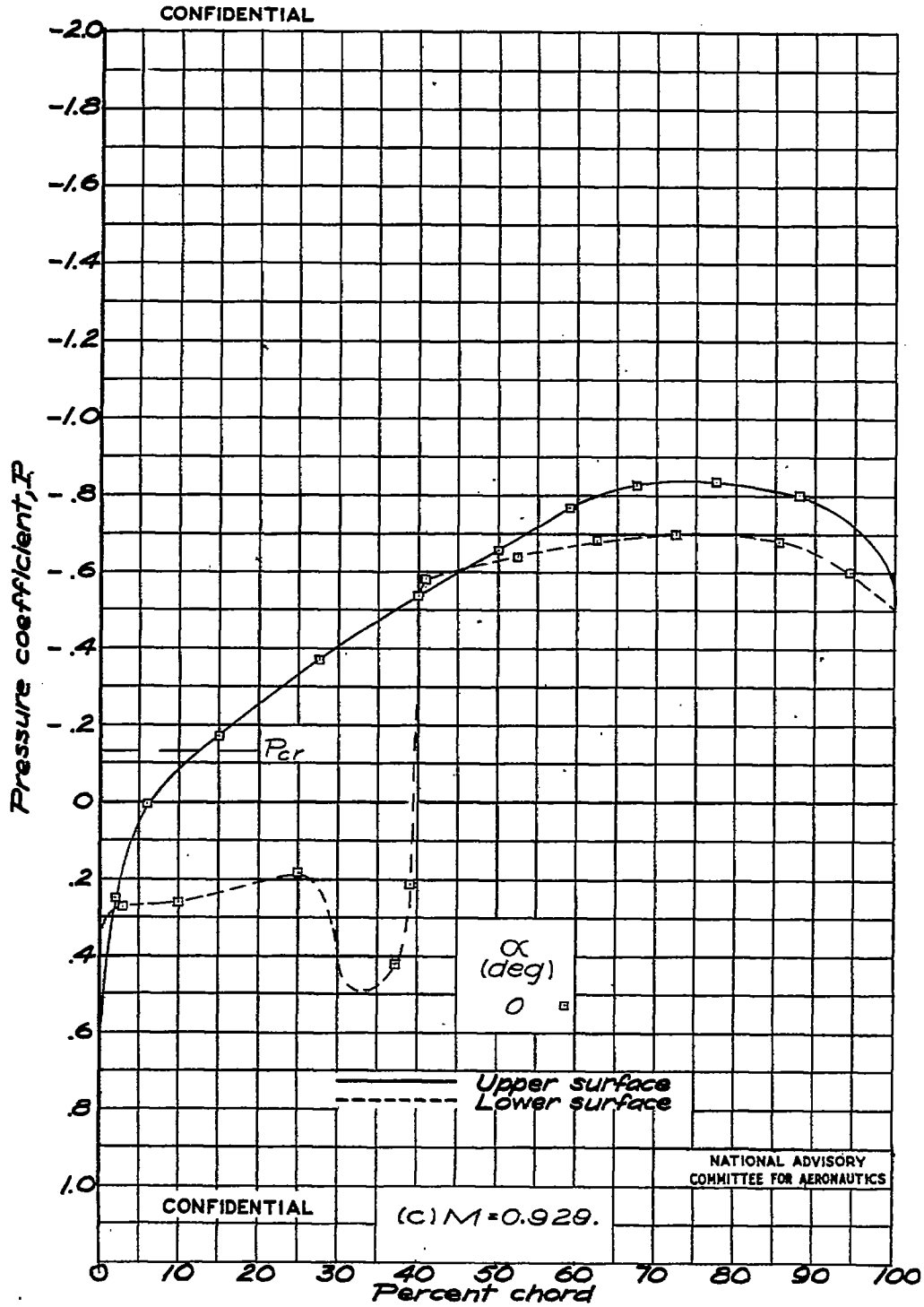


Figure 18.—Concluded.

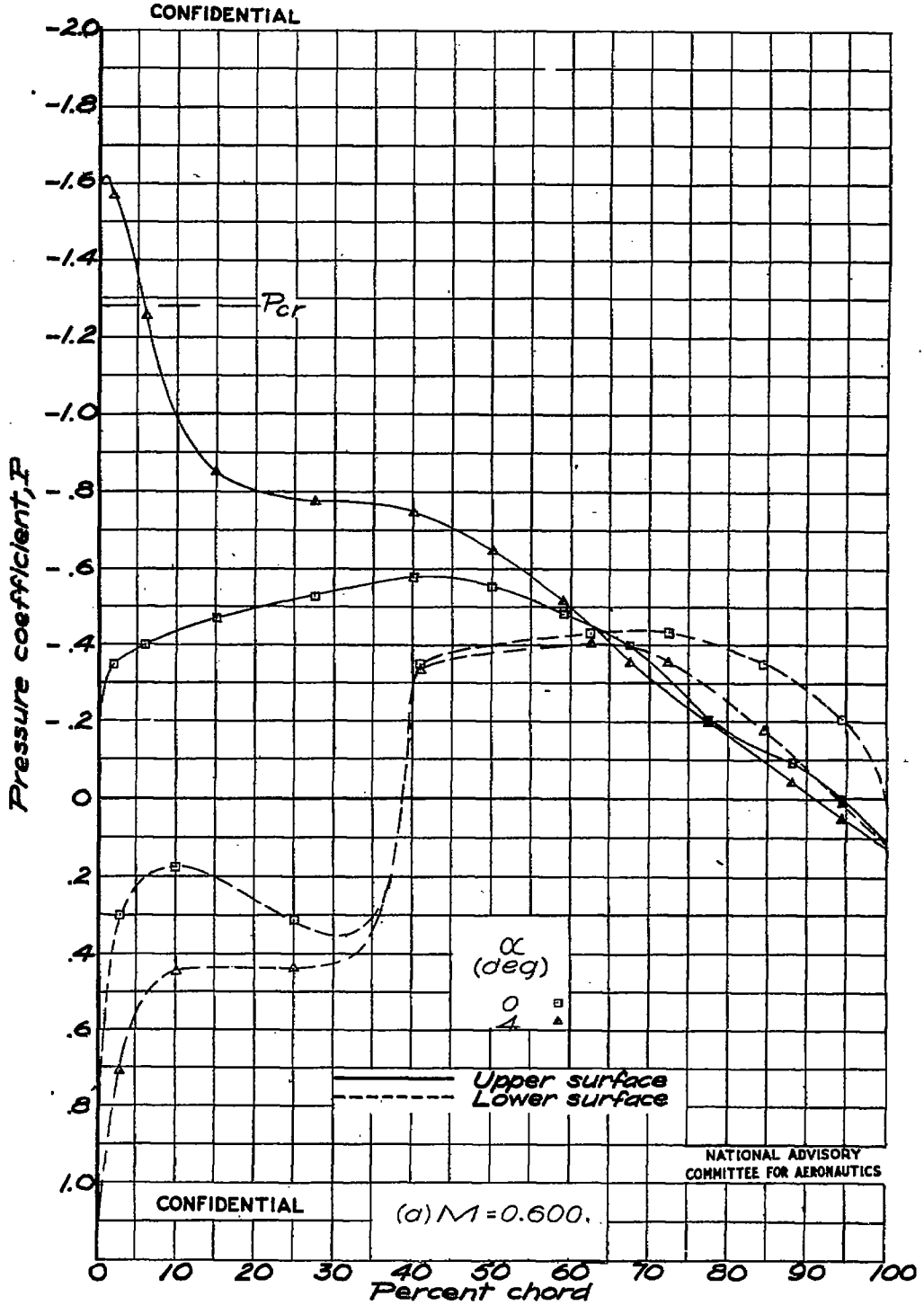


**Figure 19.**— Pressure distribution at the 30-percent-semispan station for wing with dive-recovery flap.

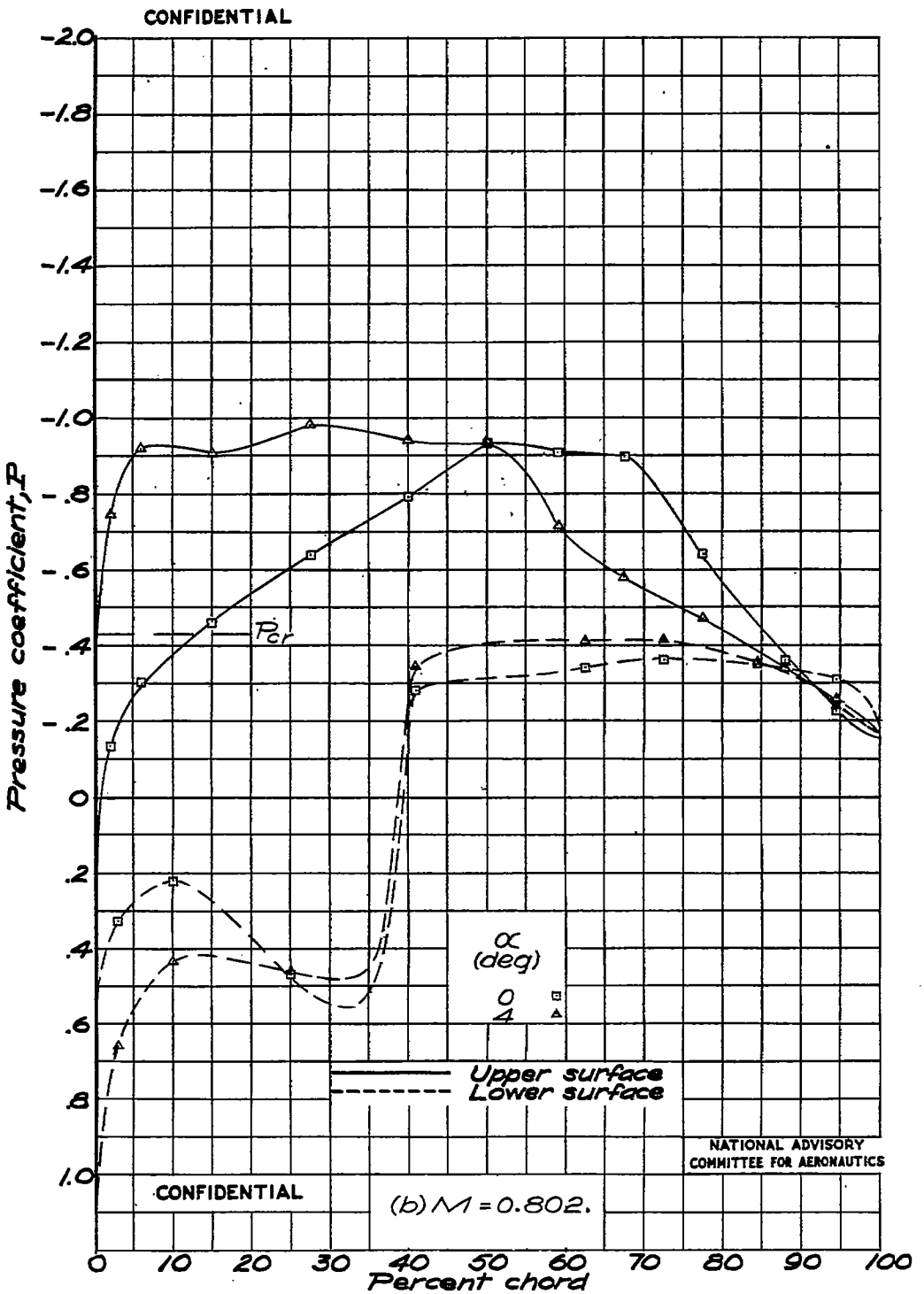


Figure 19.- Continued.

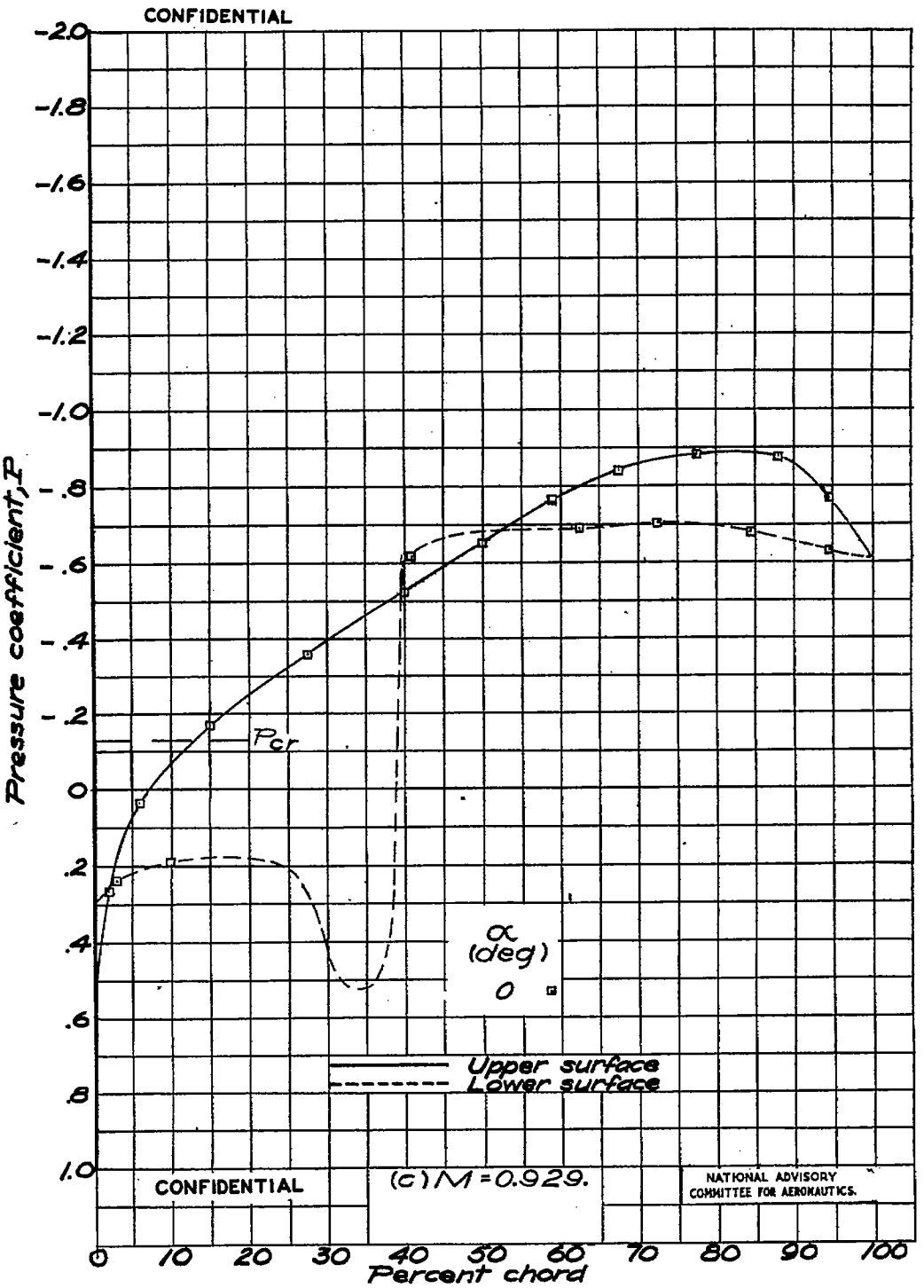


Figure 19.—Concluded.

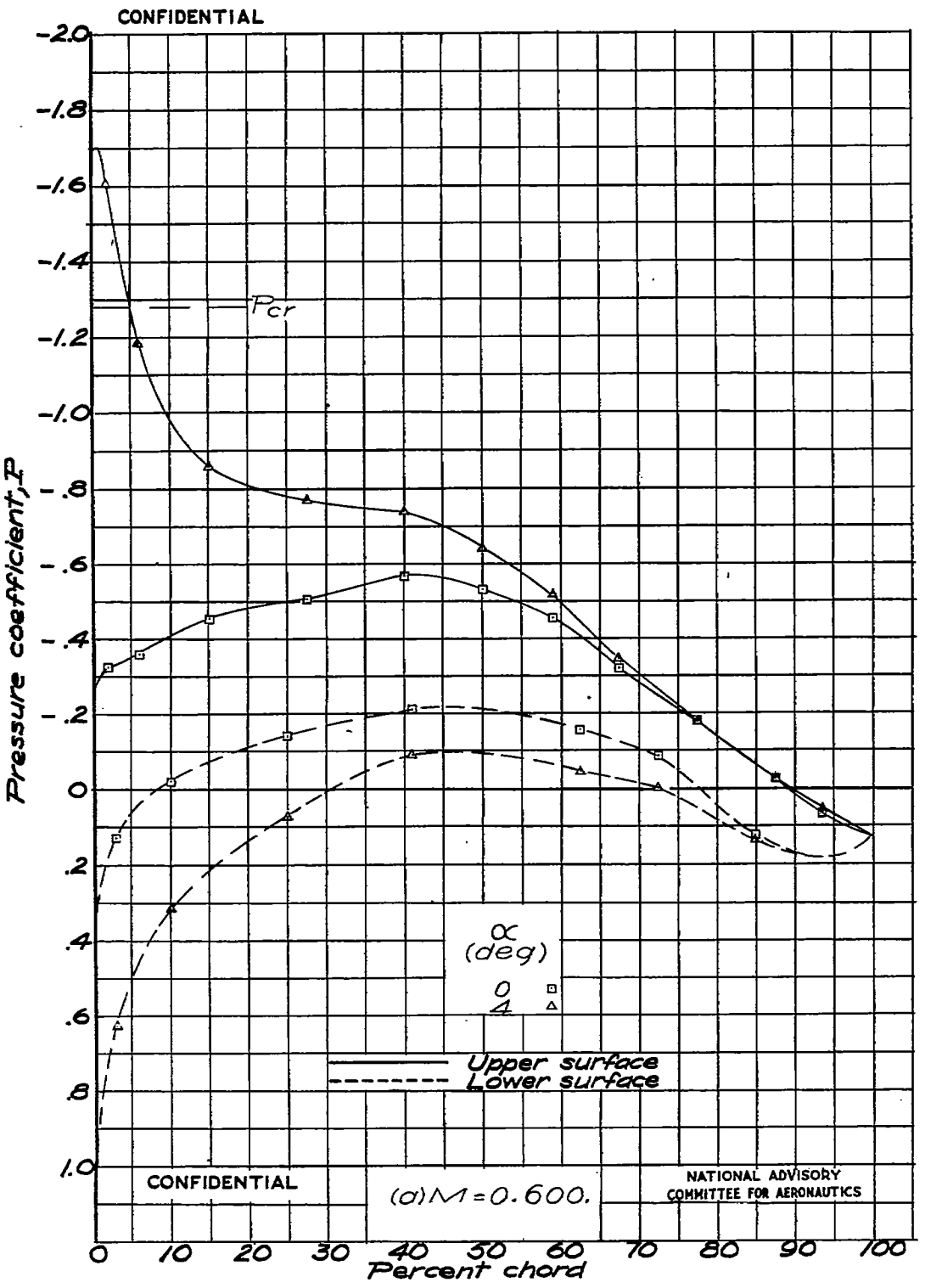


**Figure 20.**- Pressure distribution at the 43-percent-semispan station for wing with dive-recovery flap.

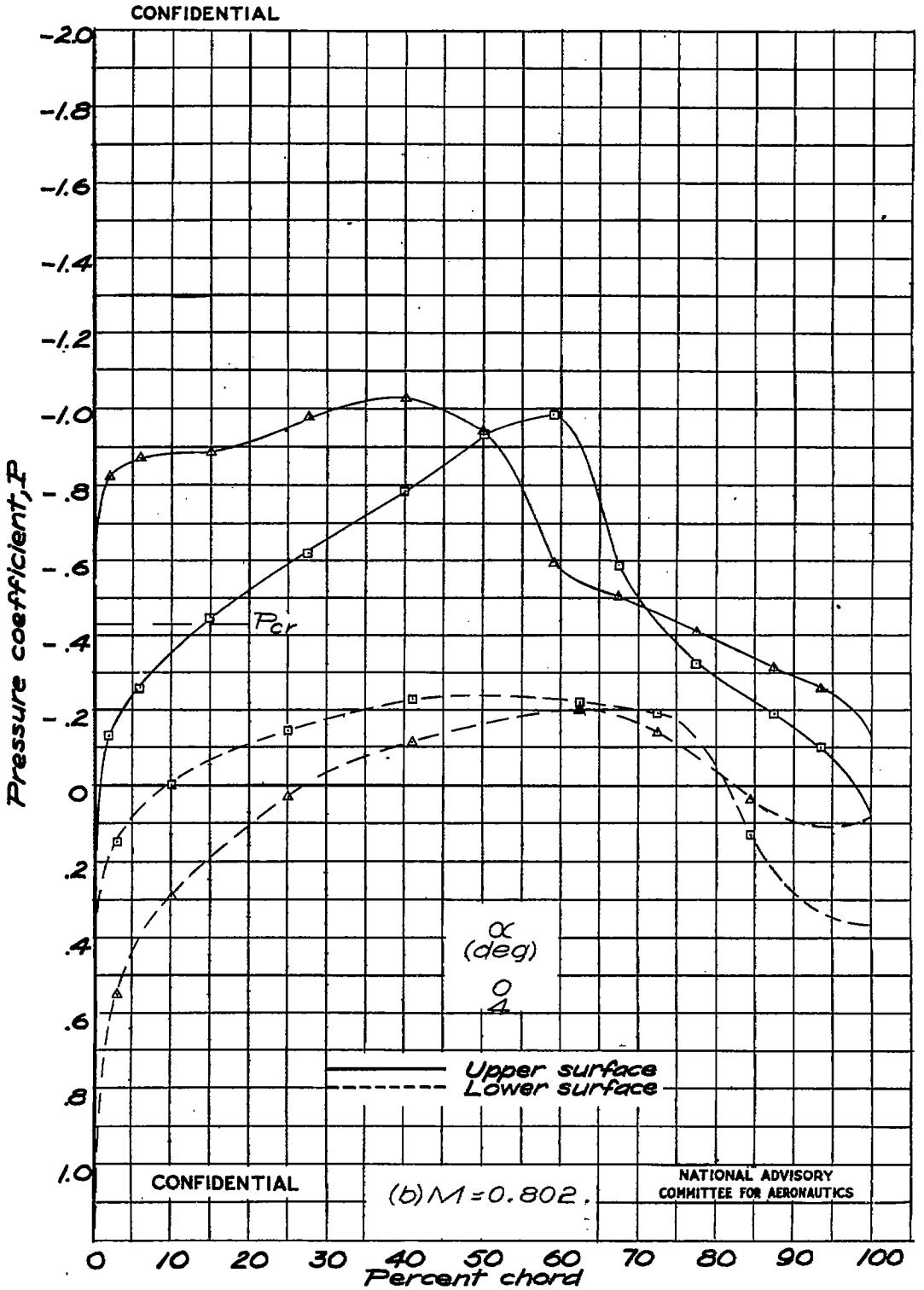


Figure 20.- Continued.

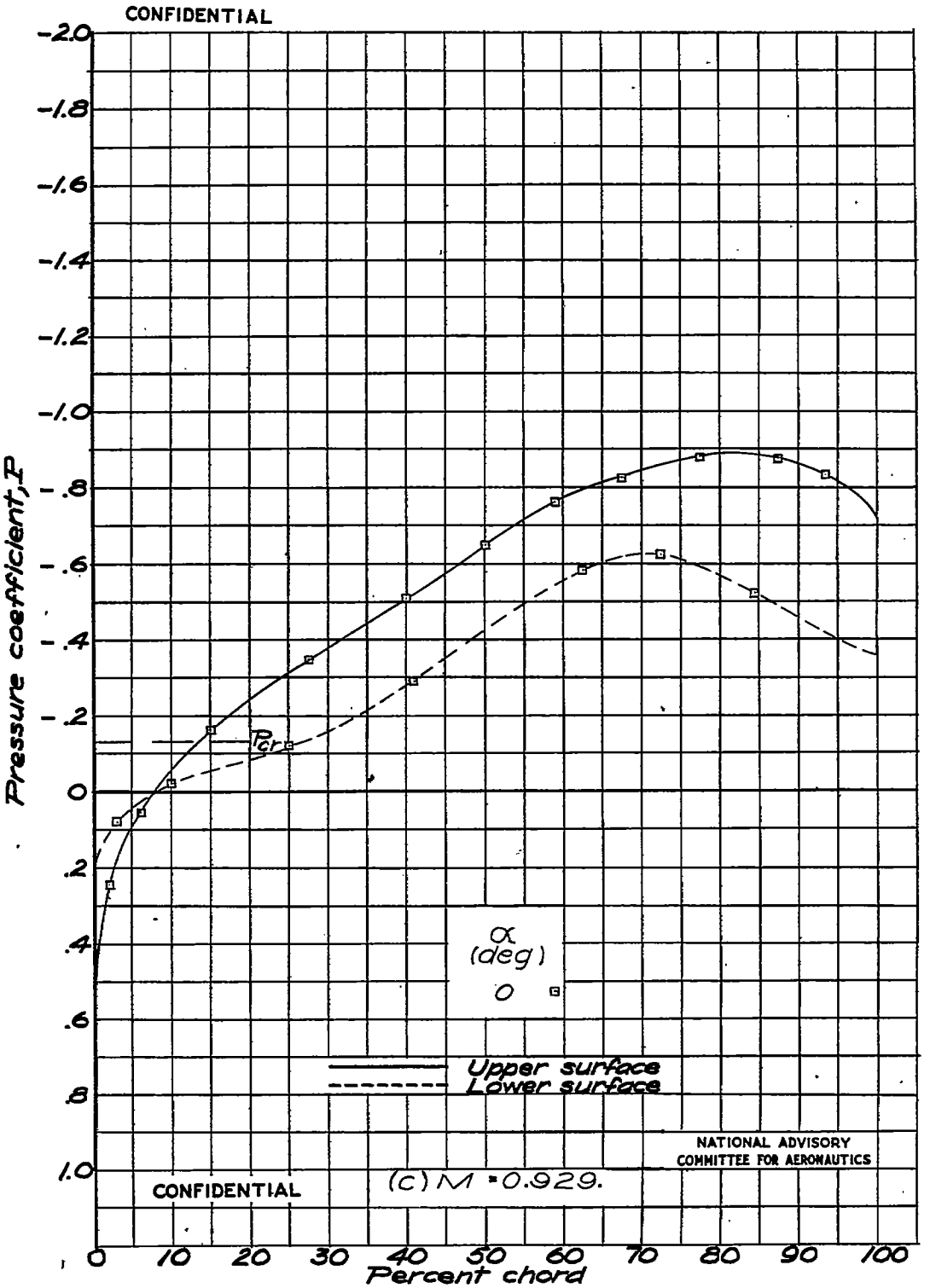


Figure 20.- Concluded.

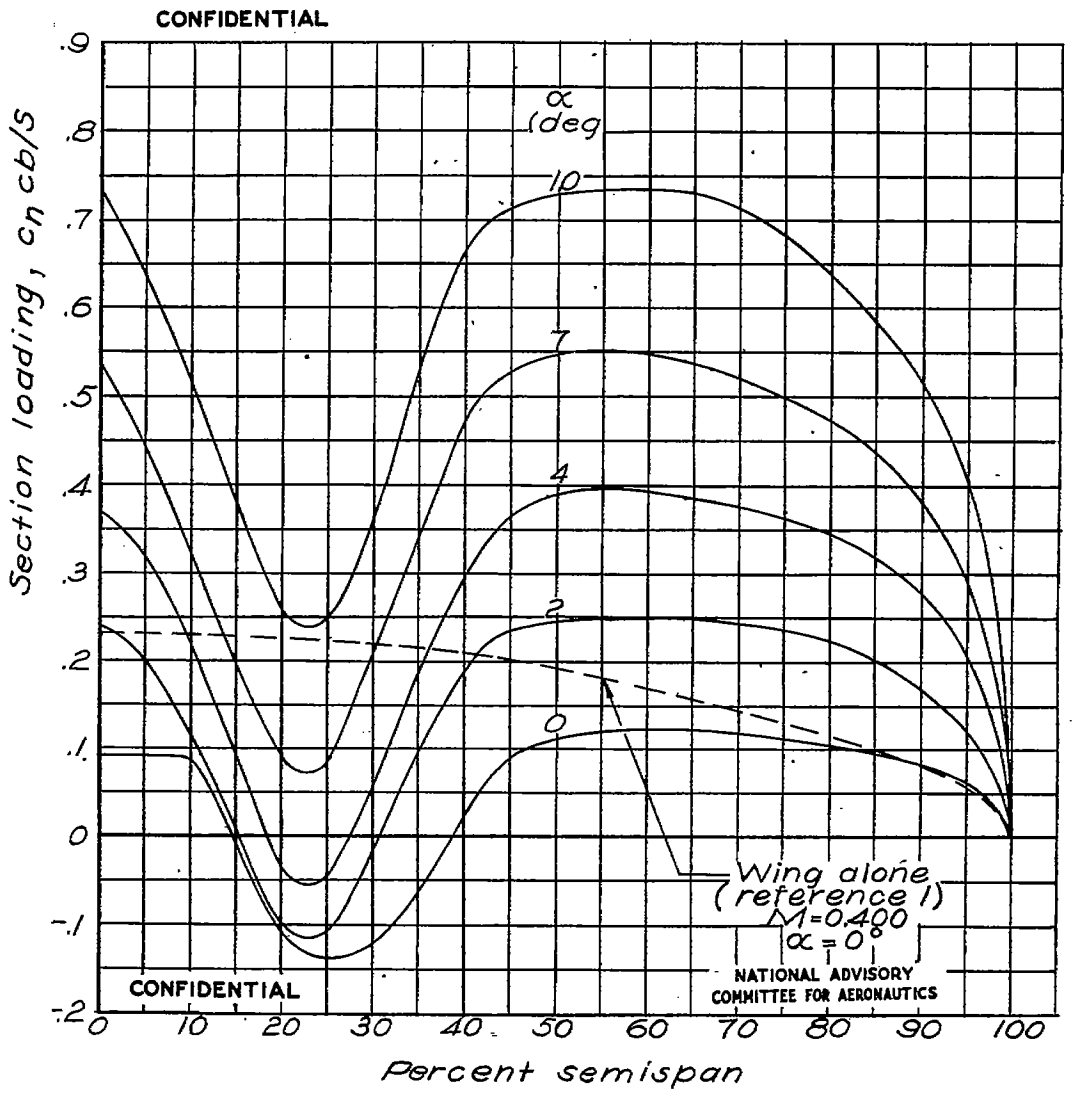


(a) M = 0.400.

Figure 21.—Spanwise variation in section loading for wing with solid brake.

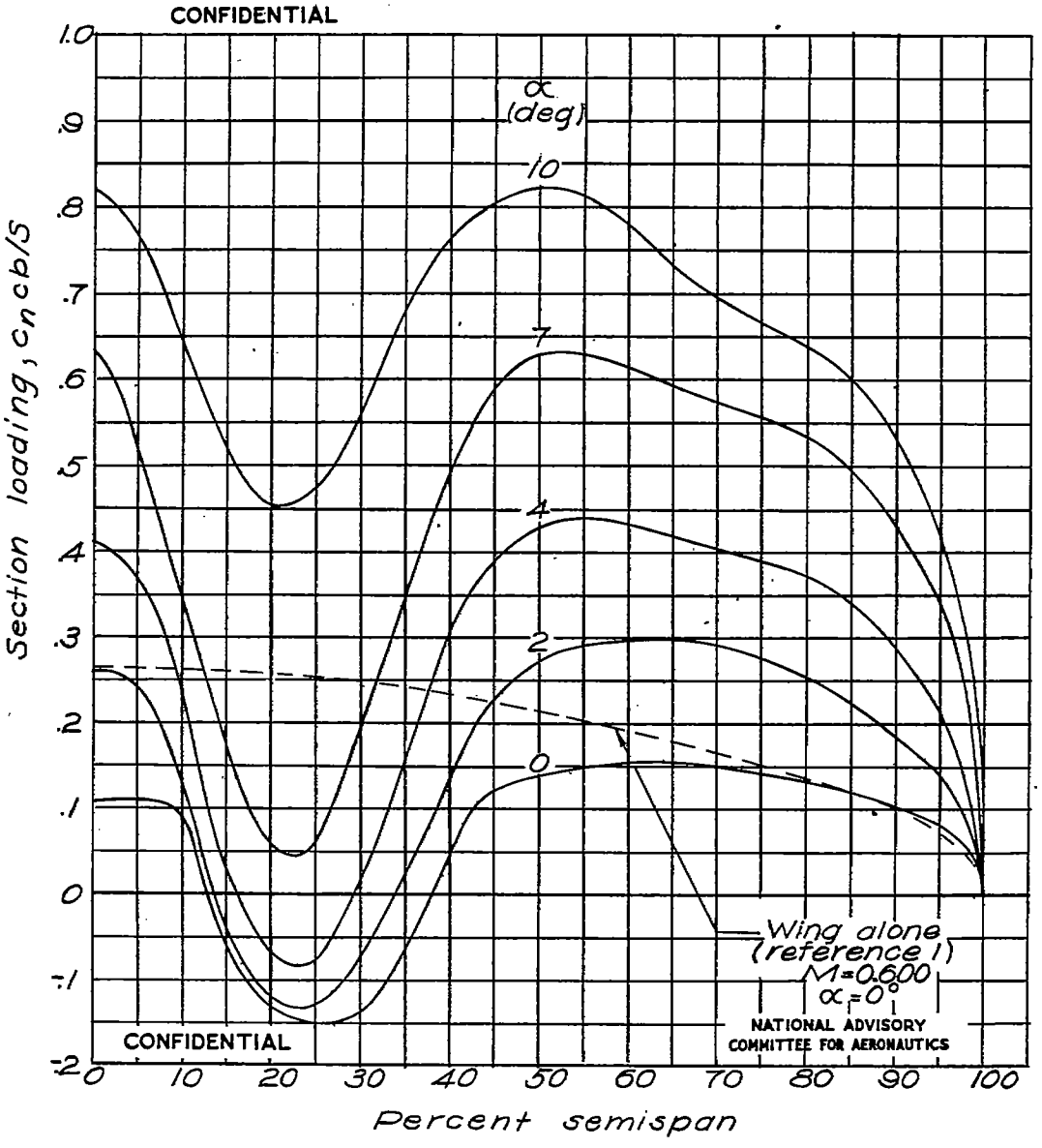


(b) $M = 0.600$.

Figure 21.-Continued.

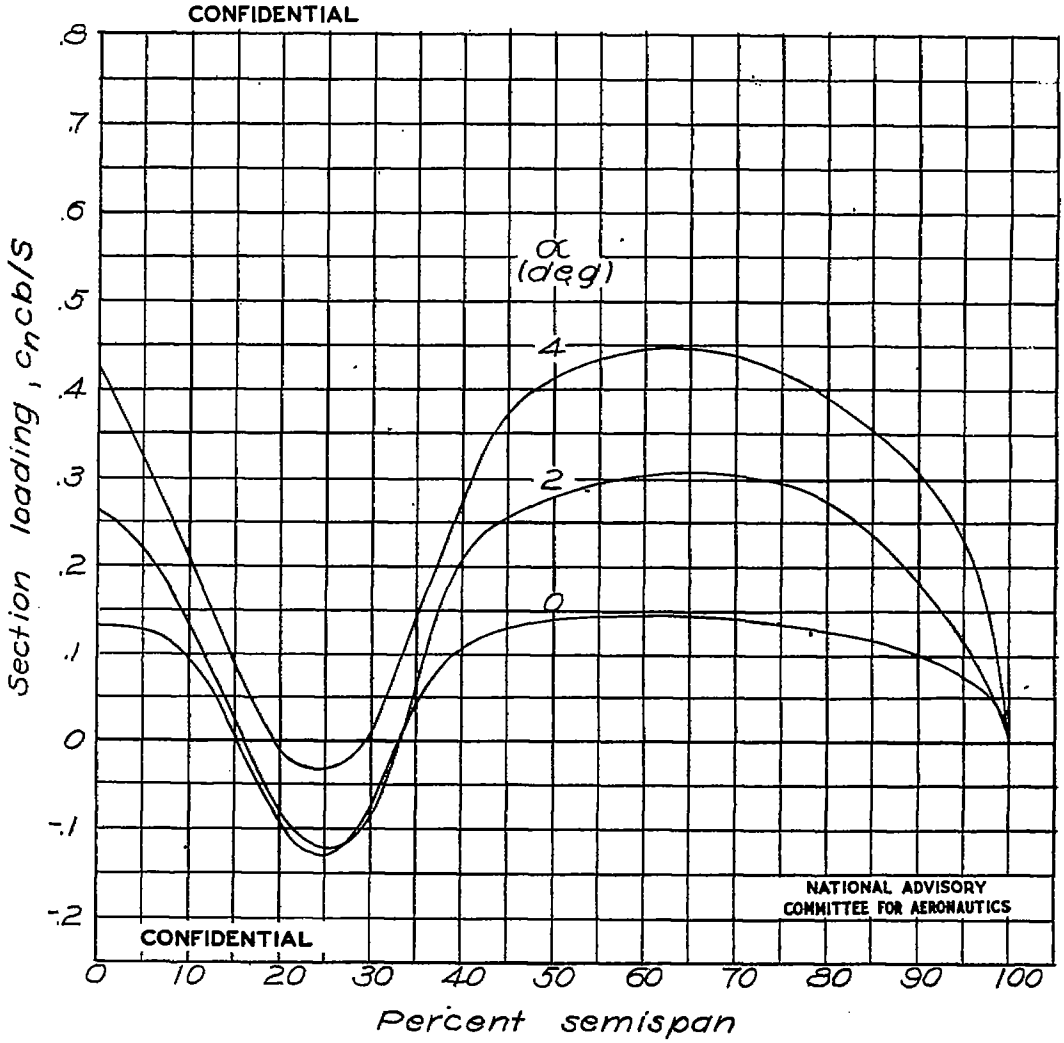


(c) $M = 0.700$.

Figure 21.-Continued.

CONFIDENTIAL

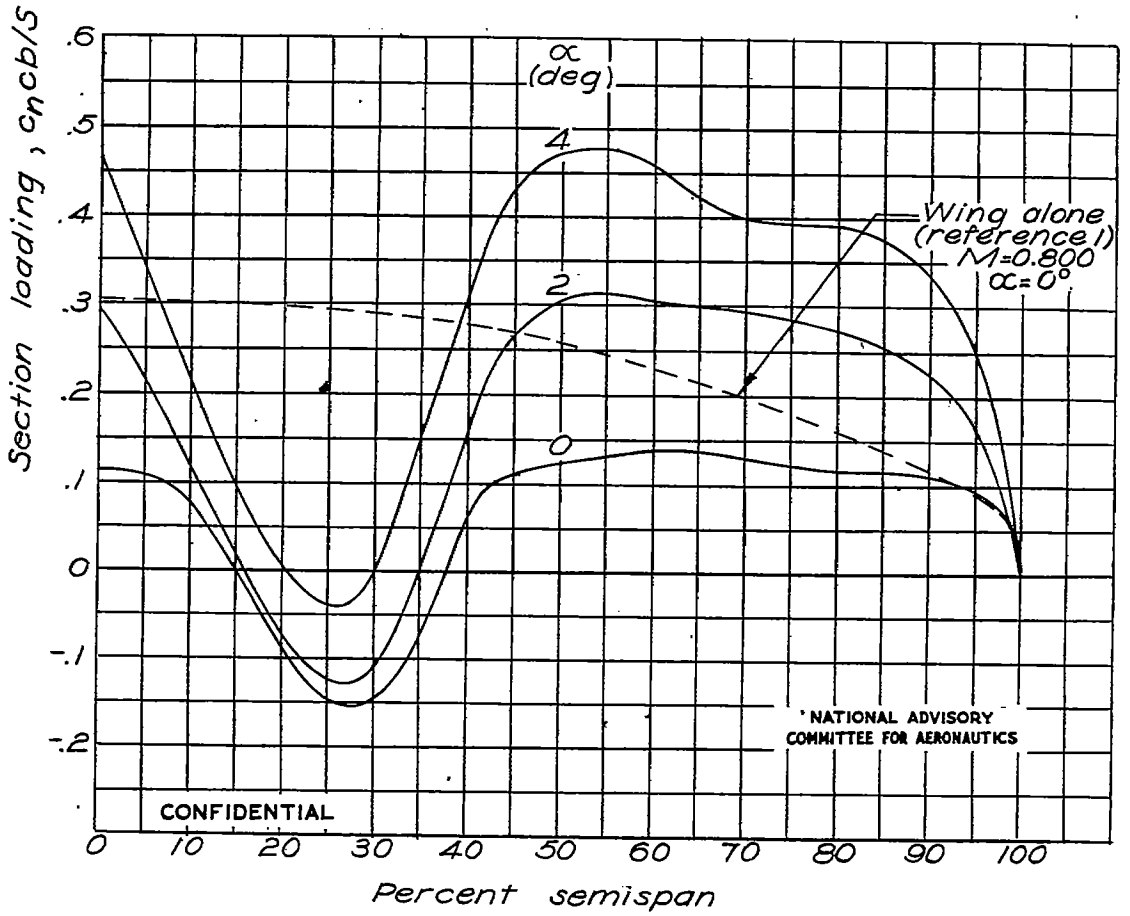


(d) $M = 0.808$.

Figure 21.- Continued.

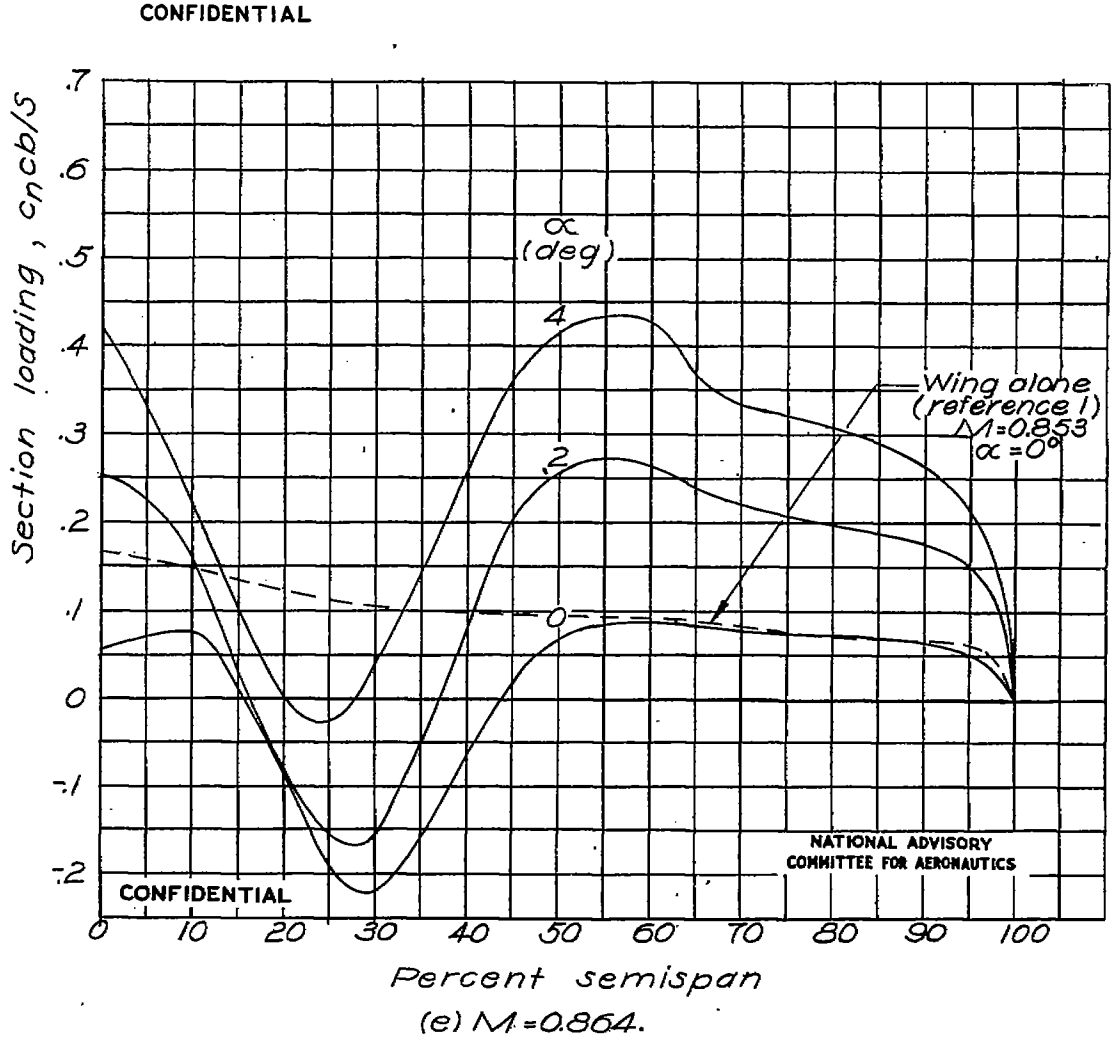


(e) M=0.864.

Figure 21.-Continued.

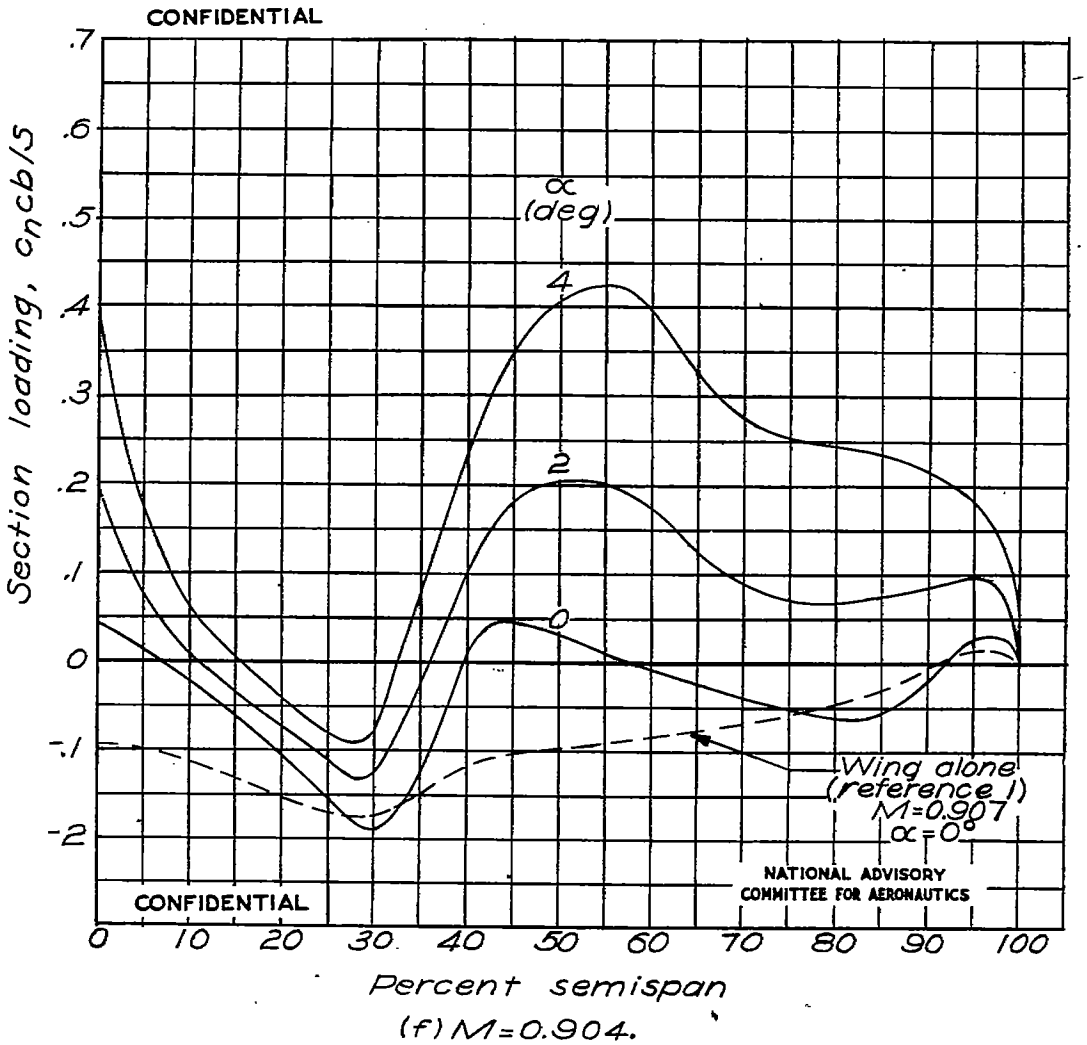


(f) $M=0.904$.

Figure 21.- Continued.

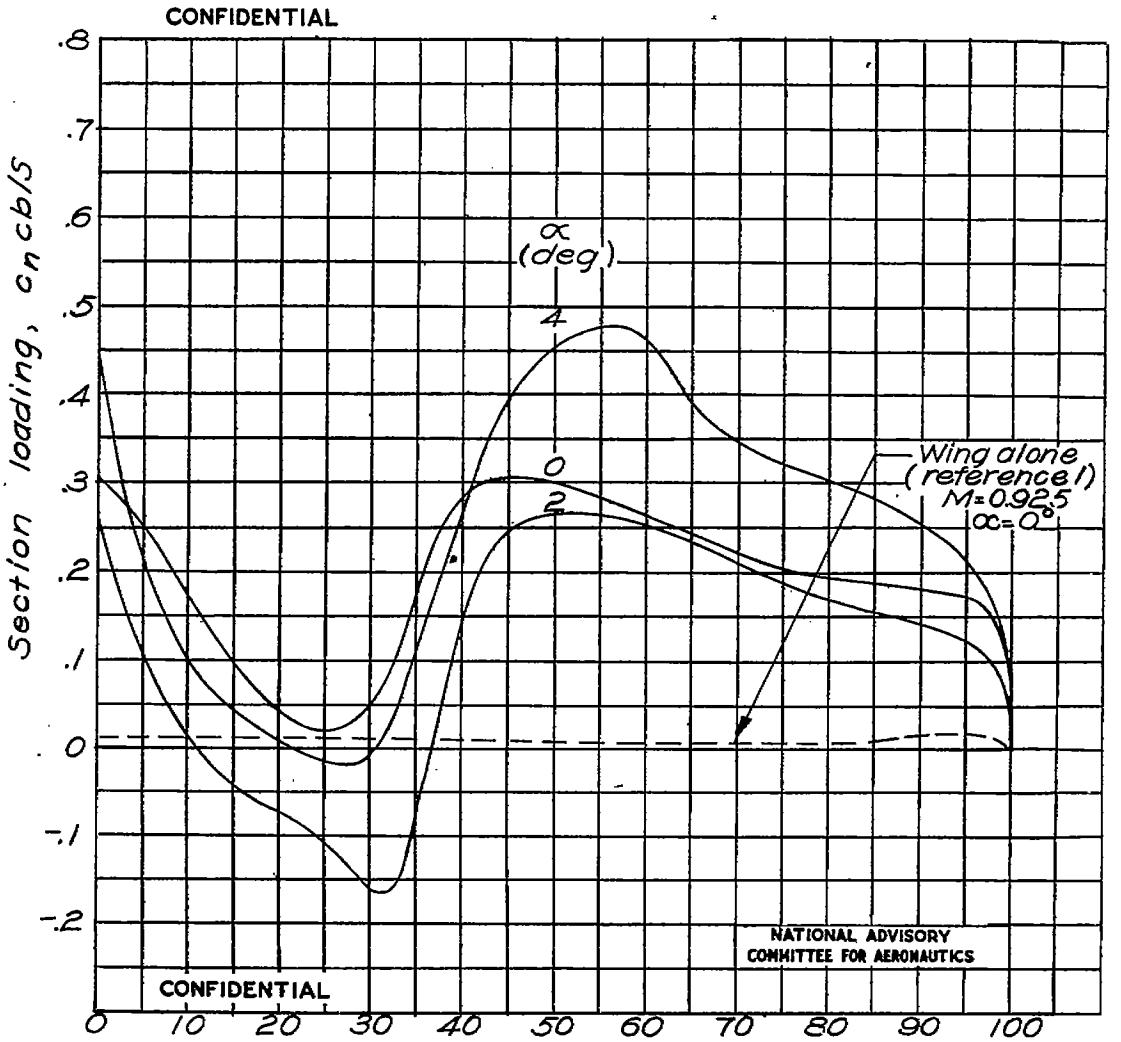


(g) $M = 0.940$.

Figure 21.- Concluded.

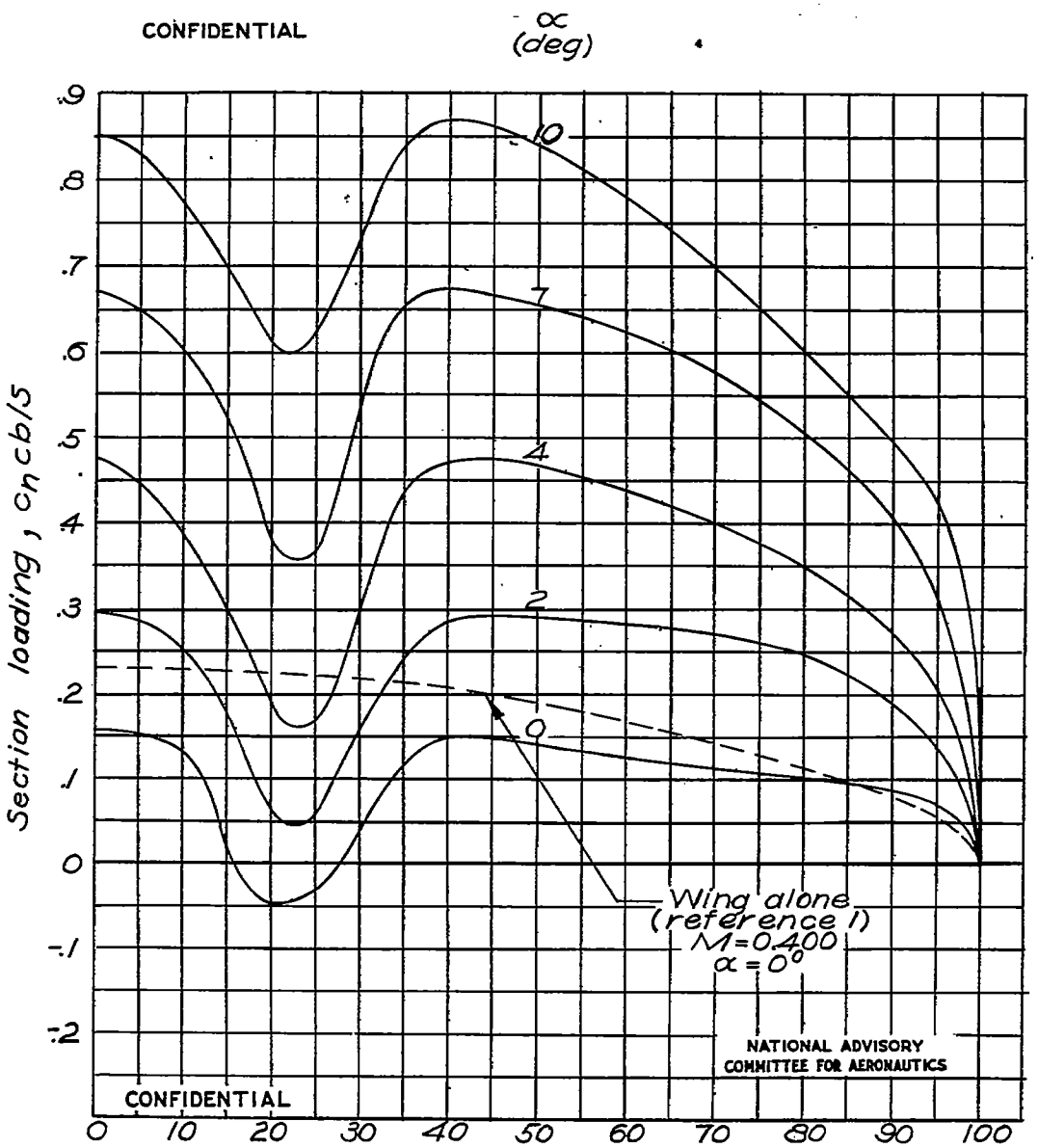


(a) $M = 0.400$.

Figure 22.—Spanwise variation in section loading for wing with slotted brake.

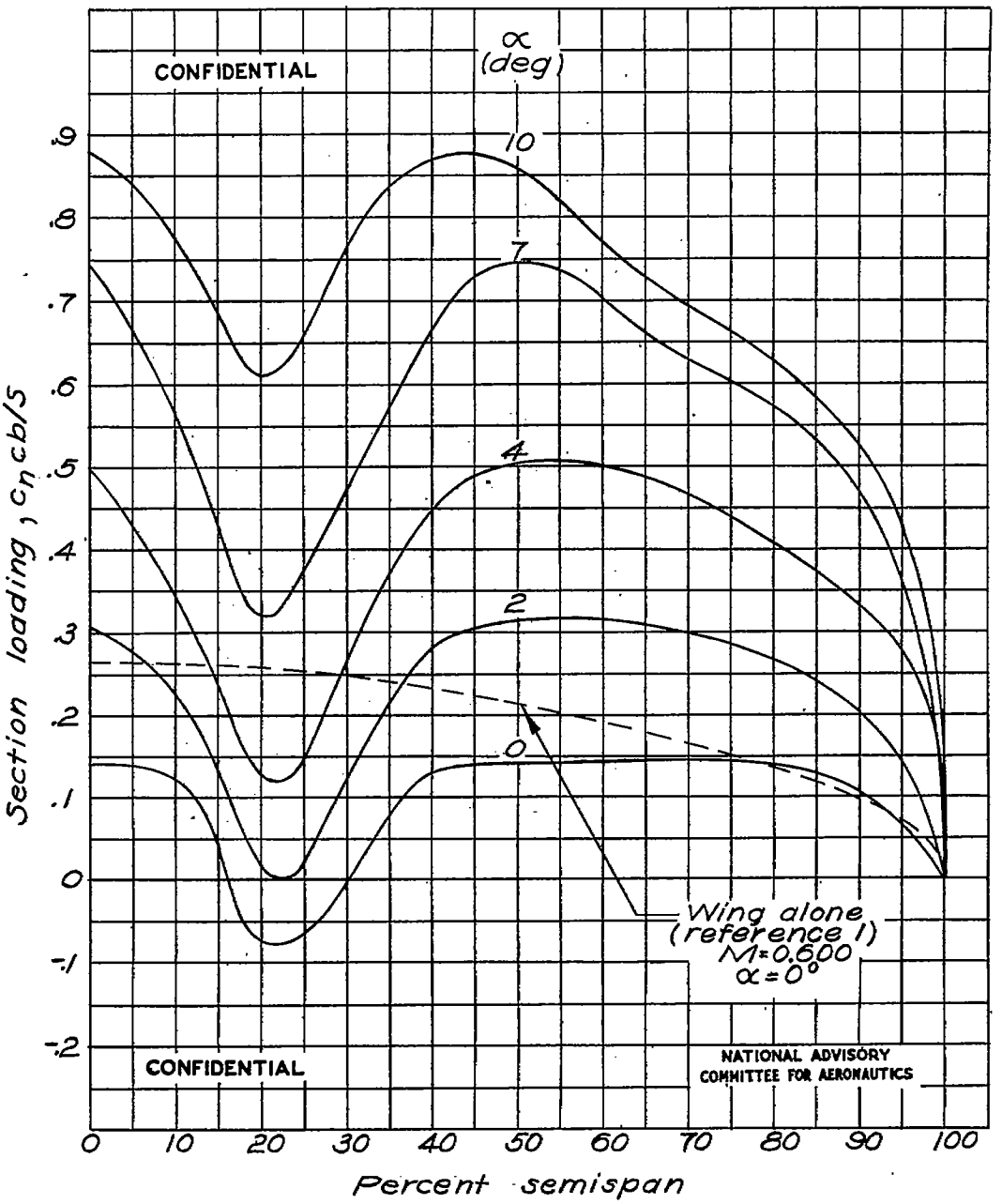


(b) $M = 0.600$.

Figure 22.-Continued.

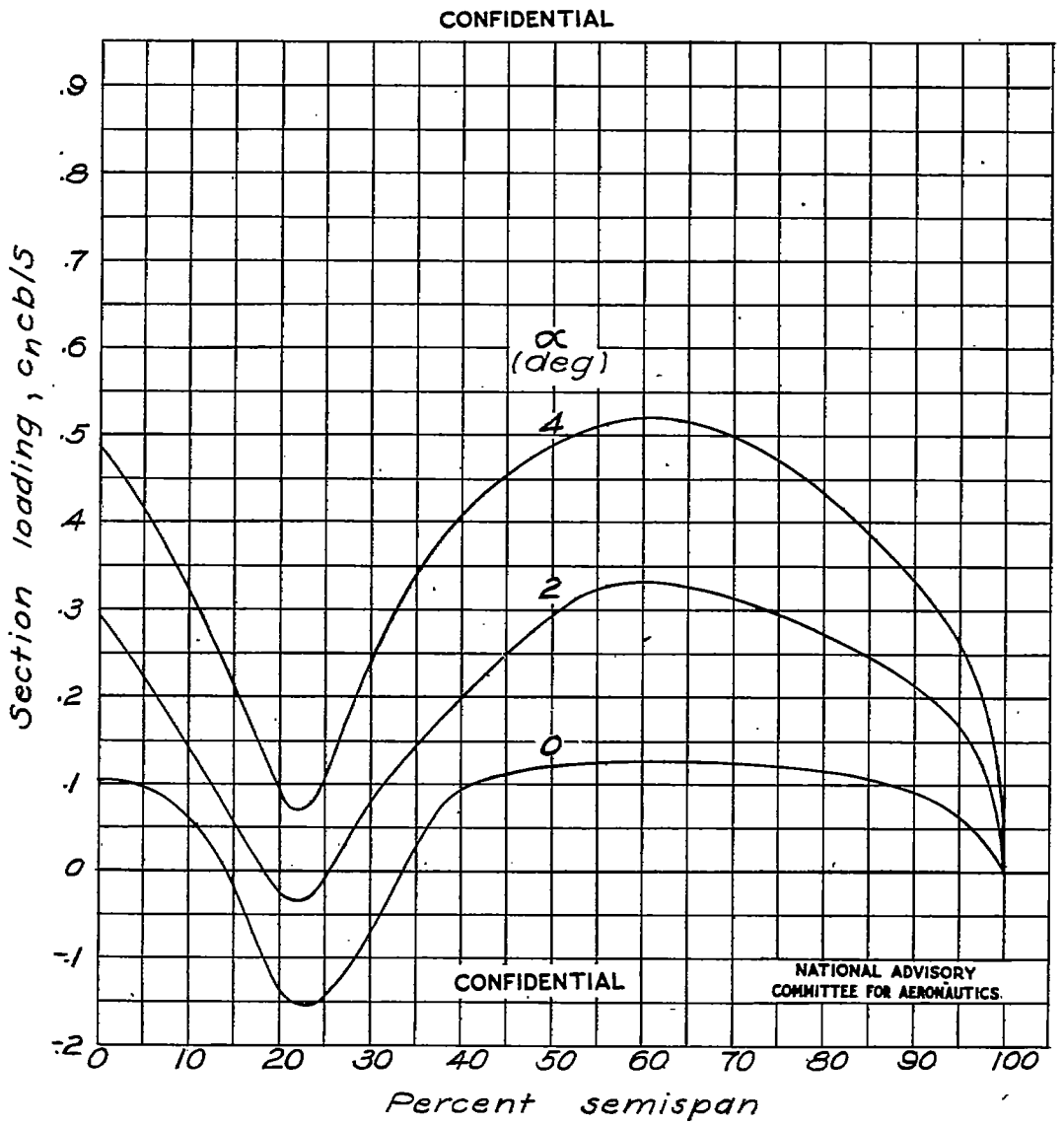


(c) $M = 0.700$.

Figure 22-Continued.

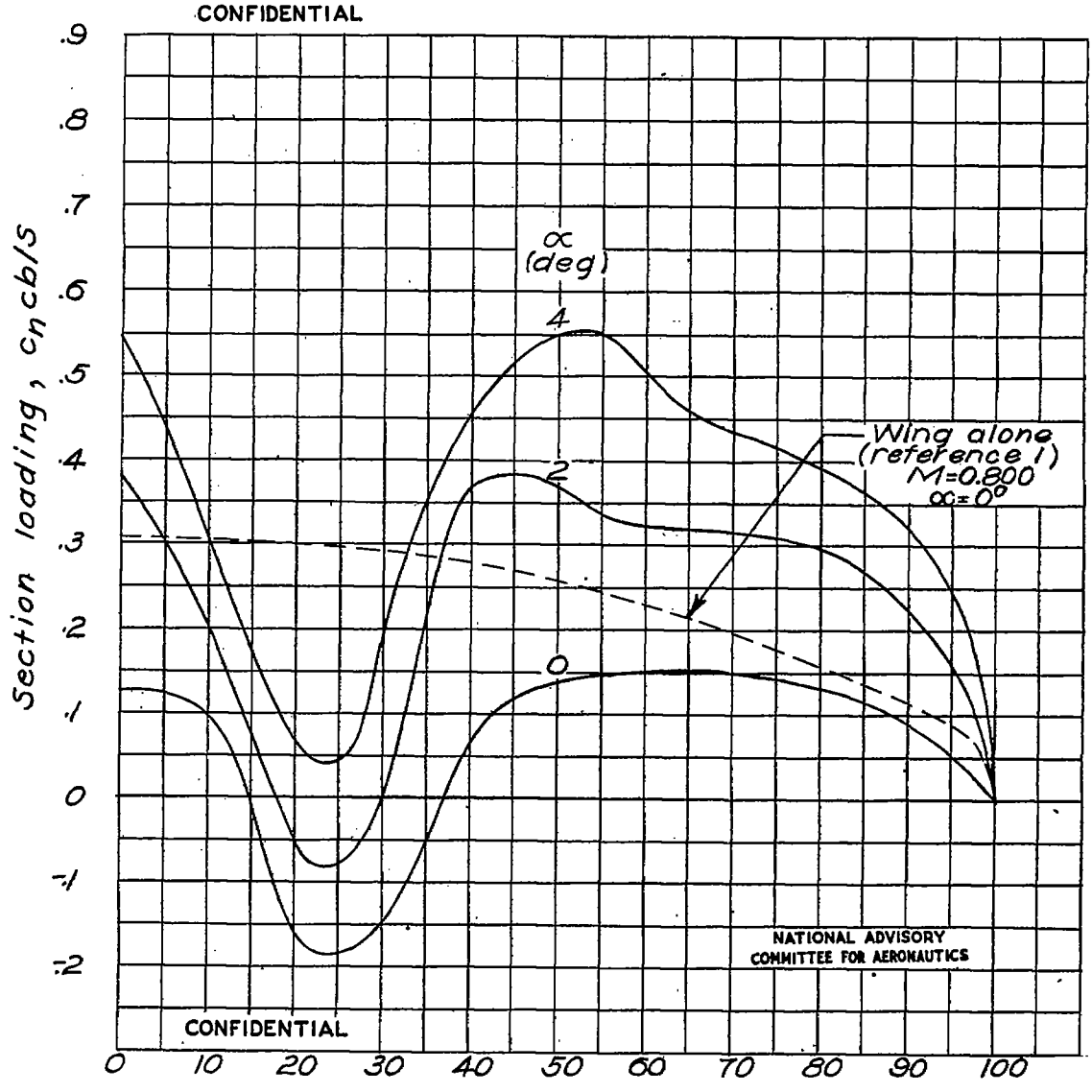


(d) $M = 0.806$.

Figure 22.-Continued.

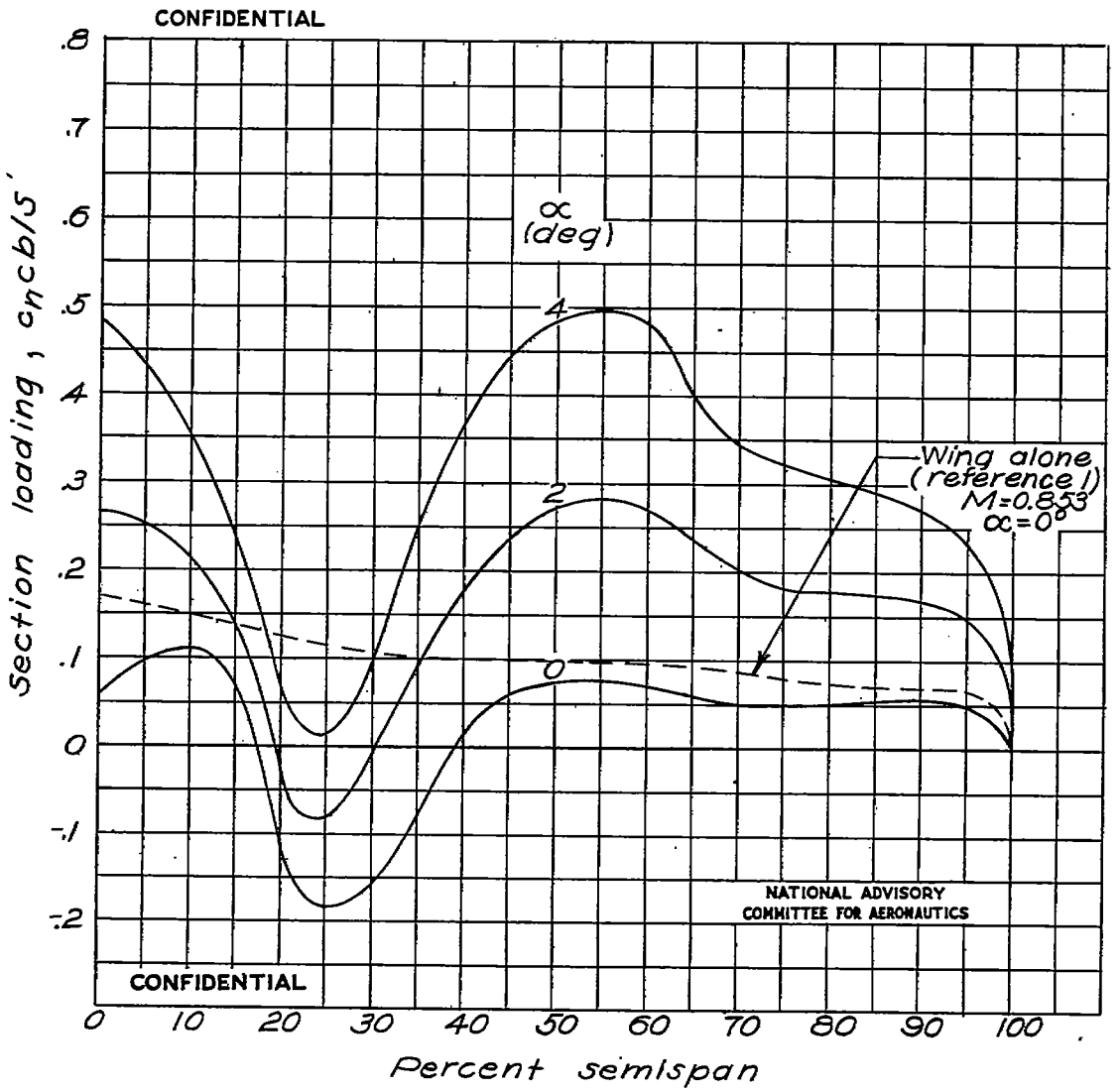


(e) $M = 0.862$.

Figure 22.-Continued.

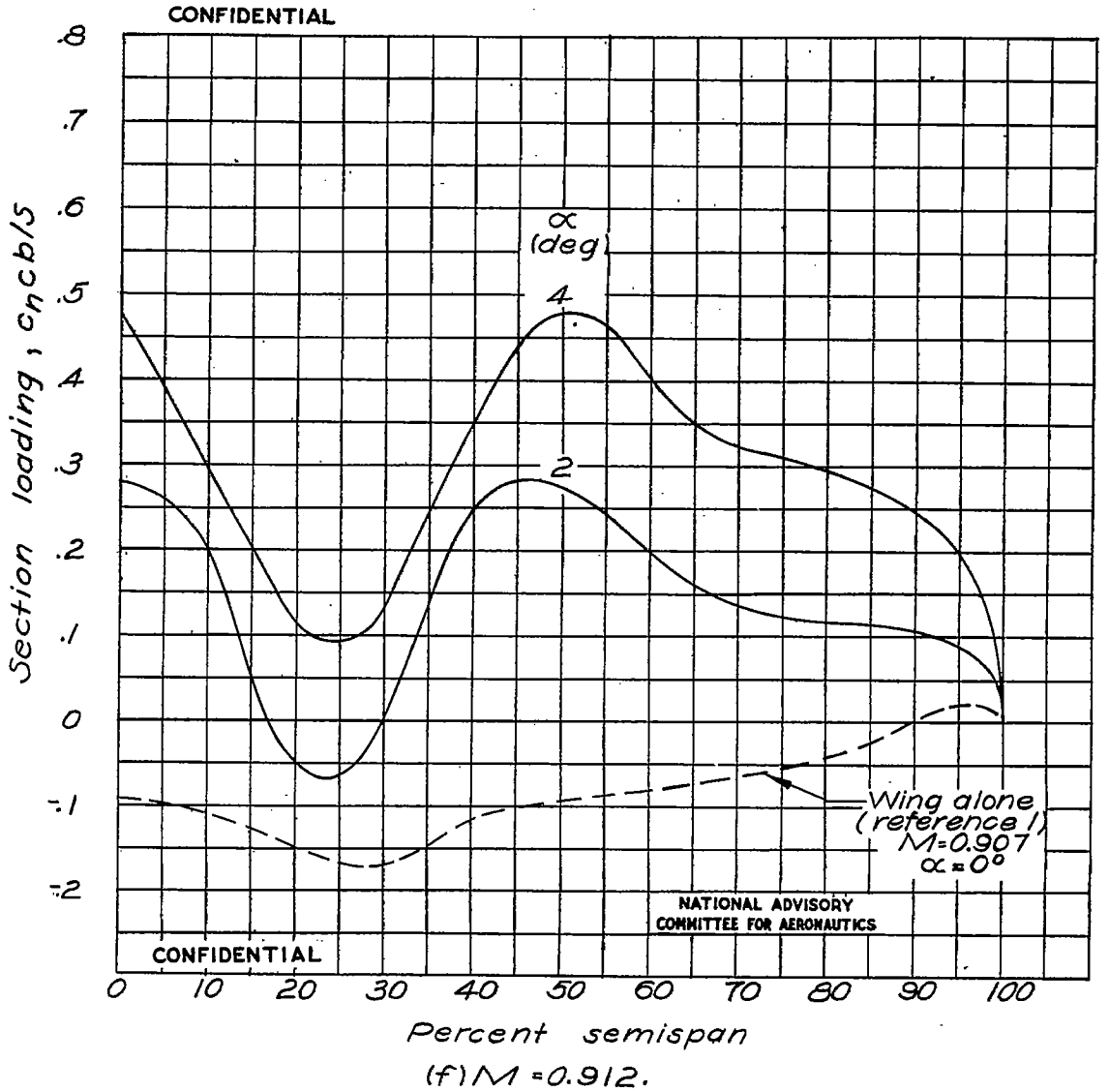


(f) $M = 0.912$.

Figure 22-Continued.

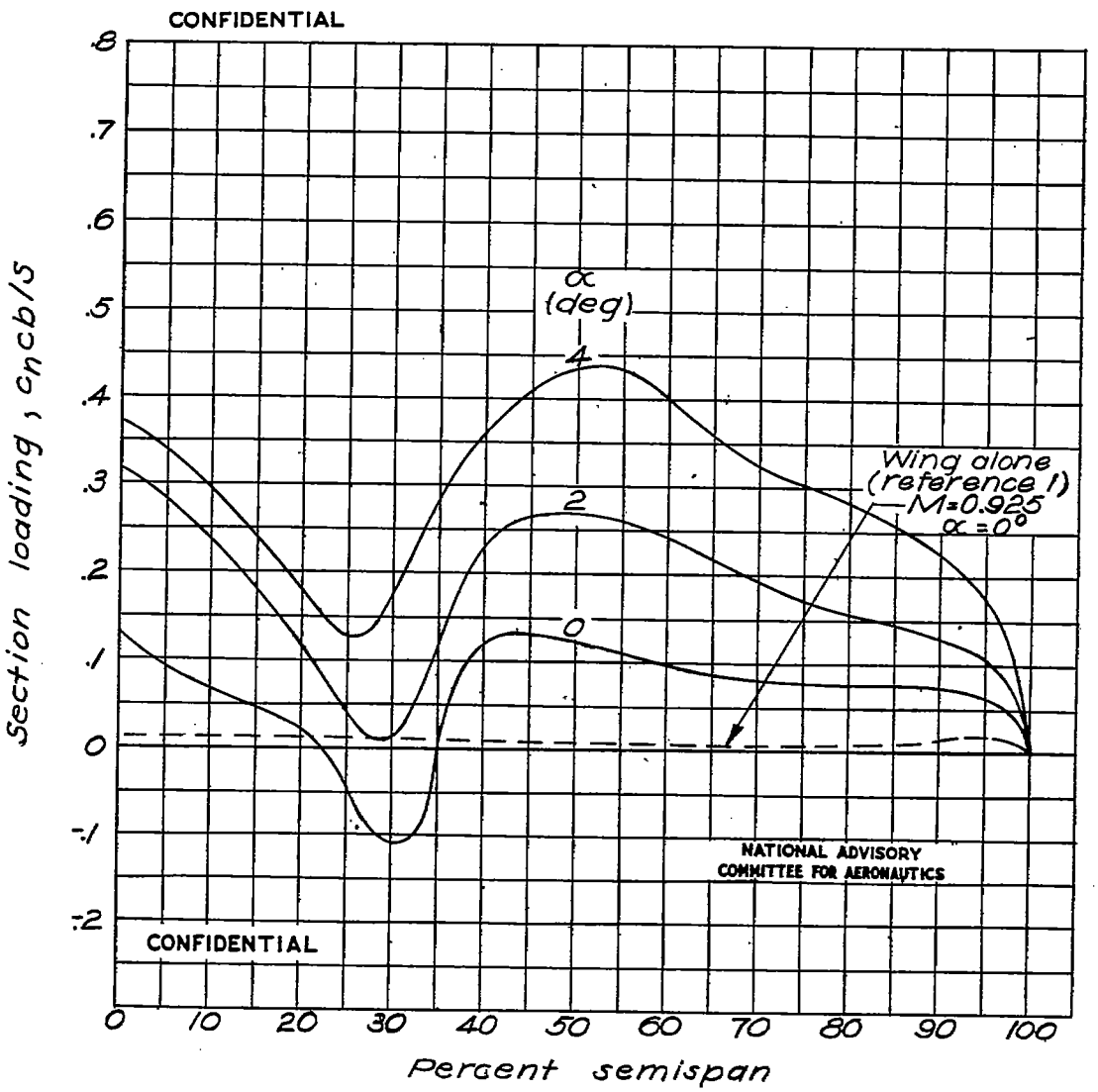


(g) $M = 0.937$.

Figure 22.-Concluded.

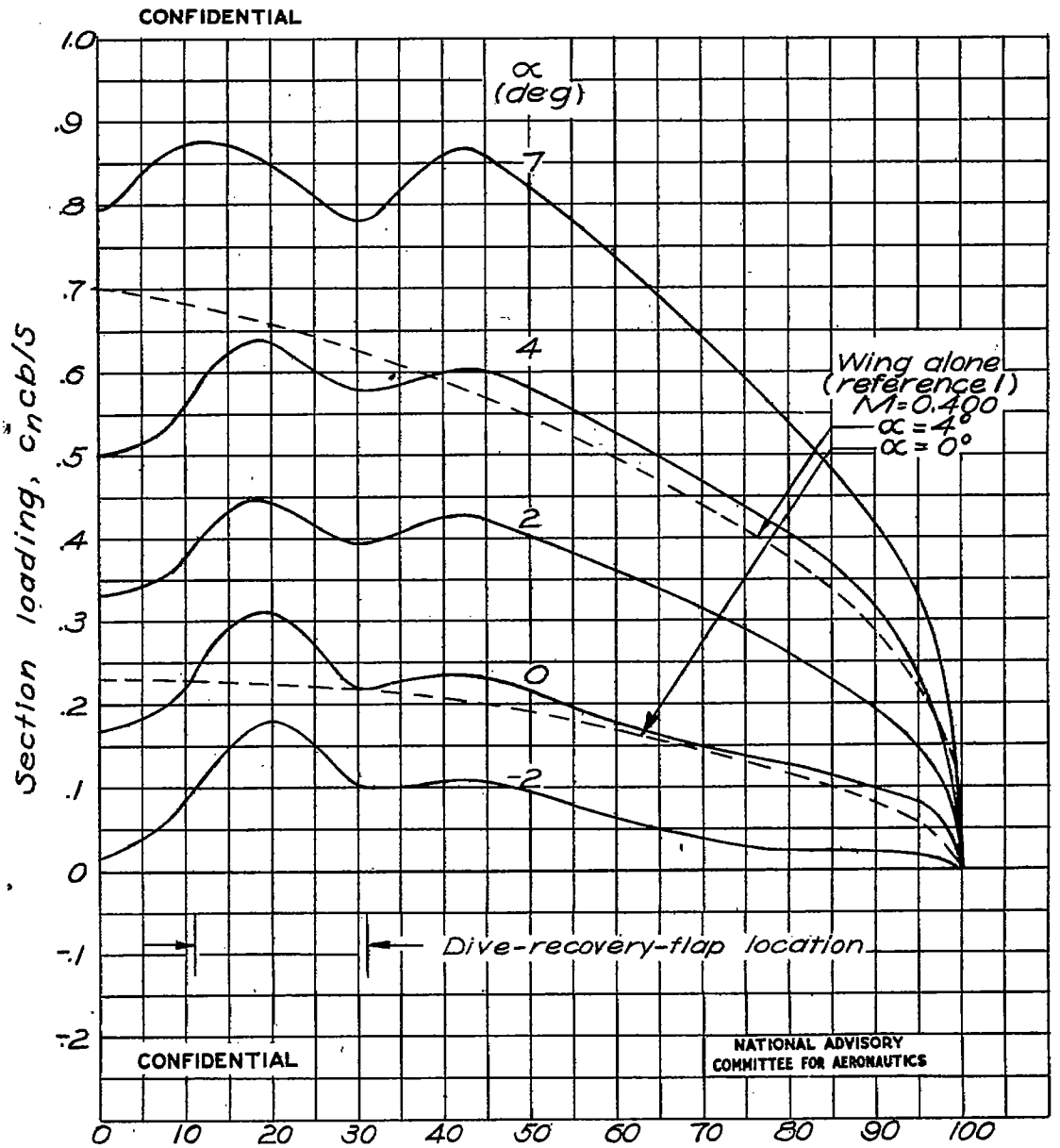


(a) M = 0.400.

Figure 23.-Spanwise variation in section loading for wing with dive-recovery flap.

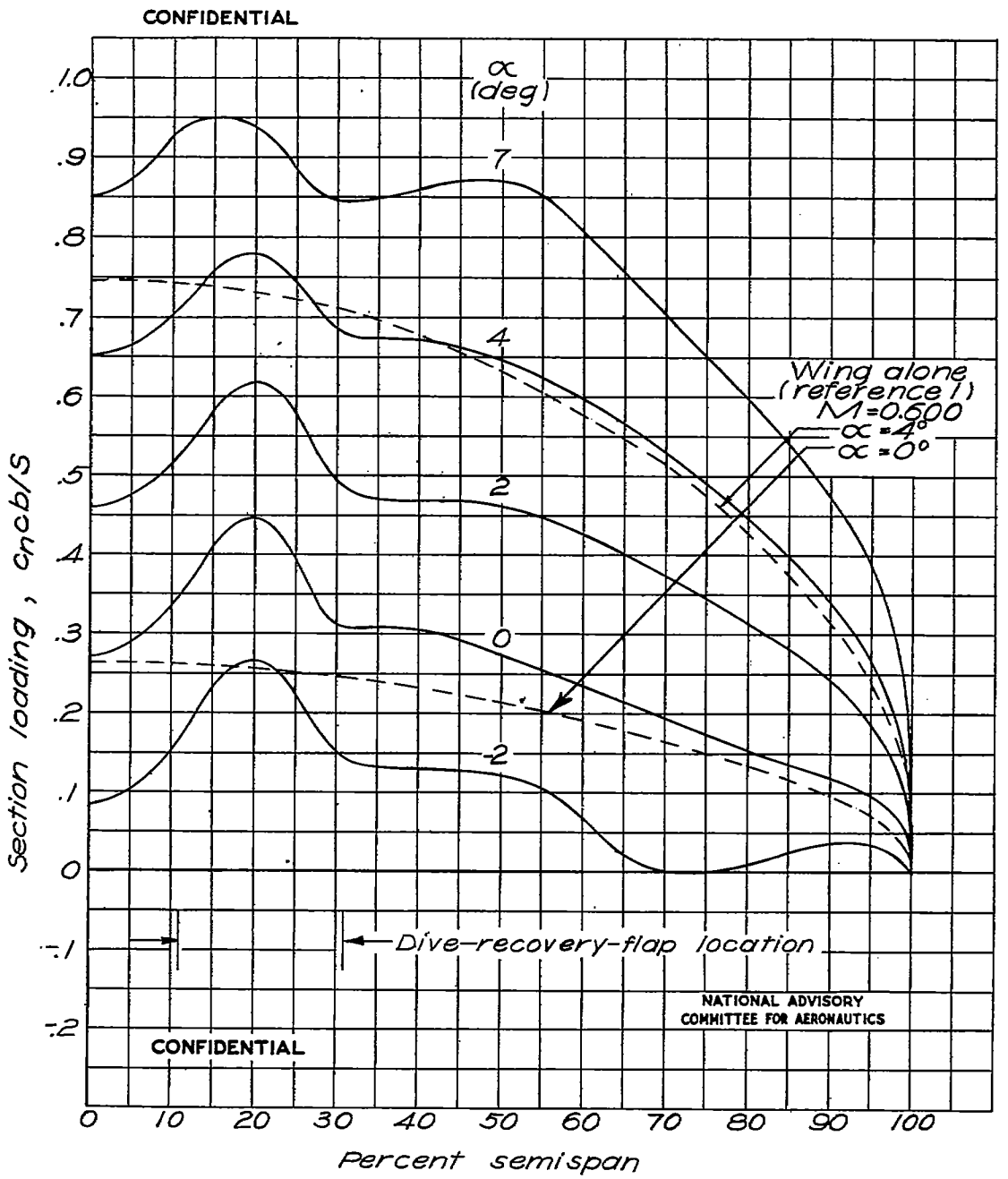


(b) M=0.600.

Figure 23.- Continued.

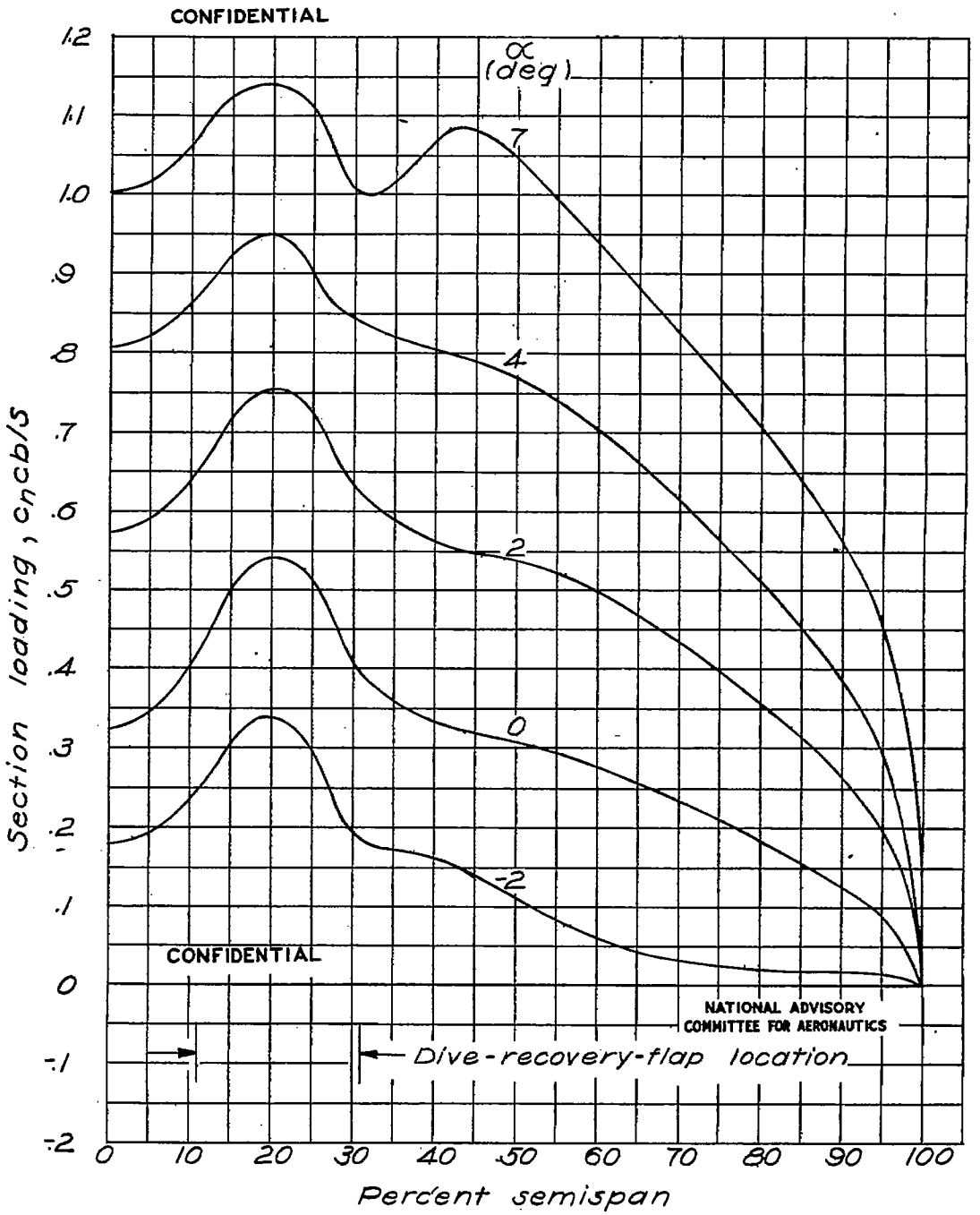


(c) $M = 0.700$.

Figure 23.- Continued.

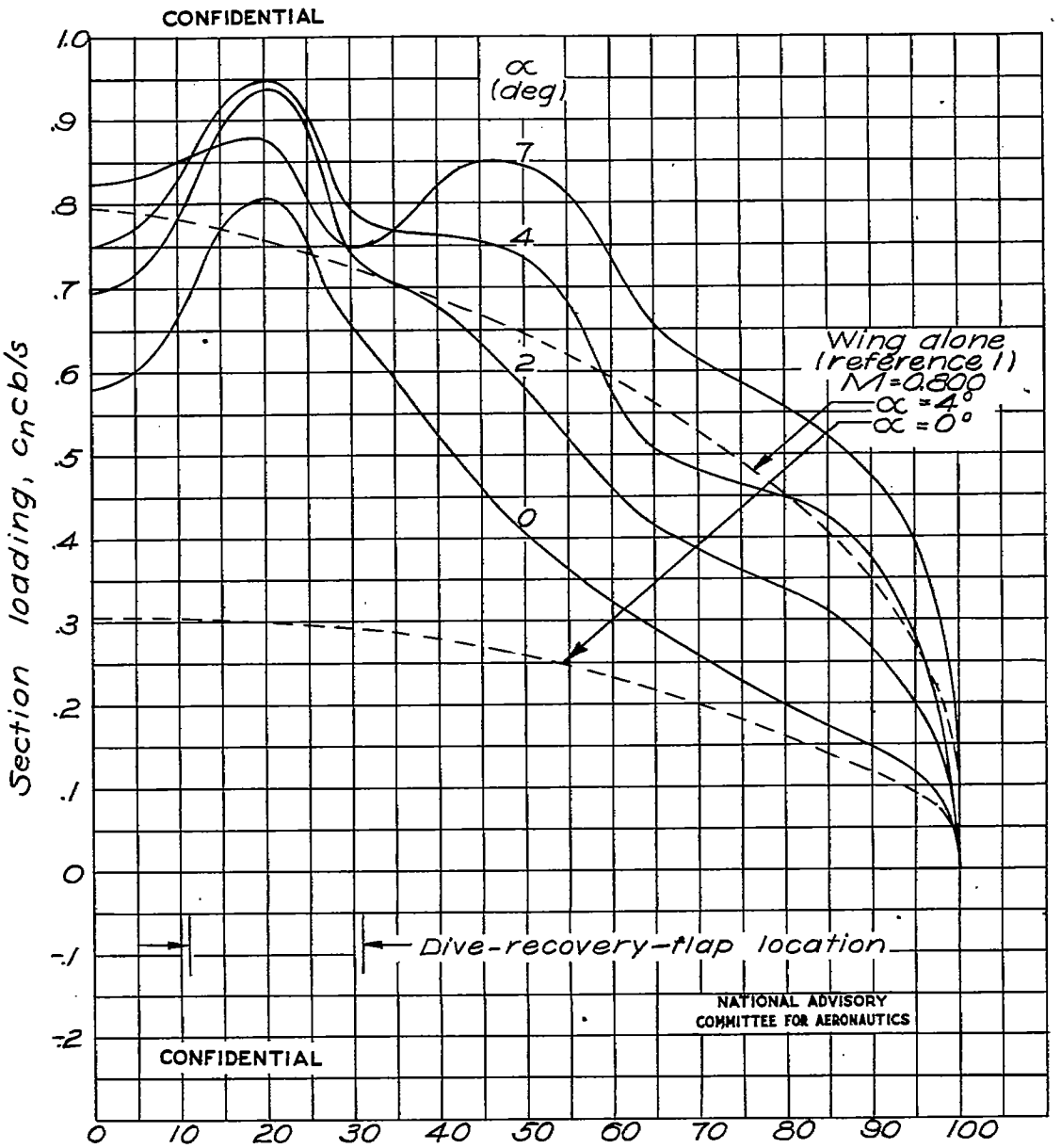


(d) $M = 0.802$.

Figure 23.-Continued.

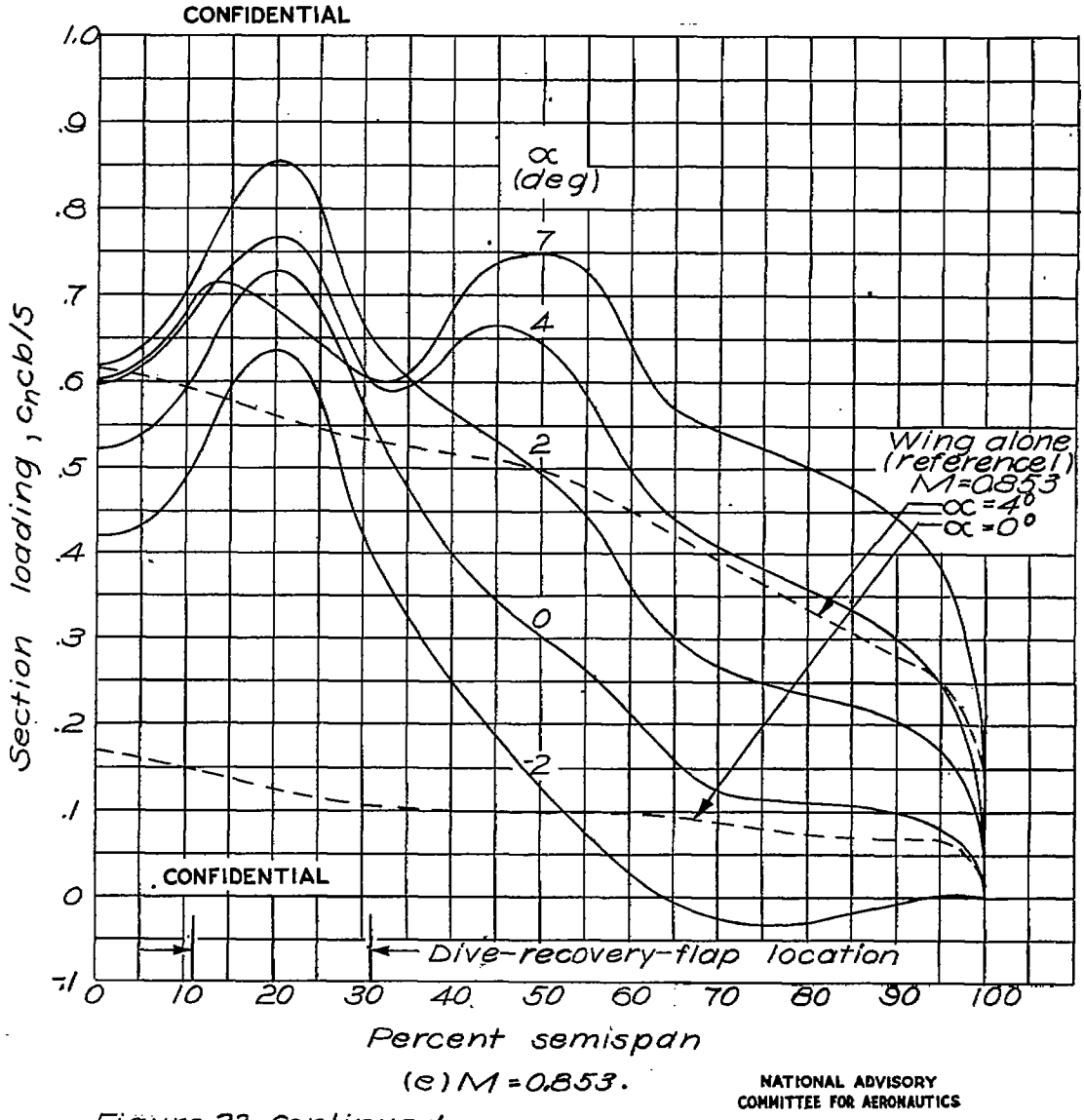


(e) $M = 0.853$.

NATIONAL ADVISORY COMMITTEE FOR AERONAUTICS

Figure 23.-Continued.

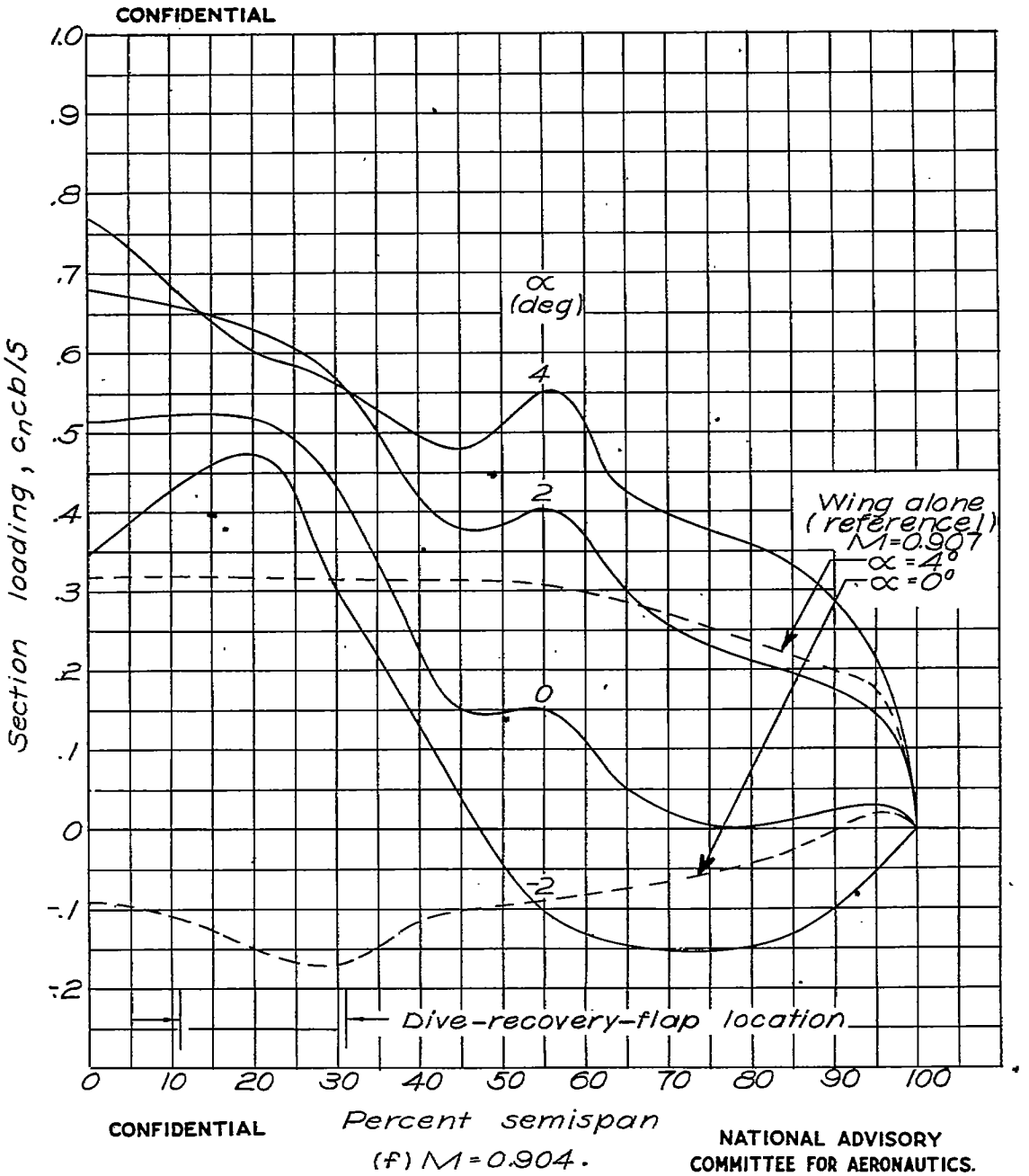


(f) $M = 0.904$.

Figure 23.- Continued.

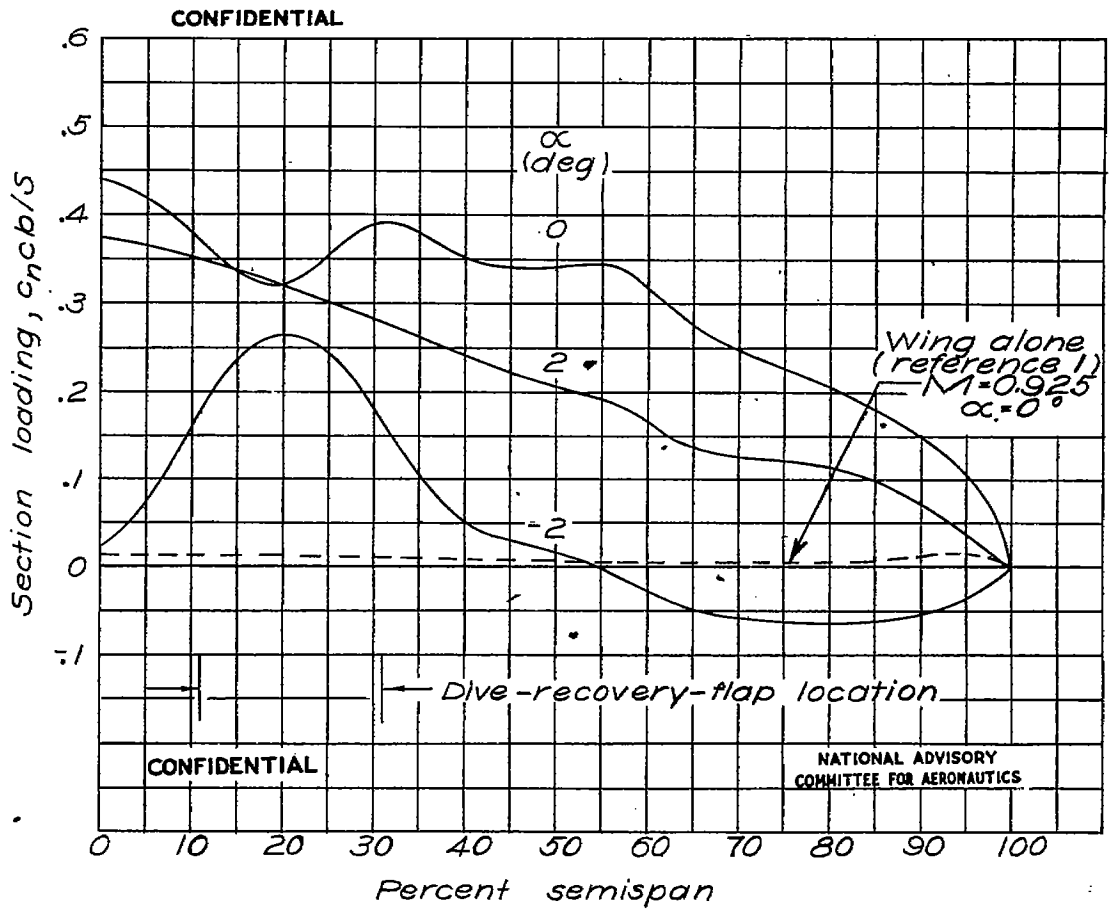


(g) $M = 0.929$.

Figure 23.- Concluded.

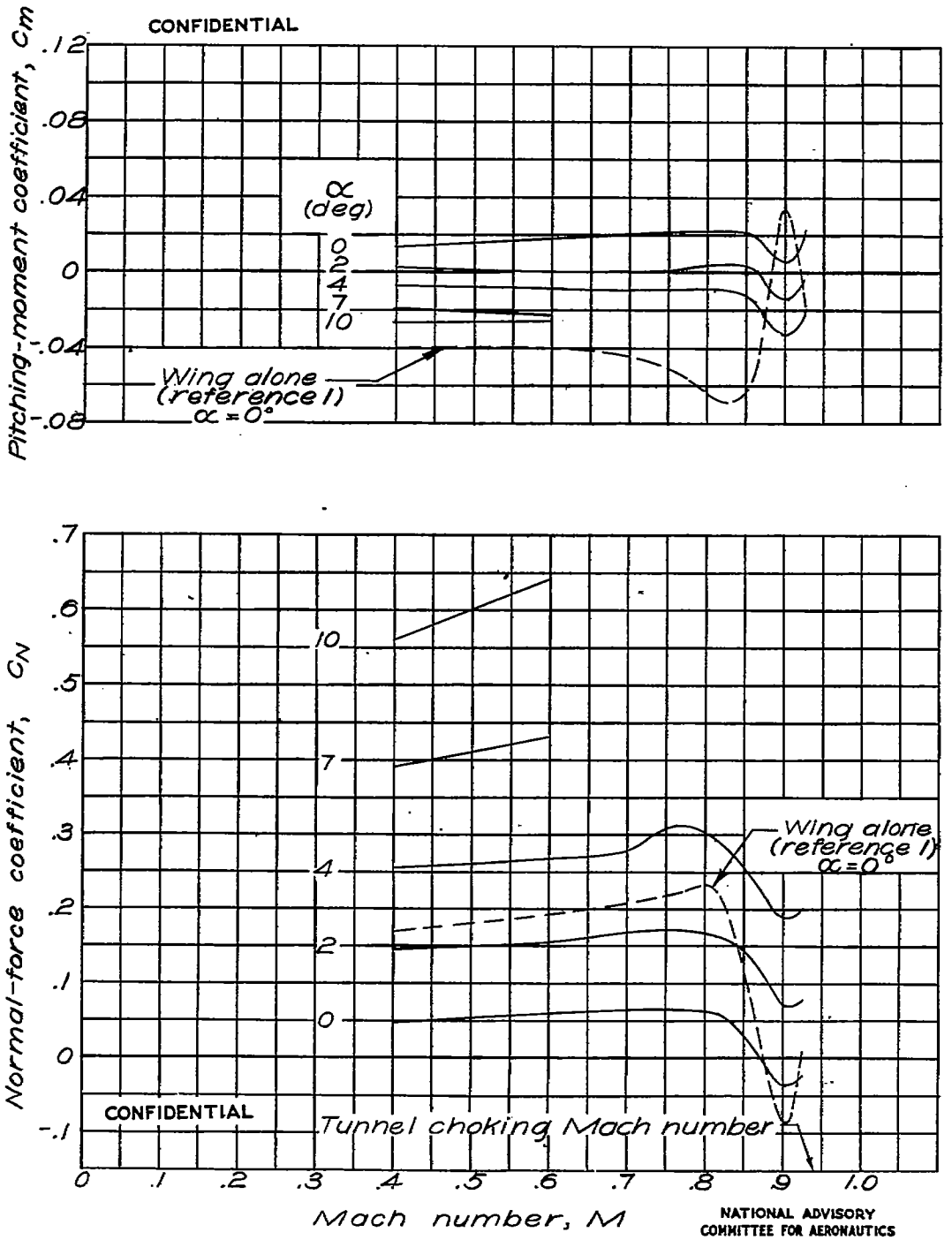


Figure 24.-Variation of normal-force and pitching-moment coefficients with Mach number for wing with solid brake.

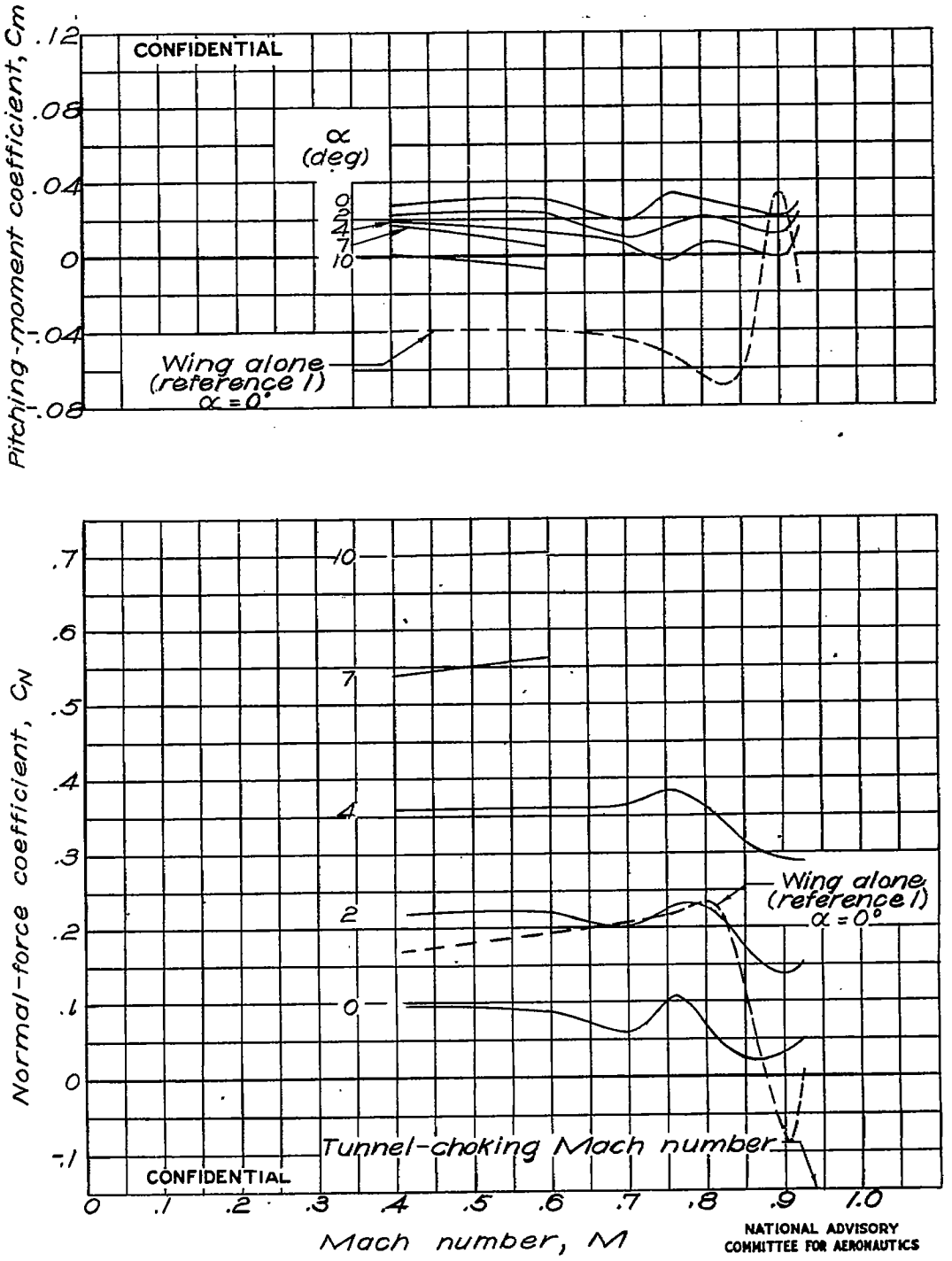


Figure 25.-Variation of normal-force and pitching-moment coefficients with Mach number for wing with slotted brake.

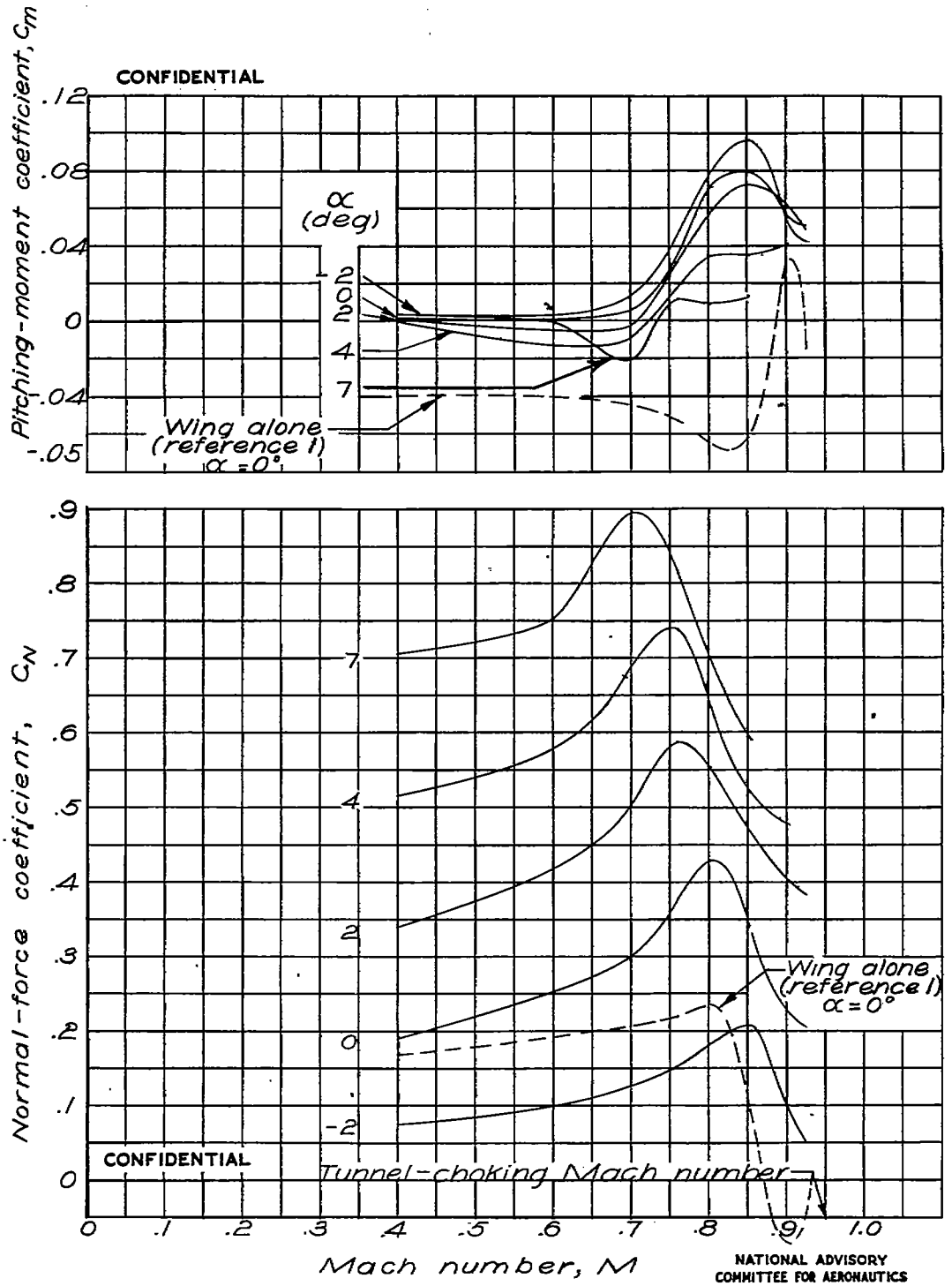


Figure 26.-Variation of normal-force and pitching-moment coefficients with Mach number for wing with dive-recovery flap.

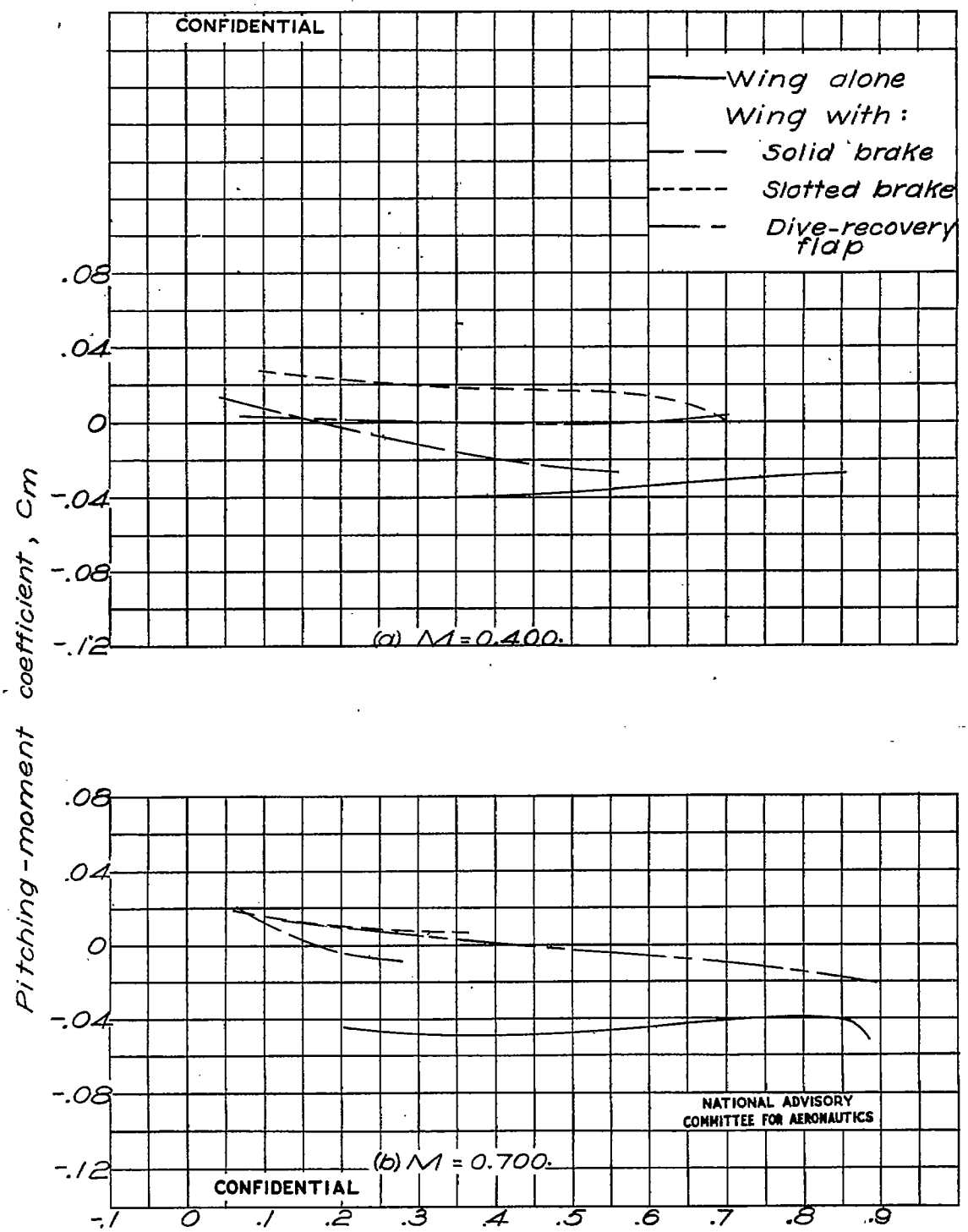


Figure 27.-Stability characteristics for various model configurations.

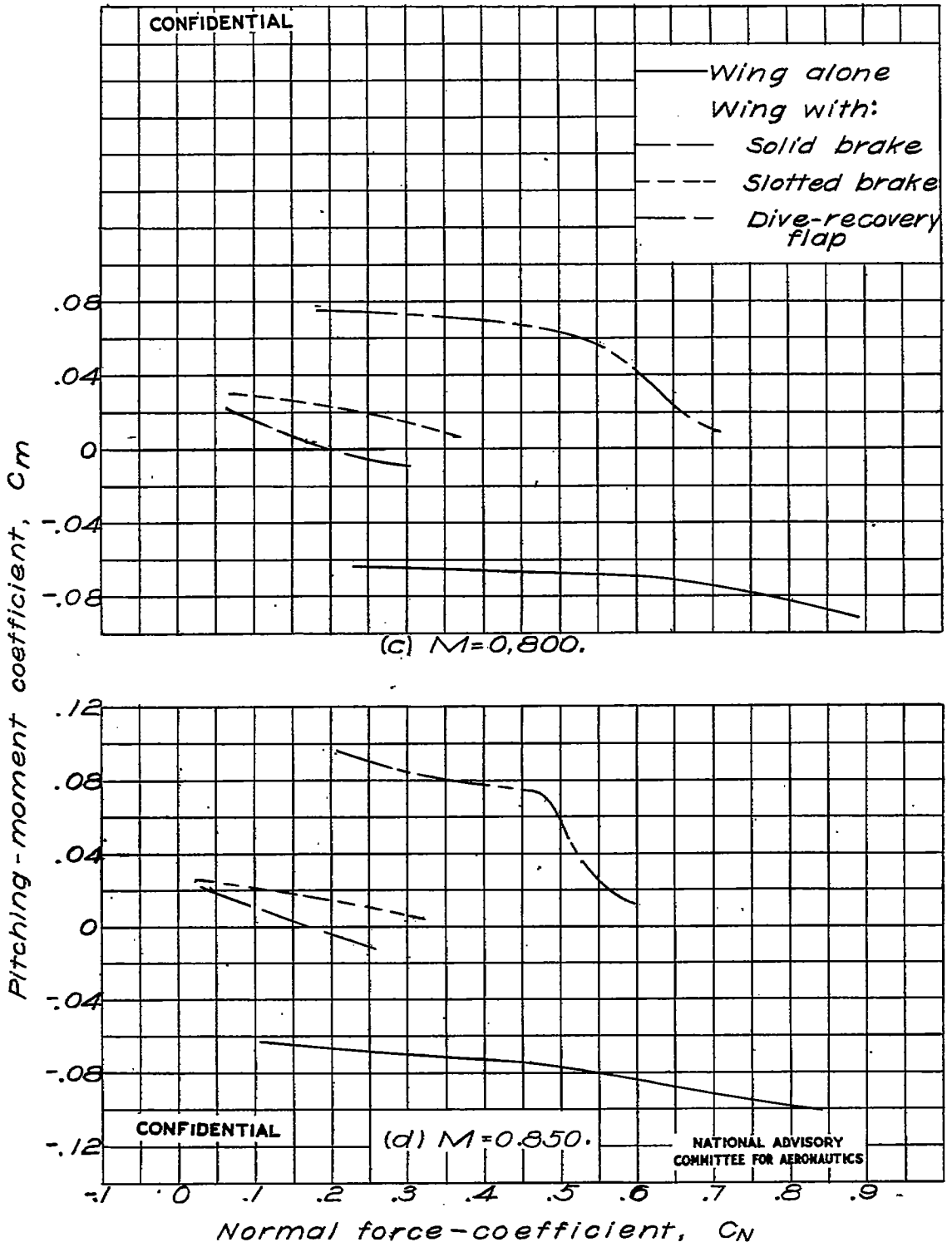


Figure 27.-Continued.

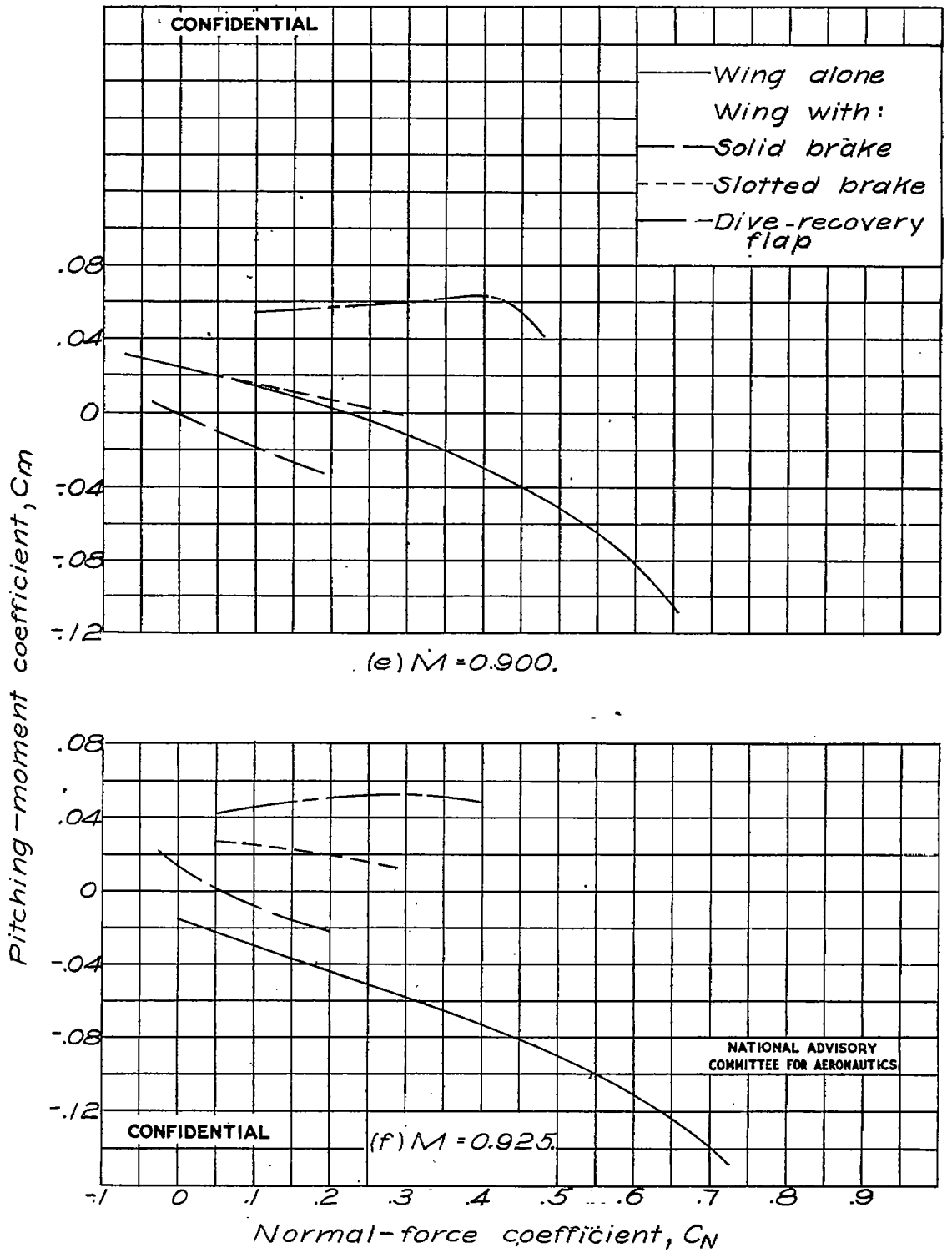


Figure 27-Concluded.

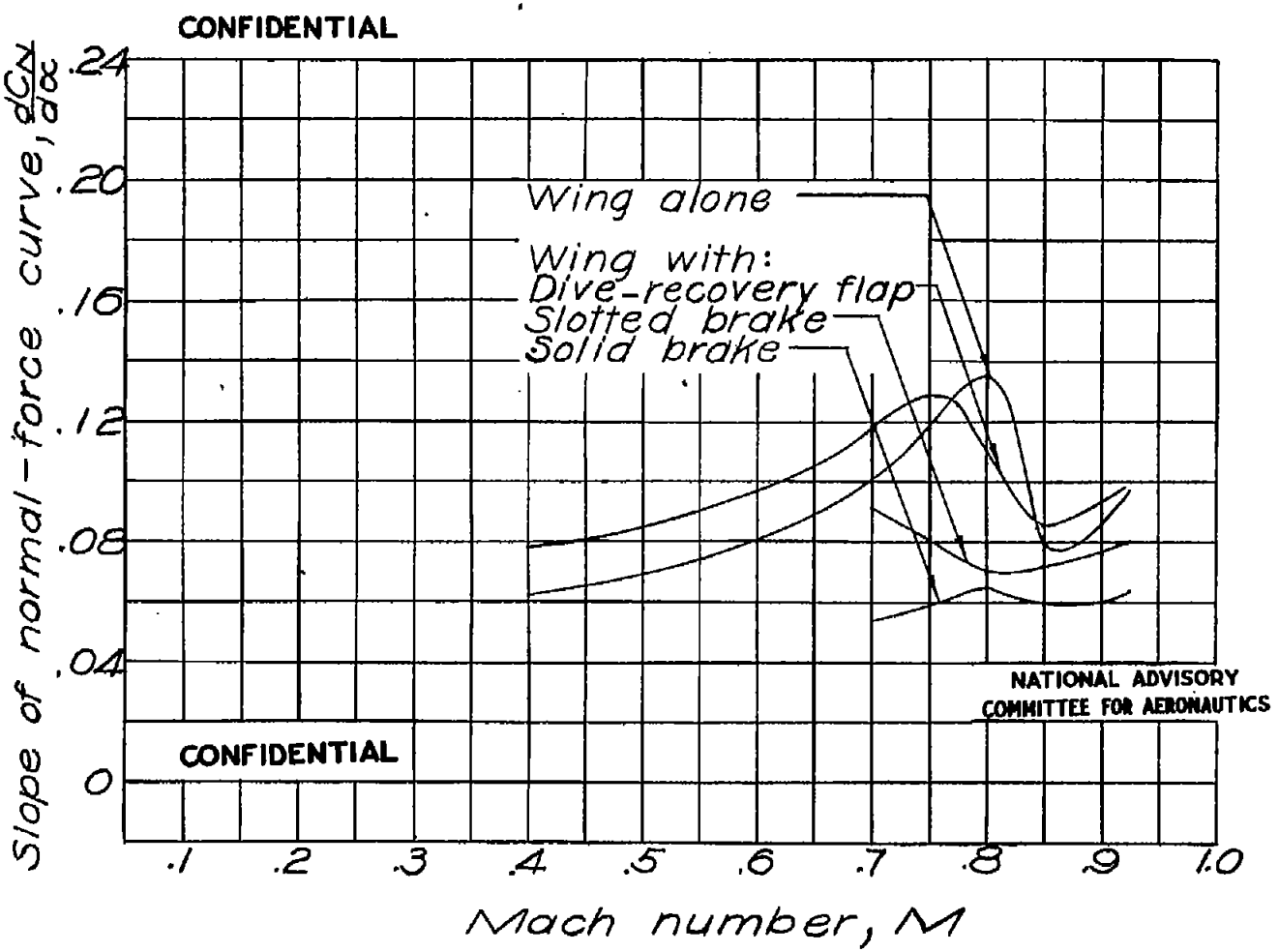


Figure 28.-Slope of normal-force-coefficient curve for a loading of 60 pounds per square foot at an altitude of 35,000 feet.

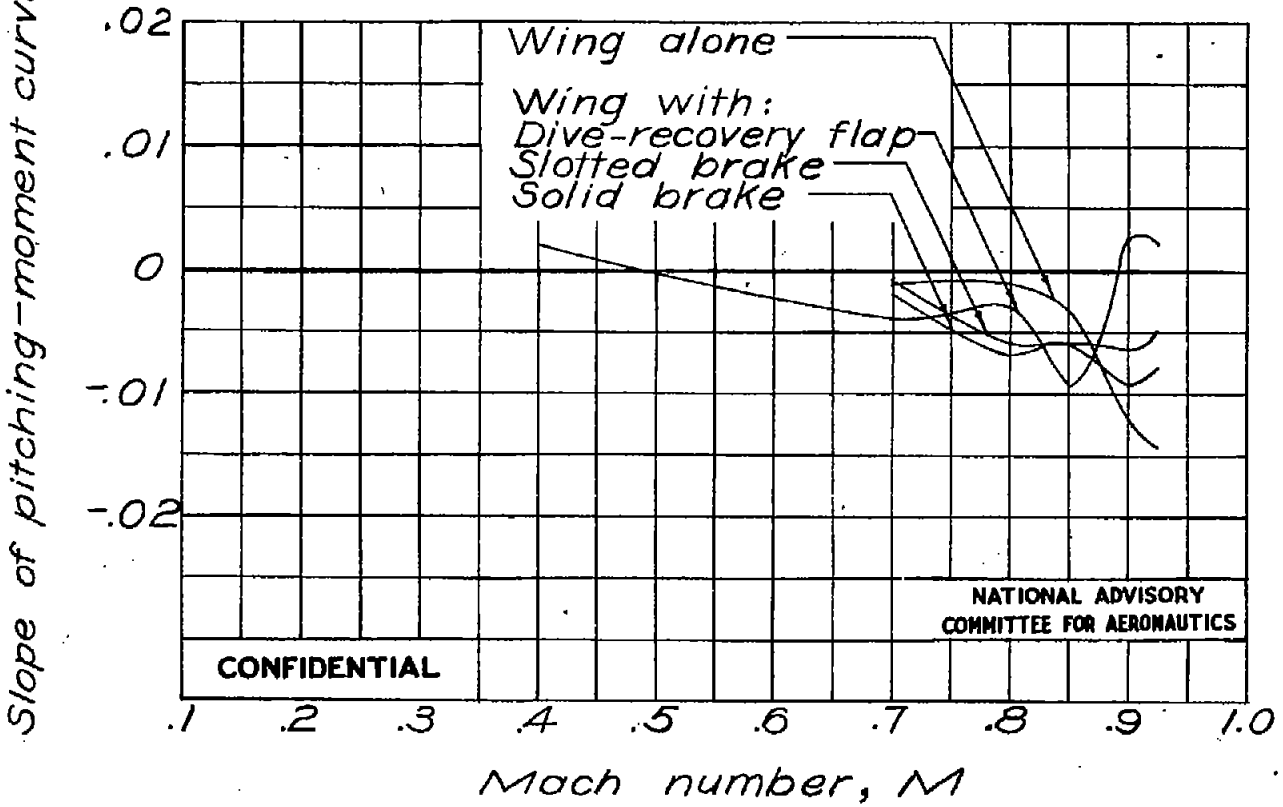


Figure 29.-Slope of pitching-moment-coefficient curve for a loading of 60 pounds per square foot at an altitude of 35,000 feet.

CONFIDENTIAL

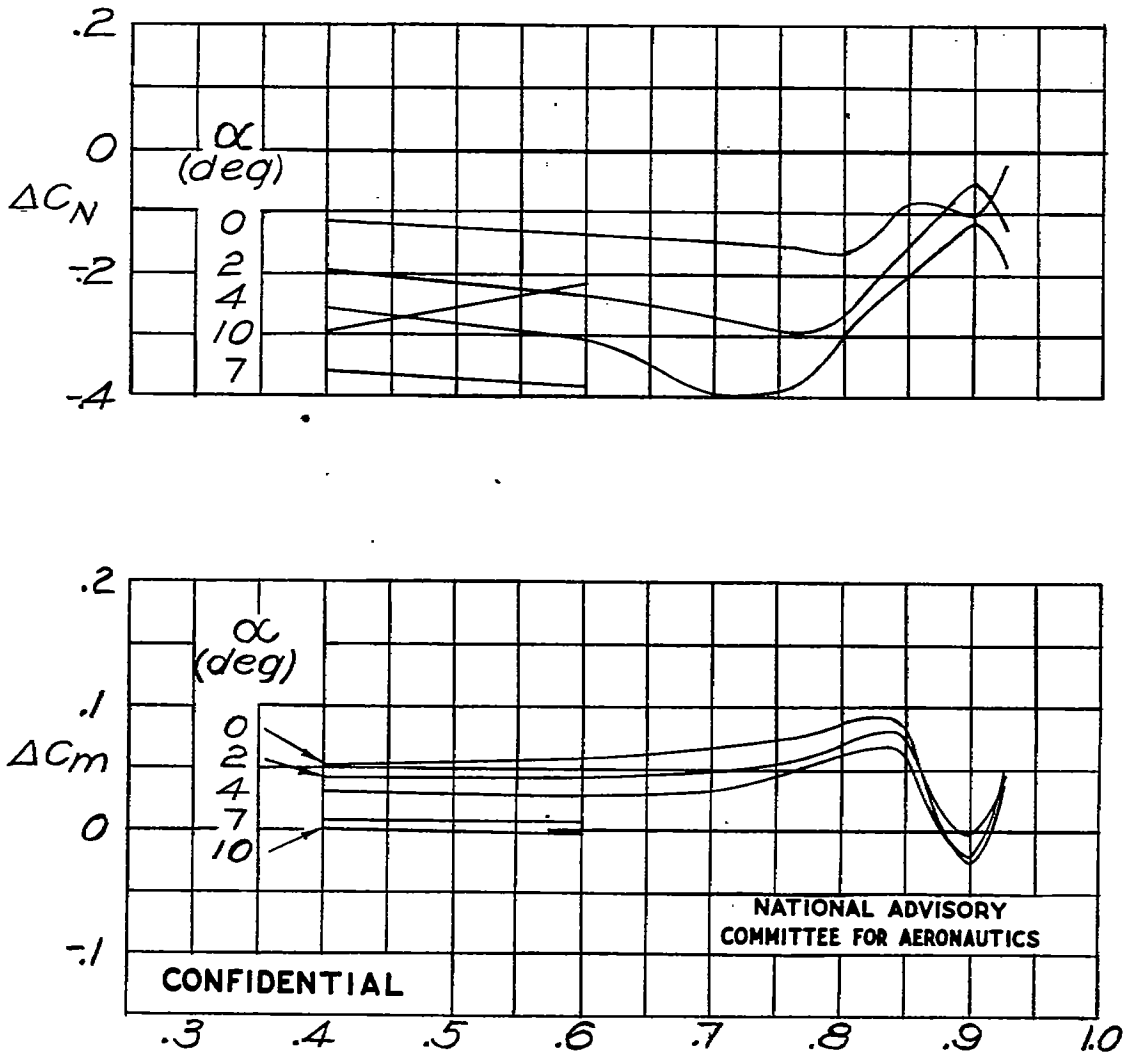


Figure 30.-Variation of incremental normal-force and pitching-moment coefficients with Mach number for solid brake.

CONFIDENTIAL

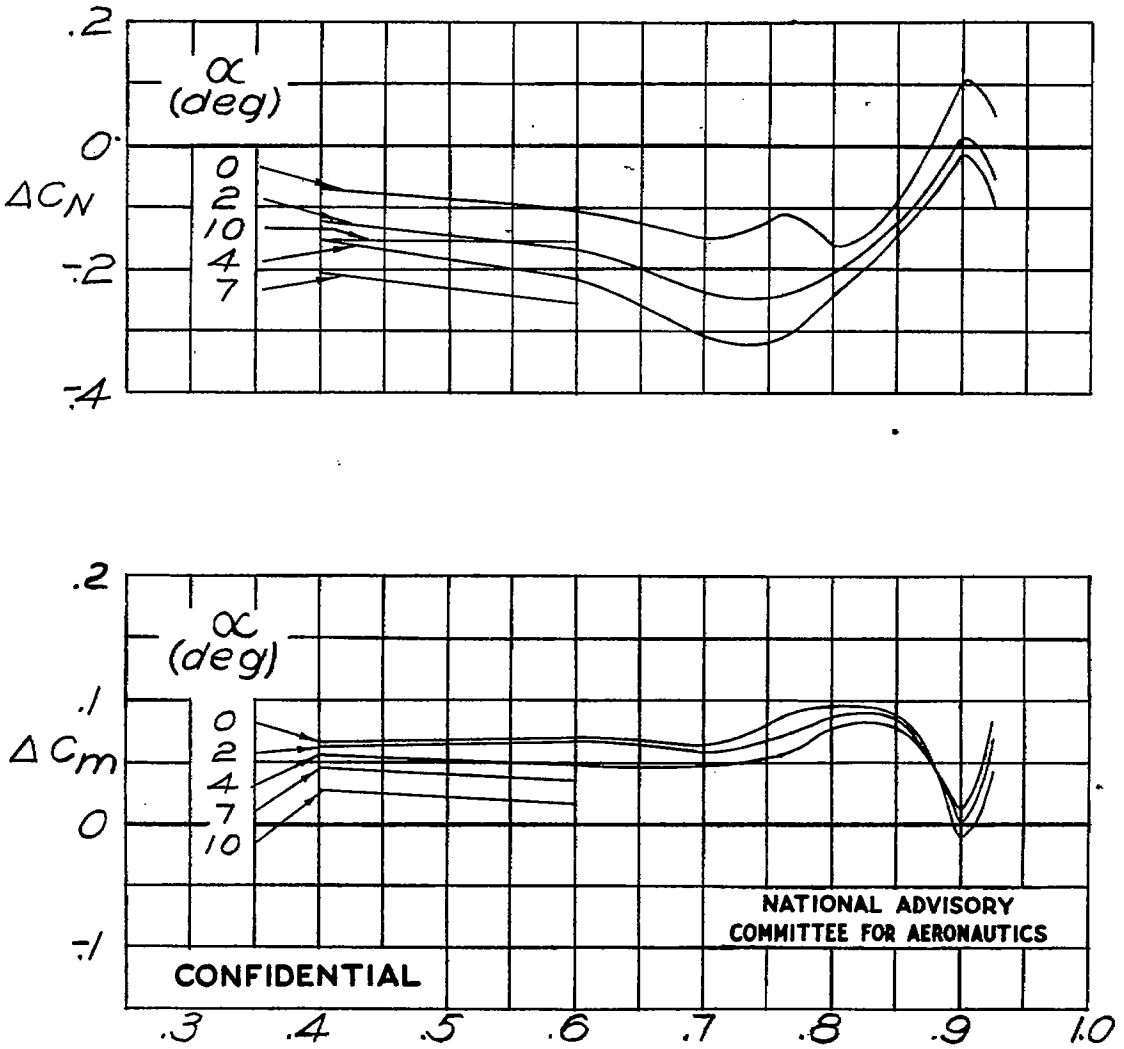


Figure 31.-Variation of incremental normal-force and pitching-moment coefficients with Mach number for slotted brake.

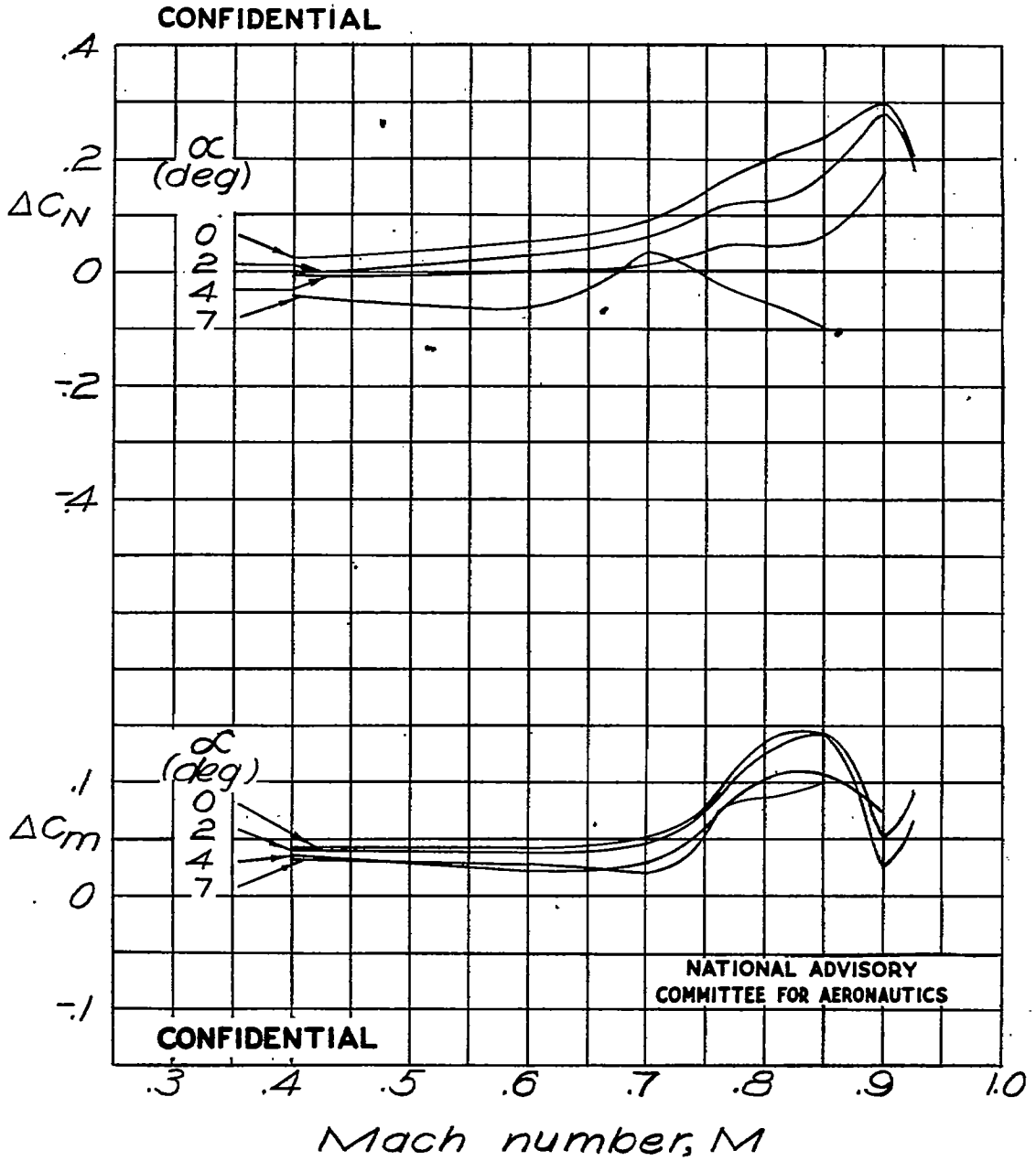


Figure 32.-Variation of incremental normal-force and pitching-moment coefficients with Mach number for dive-recovery flap.

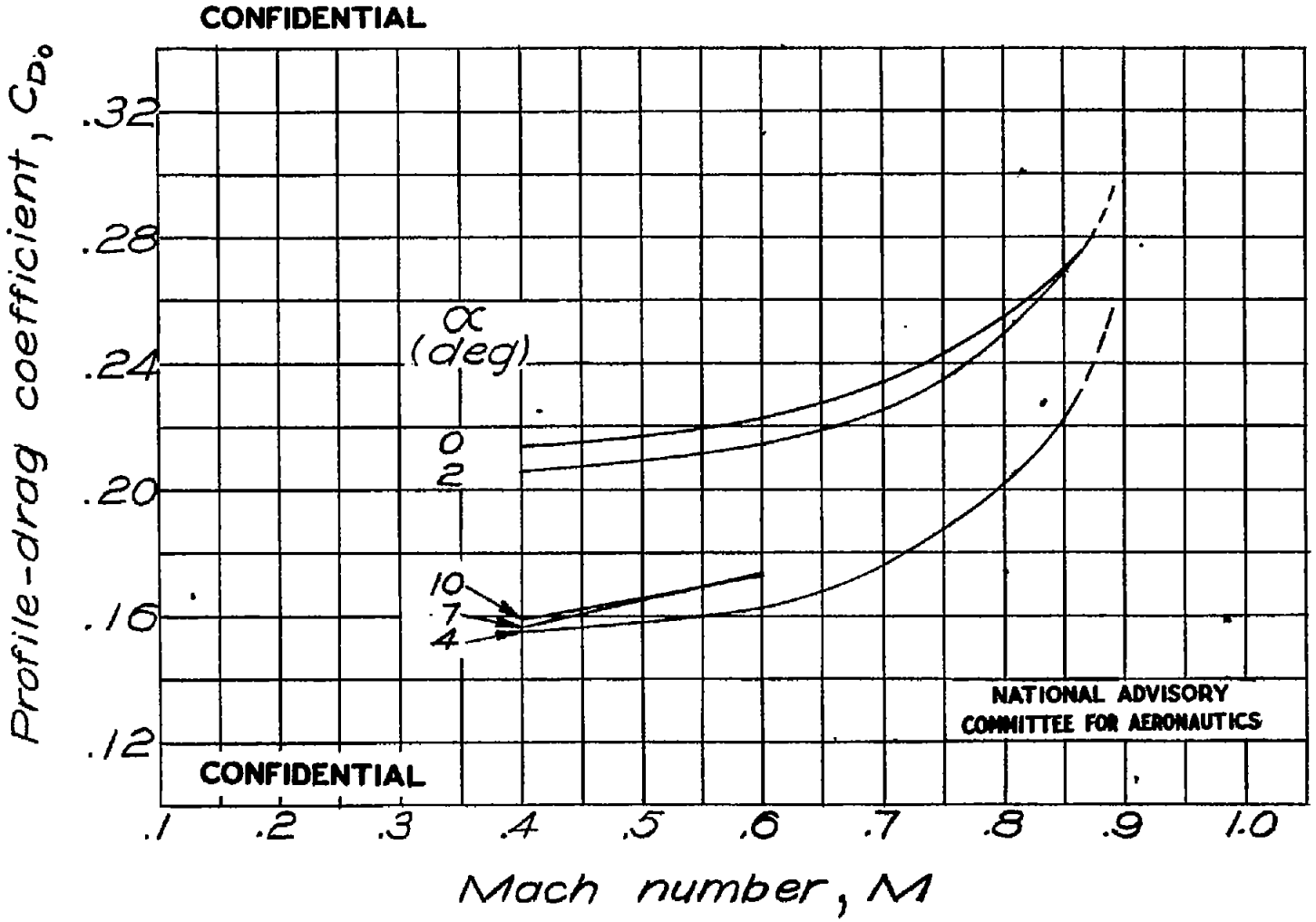


Figure 33.-Variation of profile-drag coefficient with Mach number for wing with solid brake.

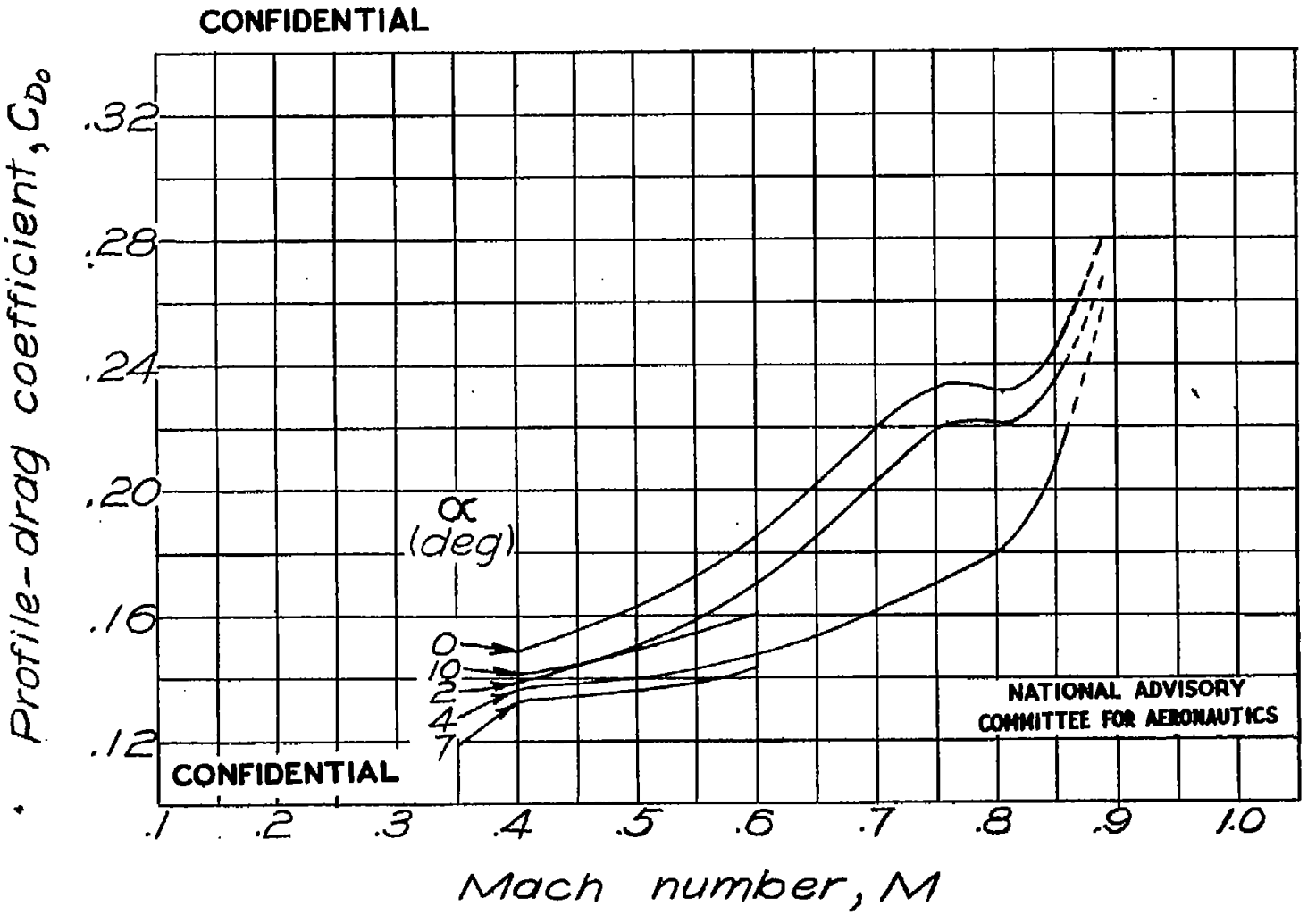


Figure 34.—Variation of profile-drag coefficient with Mach number for wing with slotted brake.

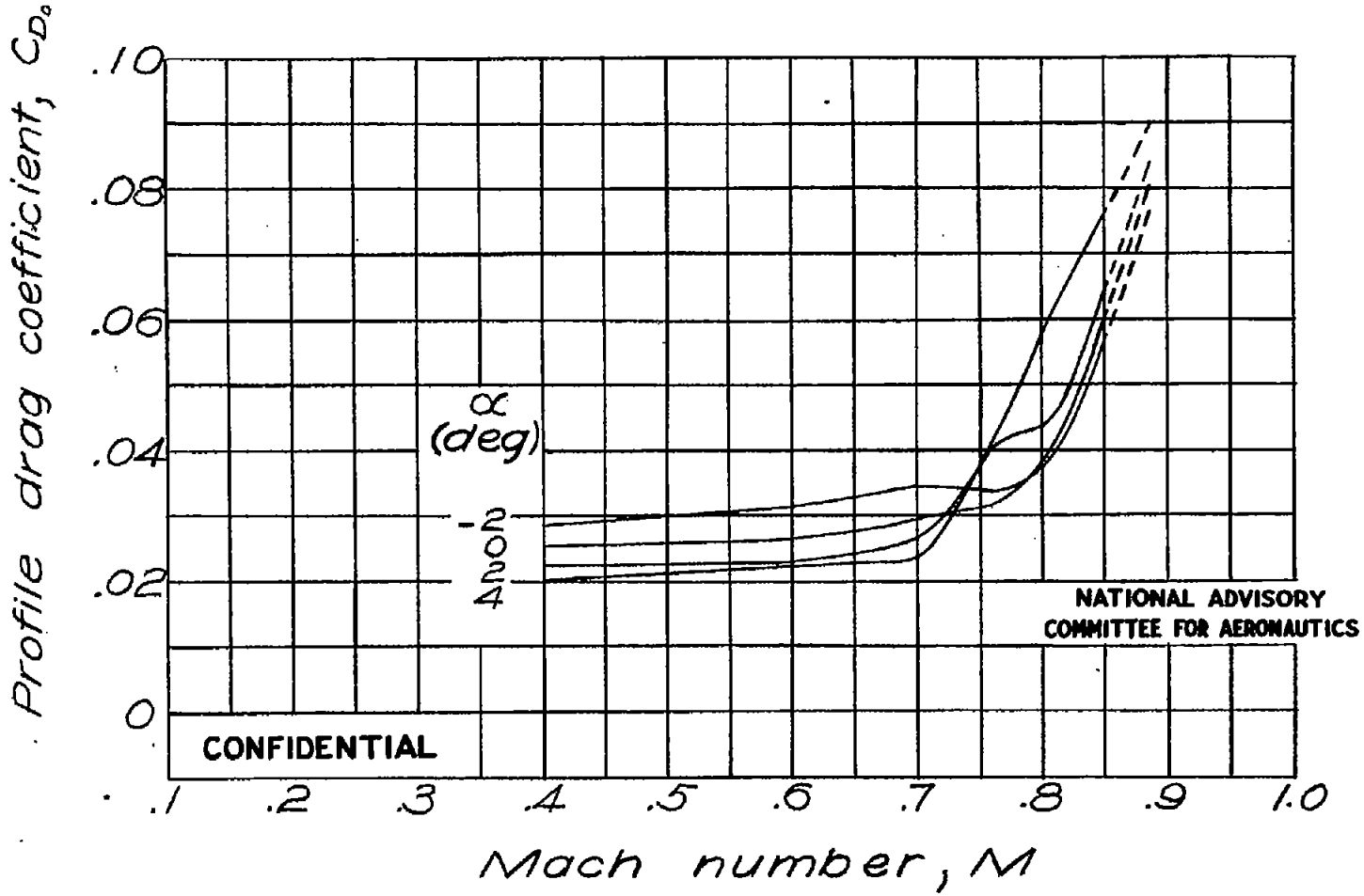


Figure 35.—Variation of profile-drag coefficient with Mach number for wing with dive-recovery flap.

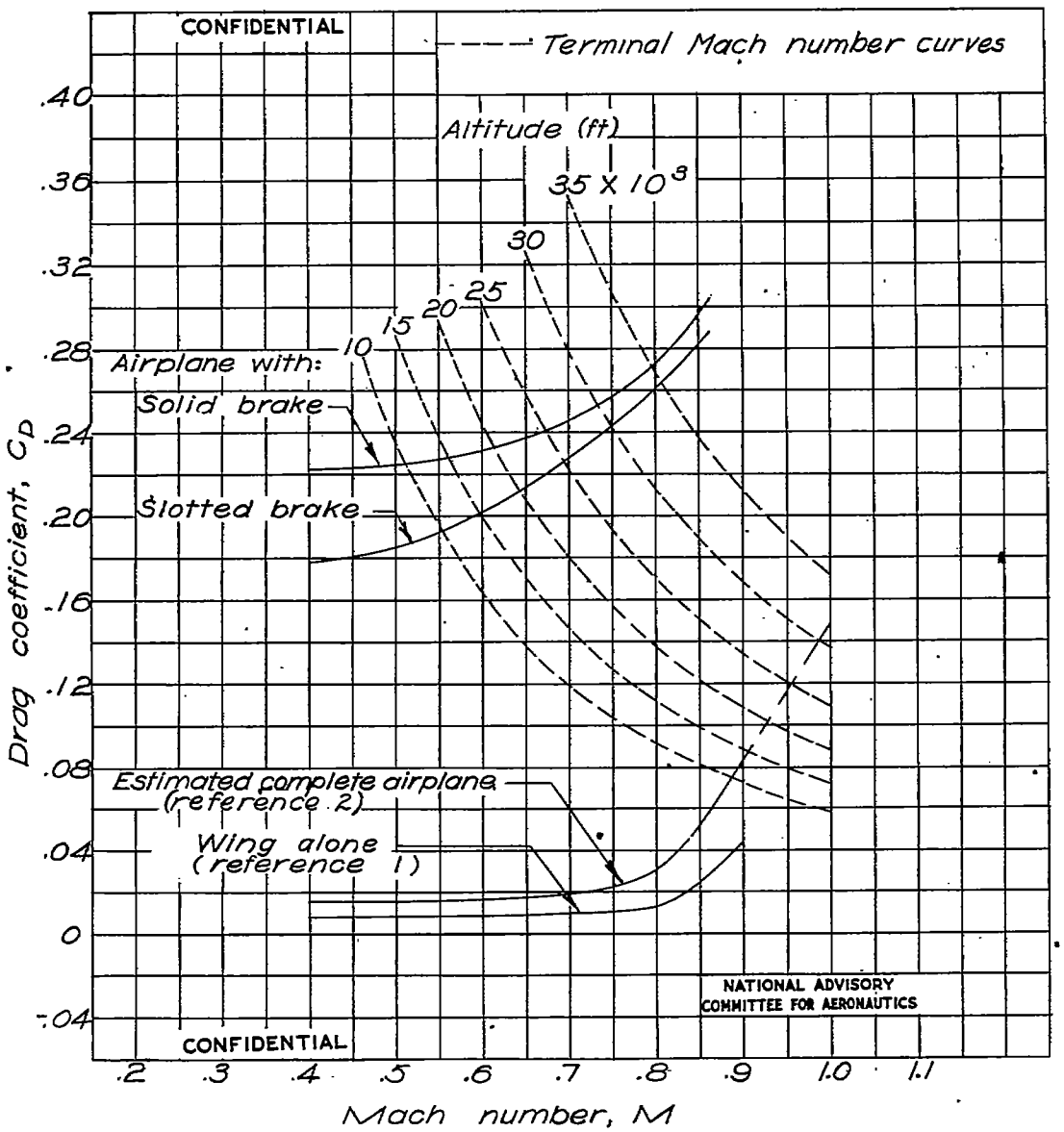


Figure 36.- Estimated variation of airplane drag coefficient with Mach number for terminal Mach number prediction for airplane wing loading of 60 pounds per square foot at various altitudes.

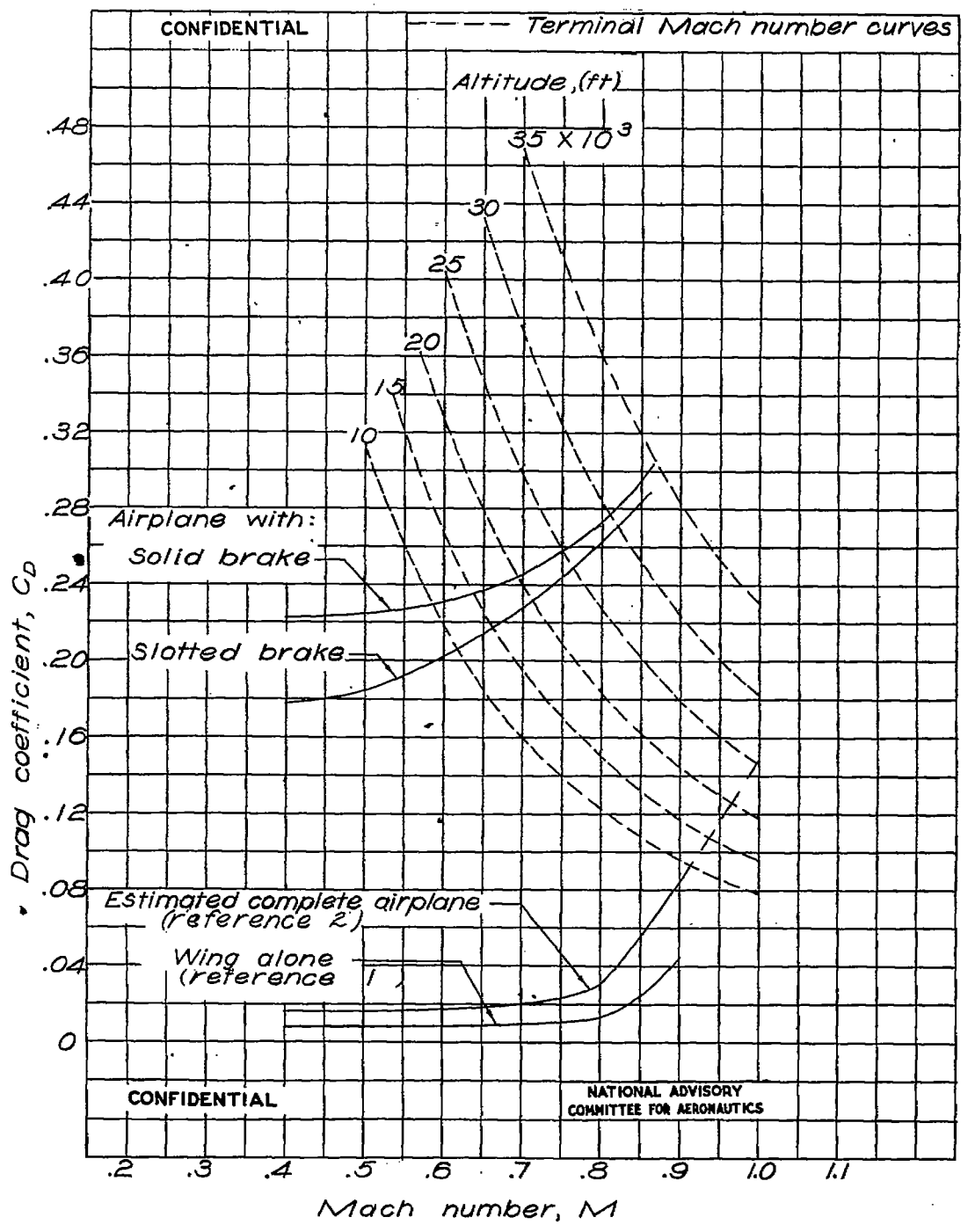


Figure 37.-Estimated variation of airplane drag coefficient with Mach number for terminal Mach number prediction for airplane wing loading of 80 pounds per square foot at various altitudes.

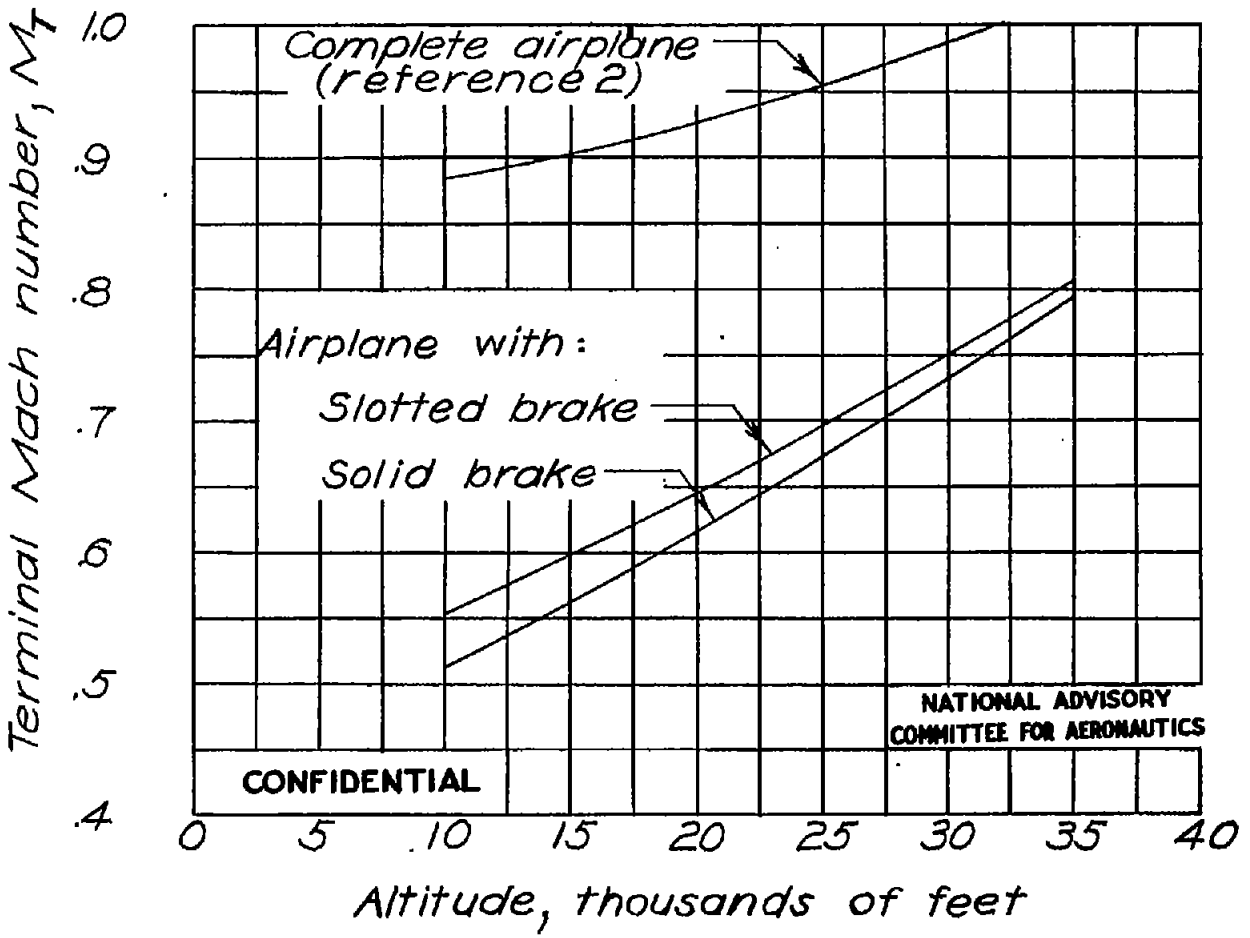


Figure 38.—Estimated variation of terminal Mach number with altitude for wing loading of 60 pounds per square foot.

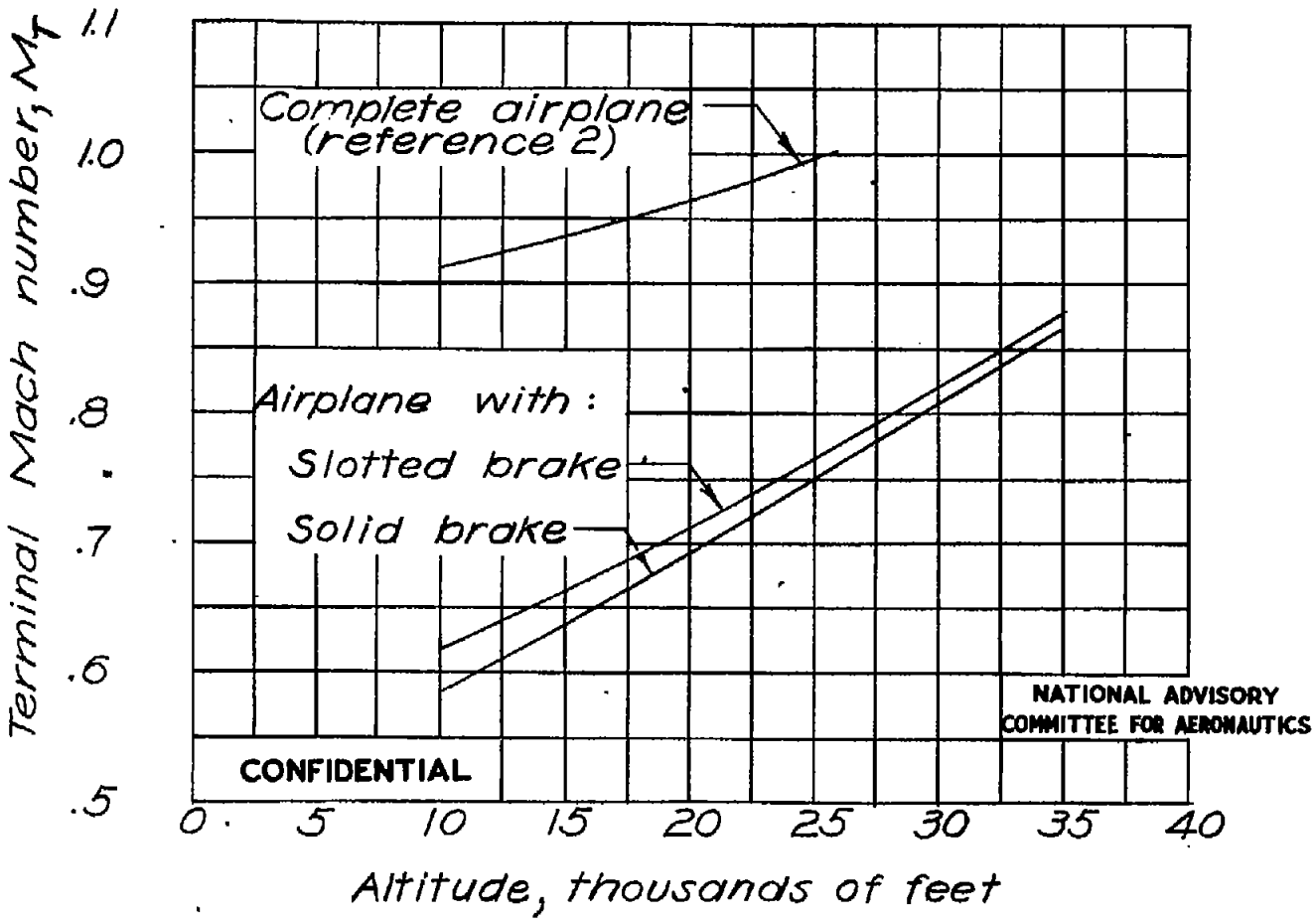


Figure 39.—Estimated variation of terminal Mach number with altitude for wing loading of 80 pounds per square foot.

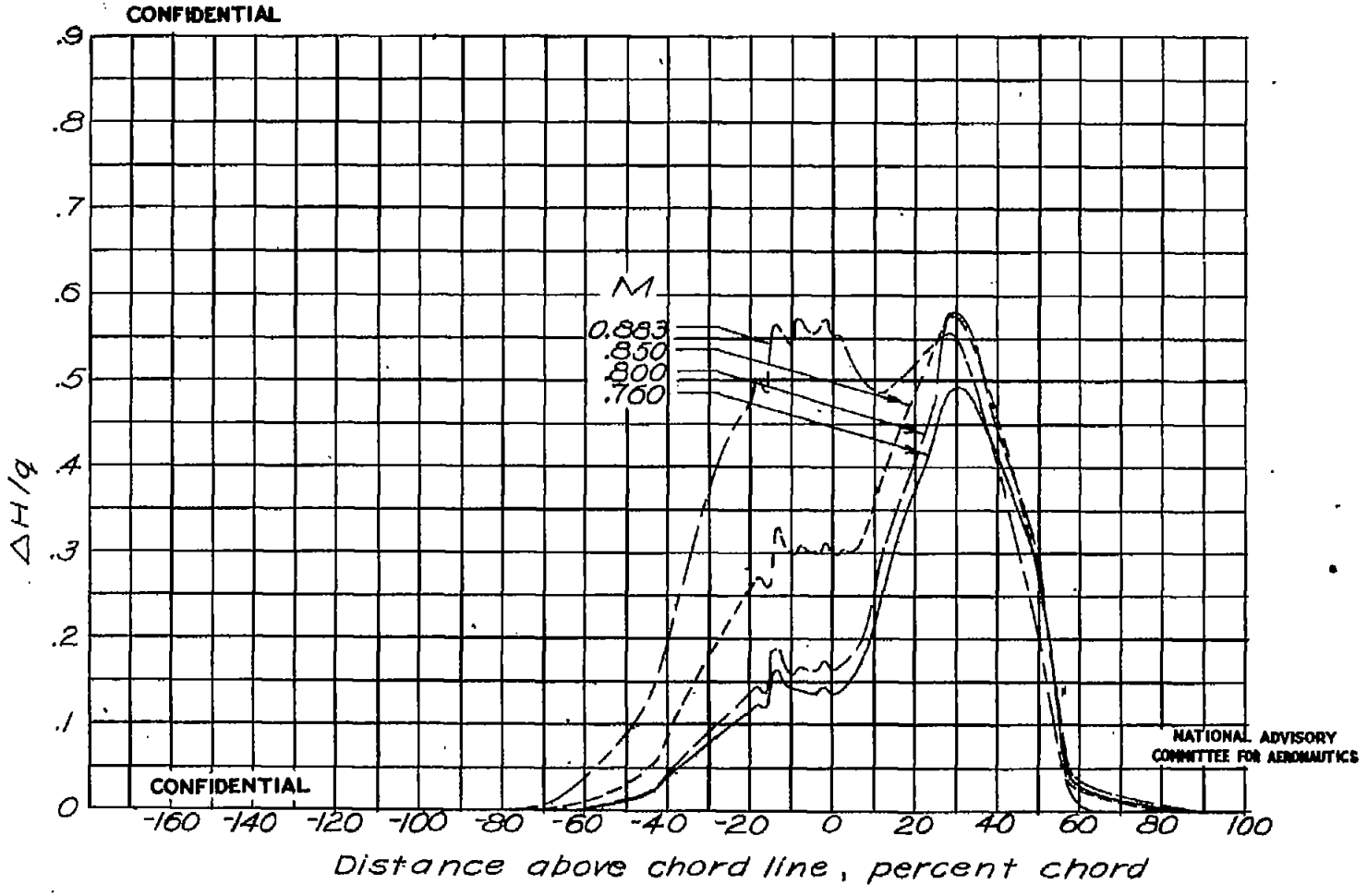


(a) $\alpha = 0°$.

Figure 40.- Wake profiles for several Mach numbers 2.82 root chords behind the 25-percent chord line for wing with solid brake.

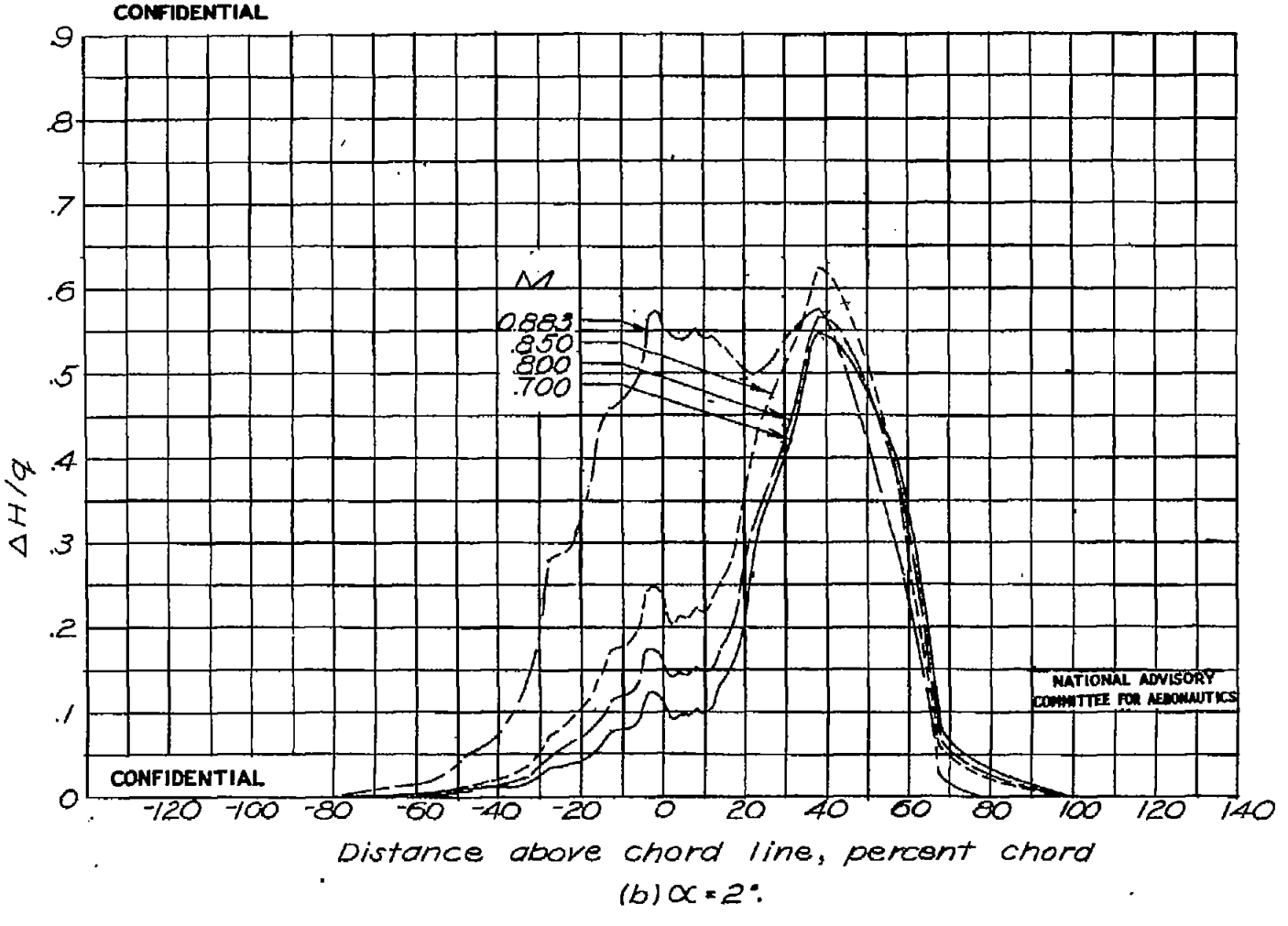


(b) $\alpha = 2°$.

Figure 40.- Continued.

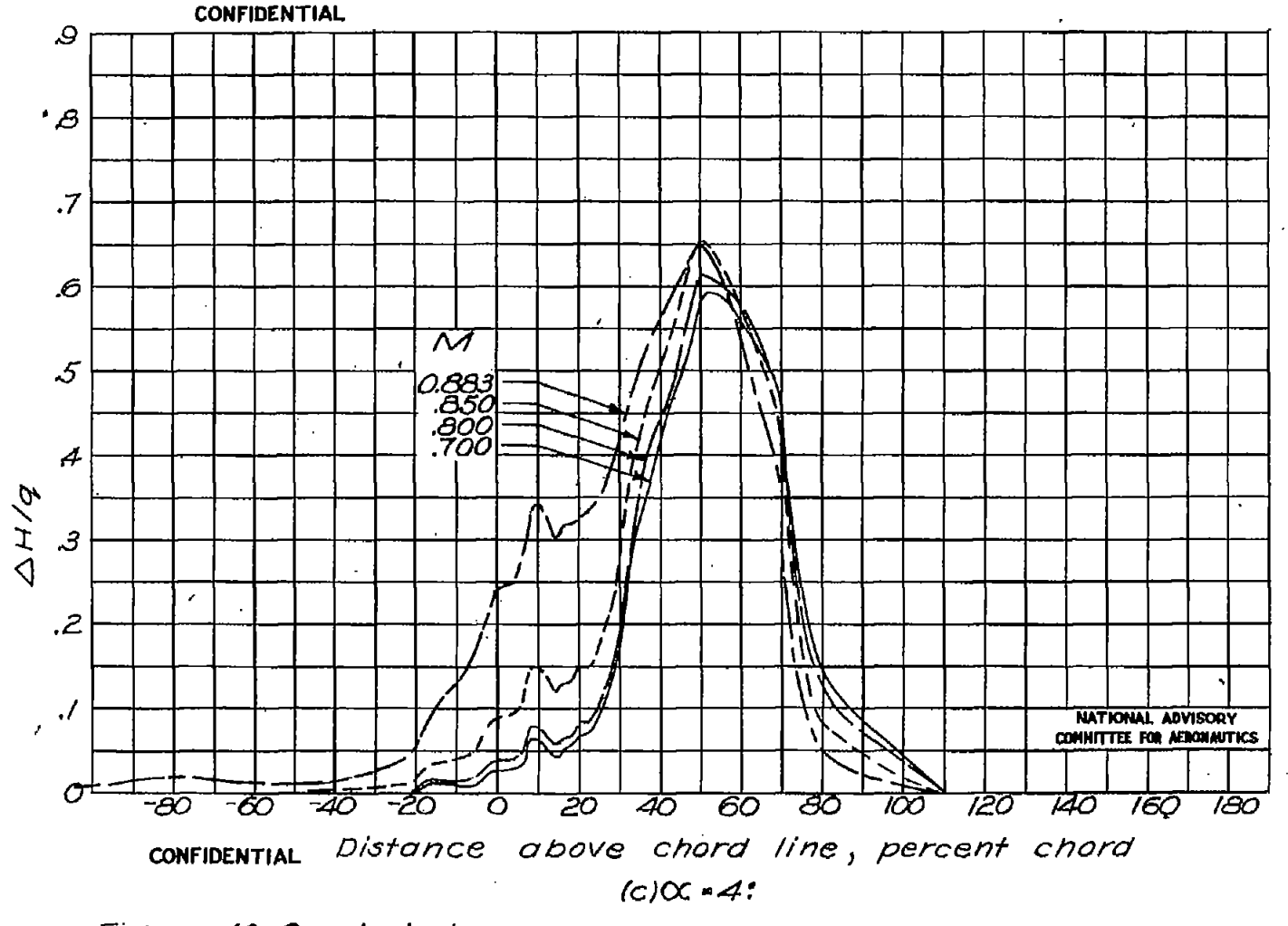


Figure 40.-Concluded.

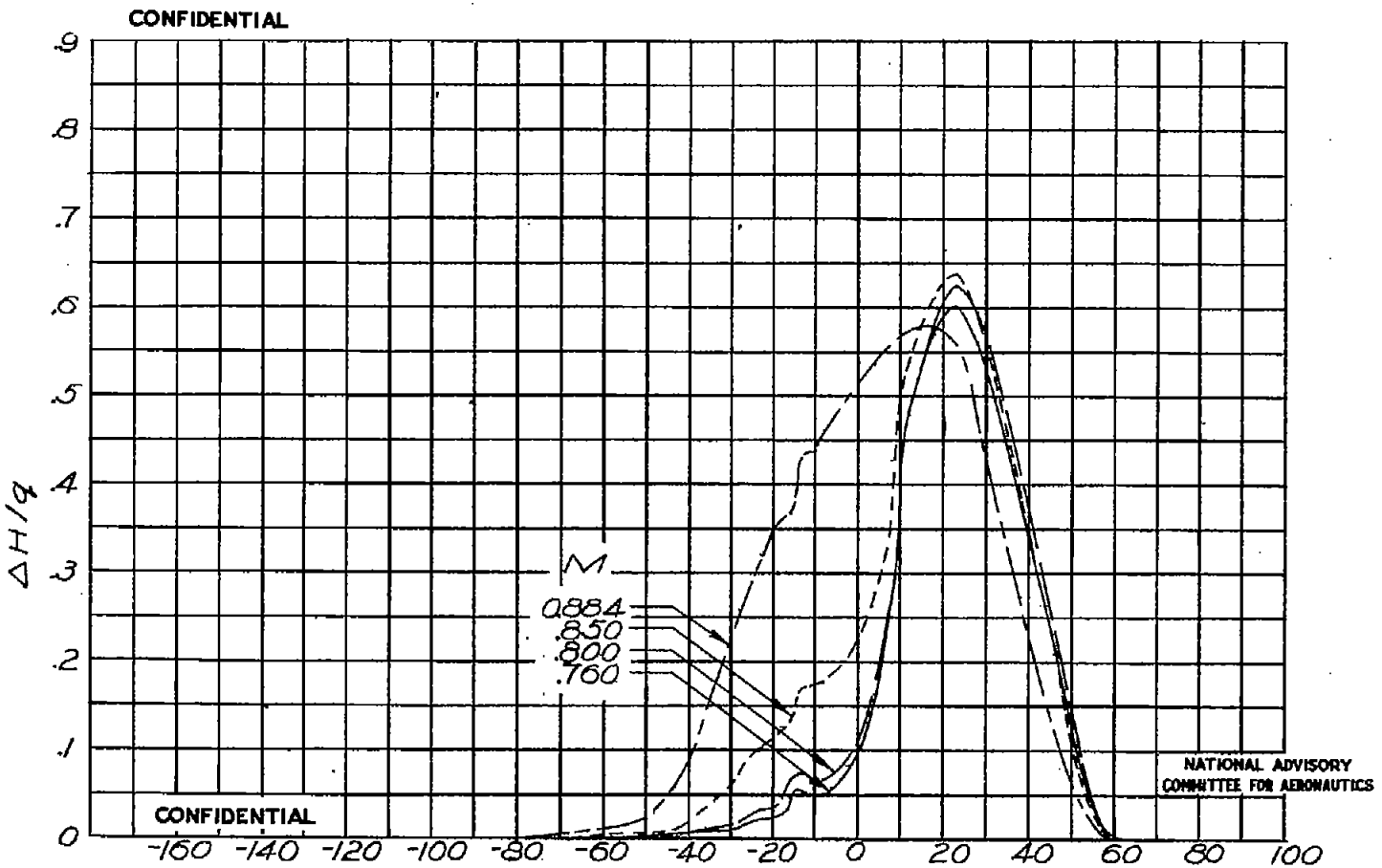


(a) $\alpha = 0°$.

Figure 41.-Wake profiles for several Mach numbers 2.82 root chords behind the 25-percent-chord line for wing with slotted brake.

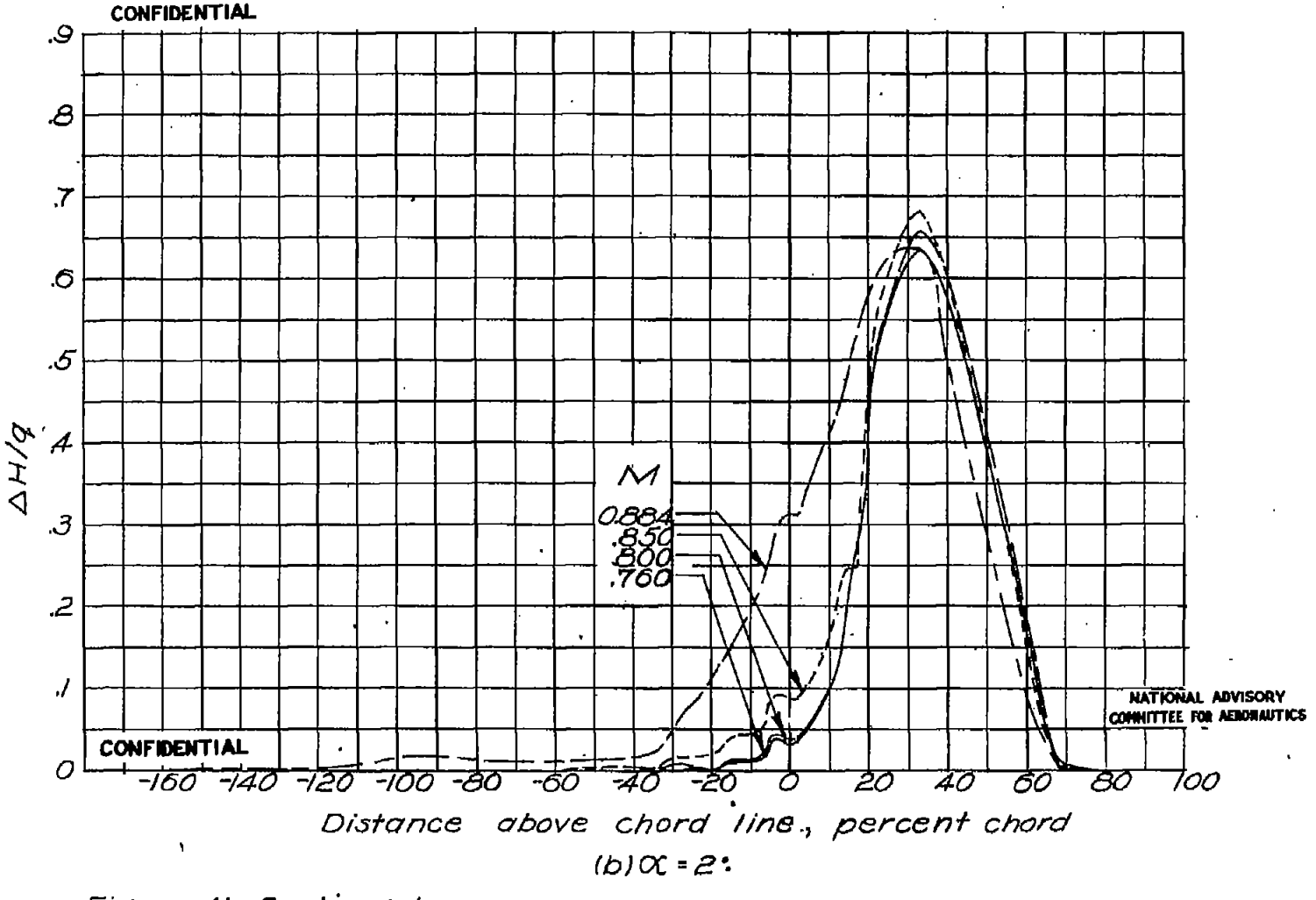


(b) $\alpha = 2°$

Figure 41.–Continued.

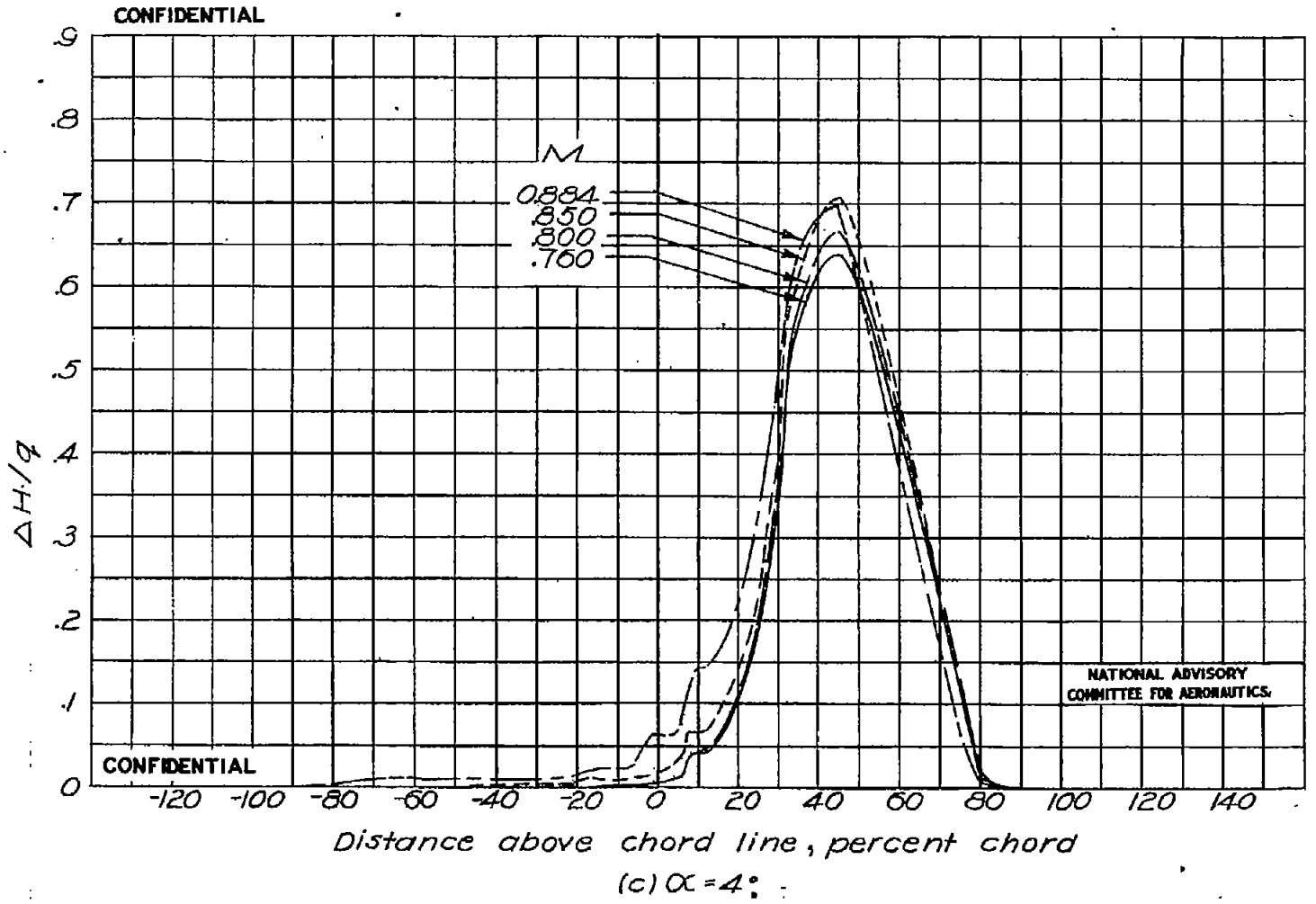


(c) $\alpha = 4°$.

Figure 41.- Concluded.

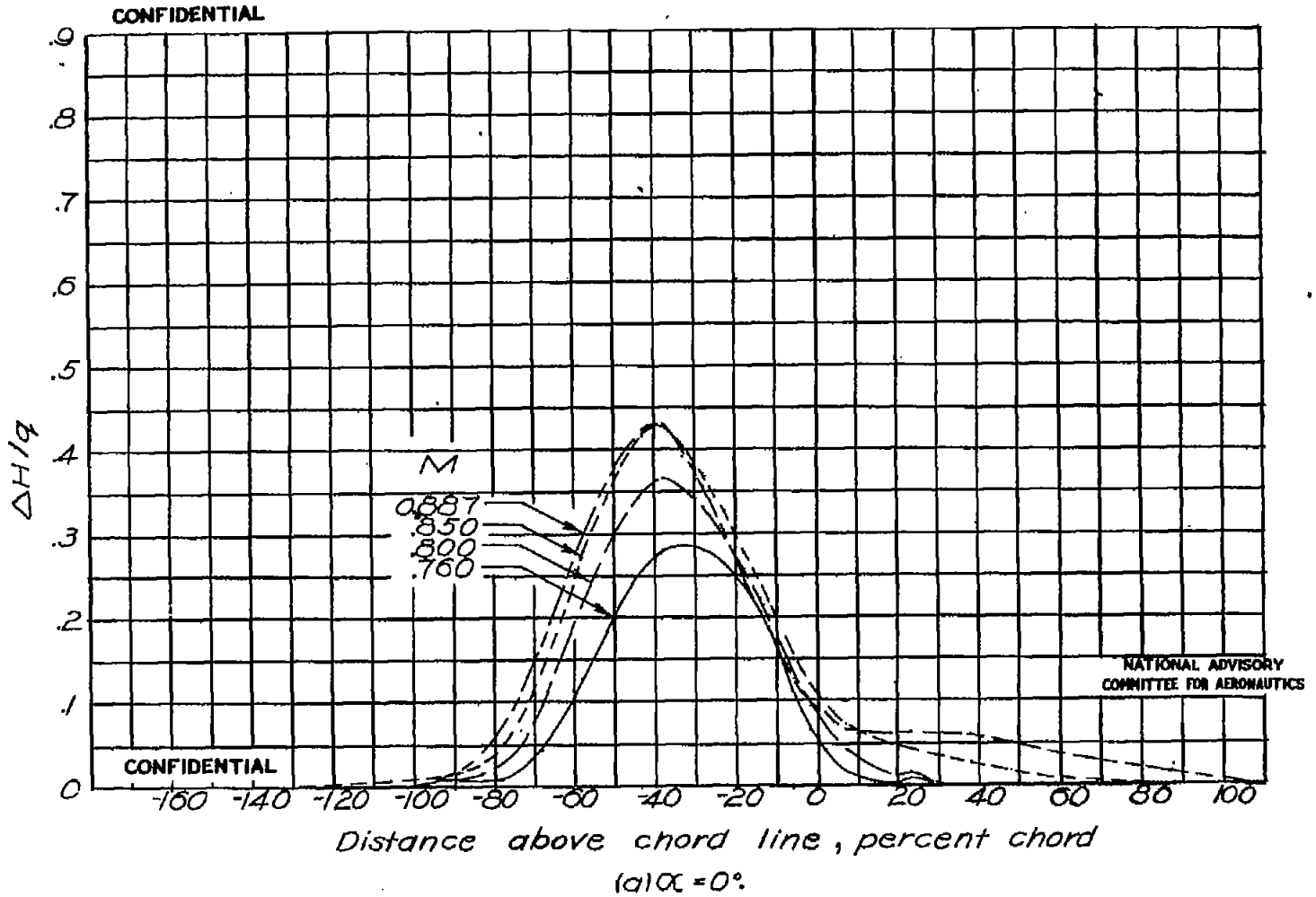


(a) $\alpha = 0°$.

Figure 42.- Wake profiles for several Mach numbers 2.82 root chords behind the 25-percent-chord line for wing with dive-recovery flap.

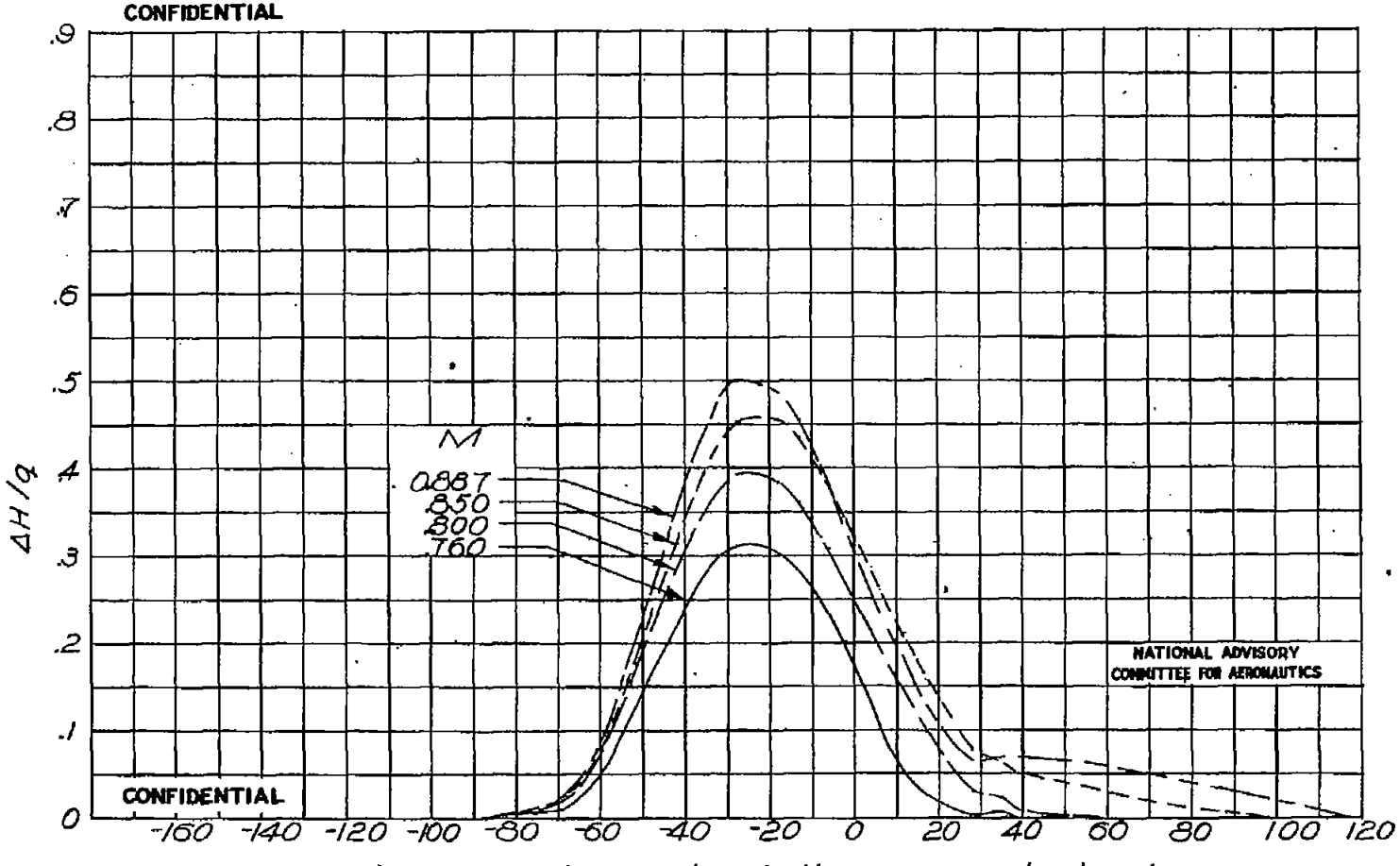


(b) $\alpha = 2°$.

Figure 42.-Continued.

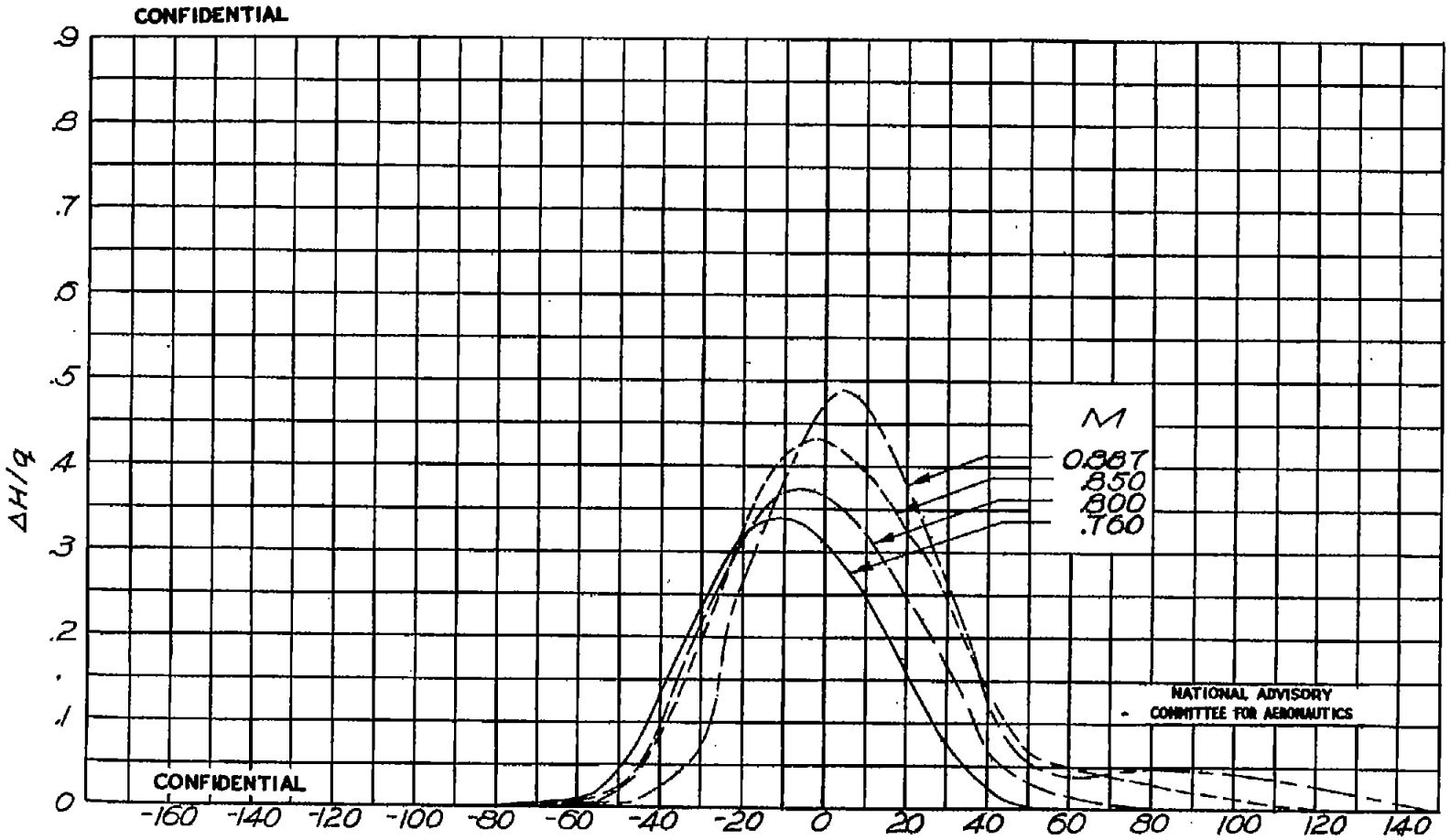


(c) $\alpha = 4°$.

Figure 42.-Concluded.

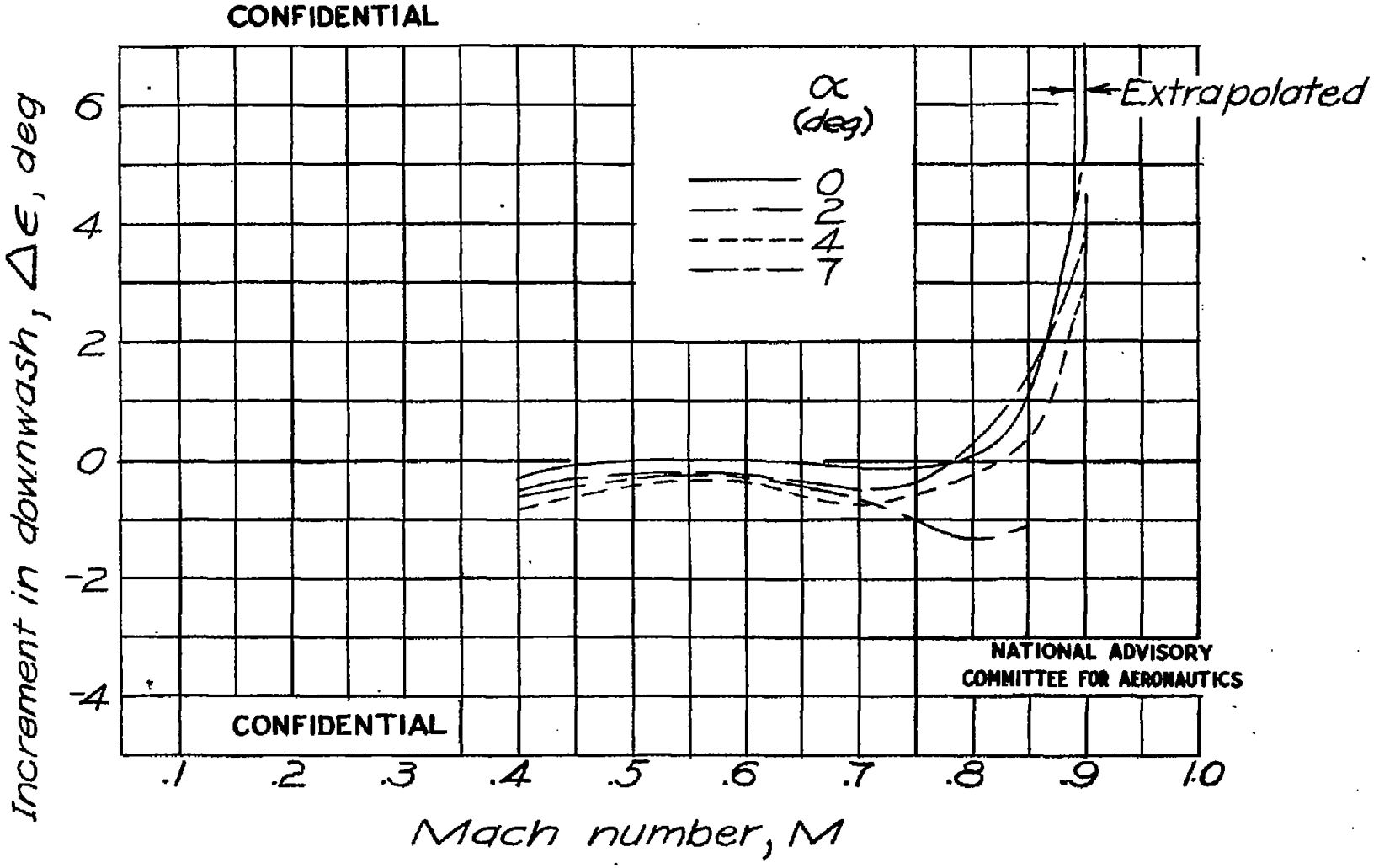


Figure 43.—Variation in increment in downwash angle with Mach number for the dive-recovery flap measured 70 percent of chord above the center line.

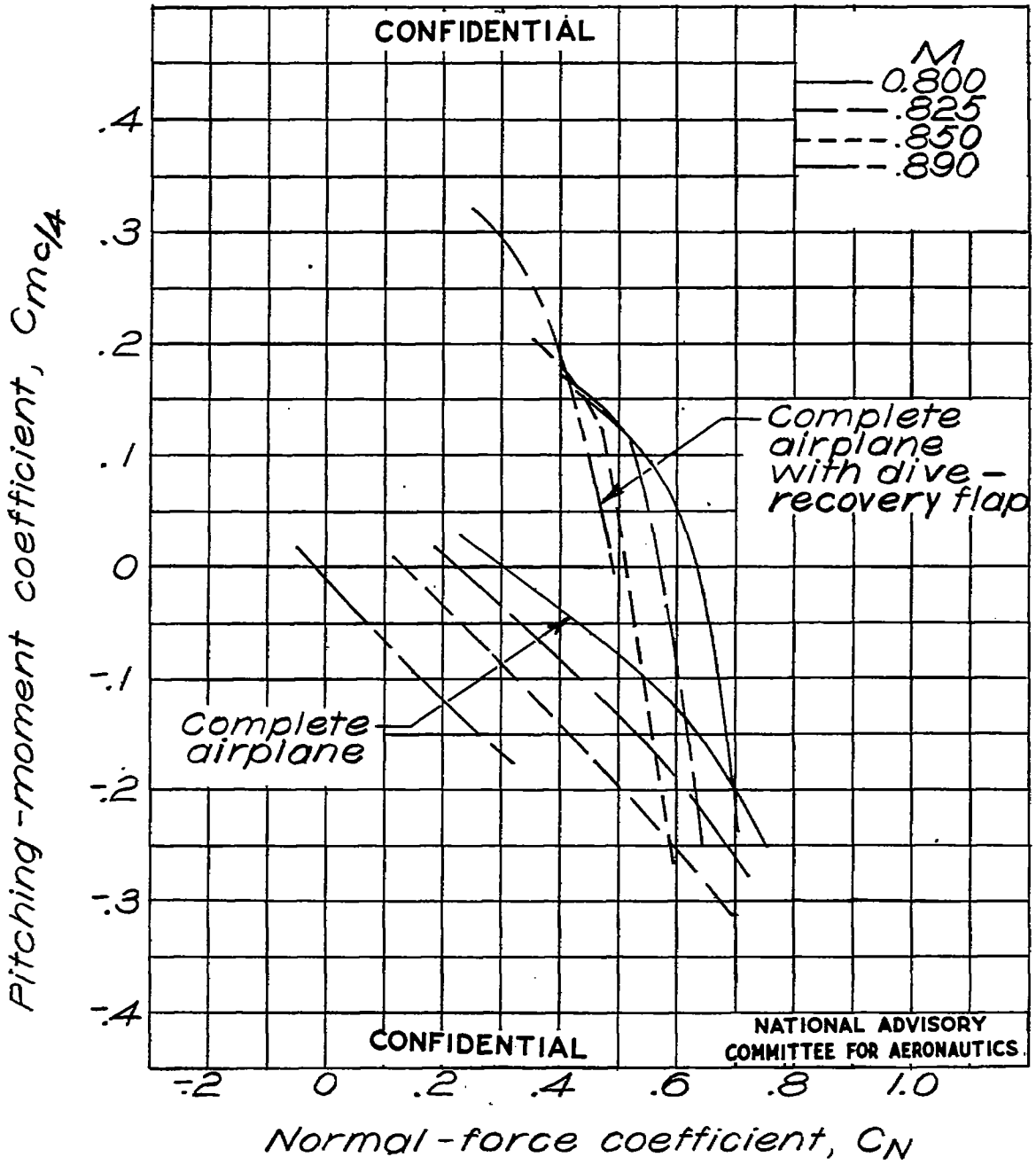


Figure 44.-Estimated comparison of elevator-fixed static longitudinal stability characteristics for complete airplane with dive-recovery flap. $i_t = 0°$.